ABSTRACT

VARIABLE PERMITTIVITY DIELECTRIC MATERIAL LOADED STEPPED-HORN ANTENNA

by
Özgür Özdemir

Stepped-horn antenna loaded with dielectric material of variable permittivity is proposed to improve radiation characteristics and/or to increase the electrical dimensions of the radiating structure compared to unloaded empty one. A hybrid numerical technique is used to analyze such an antenna. The tapered section of the horn antenna is modeled by multi-stepped waveguide structures filled with variable dielectric constant material. Generalized scattering matrix representation of the tapered section of the horn antenna is obtained using mode matching technique. The radiating aperture problem is solved by the method of moments, under the assumption that the horn is terminated by an infinite metallic flange. Input return loss, gain, aperture efficiency and cross-polarization characteristics are studied. Comparisons indicate that any kind of loading with dielectric material along the taper tend to improve the gain level for the entire bandwidth, aperture efficiency may increase and cross-polarization level may decrease for relatively narrow bandwidths. It is observed that this is partly due to increase in the electrical size of the aperture and partly due to excitation of higher order modes. The goal of the optimization in a stepped-horn antenna is to adjust the magnitude and phase of the excited TE_{30} mode to achieve more uniform aperture field distribution. This has been accomplished by optimizing step length and permittivity of the enclosed dielectric material. As a result of optimization, improved gain, reduced cross-polarization and enhanced aperture efficiency characteristics have been achhieved in a stepped-horn antenna. Instead of loading only one material, using materials with different permittivities gave extra parameters to control characteristics such as the input return loss. These study can be extended for further multi-stepped structures with variable dielectric materials.

VARIABLE PERMITTIVITY DIELECTRIC MATERIAL LOADED STEPPED-HORN ANTENNA

by
Özgür Özdemir

A Dissertation
Submitted to the Faculty of
New Jersey Institute of Technology
in Partial Fulfillment of the Requirements for the Degree of
Doctor of Philosophy in Electrical Engineering

Department of Electrical and Computer Engineering

August 2005

APPROVAL PAGE

VARIABLE PERMITTIVITY DIELECTRIC MATERIAL LOADED STEPPED-HORN ANTENNA

Özgür Özdemir

August 18, 2005

Dr. Edip Niver, Dissertation Advisor — Date
Associate Professor of Electrical and Computer Engineering, NJIT

Aug 18, 2005

Dr. Gerald Whitman, Committee Member — Date
Professor of Electrical and Computer Engineering, NJIT

Aug 18, 05

Dr. Haim Grebel, Committee Member — Date
Professor of Electrical and Computer Engineering, NJIT

Aug 18, 2005

Dr. Koray E. Akdogan , Committee Member — Date
Research Faculty of Ceramic and Materials Engineering, Rutgers University

Aug. 18, 2005

Dr. Ken Chin, Committee Member — Date
Professor of Physics, NJIT

BIOGRAPHICAL SKETCH

Author: Özgür Özdemir

Degree: Doctor of Philosophy

Date: August 2005

Undergraduate and Graduate Education:

- Doctor of Philosophy in Electrical Engineering,
  New Jersey Institute of Technology, Newark, NJ, 2005
- Master of Engineering in Electrical Engineering,
  Istanbul Technical University, Istanbul, Turkey, 2000
- Bachelor of Engineering in Electrical Engineering,
  Istanbul Technical University, Istanbul, Turkey, 1998

Major: Electrical Engineering

Presentations and Publications:

Ozgur Ozdemir, Edip Niver, Koray E. Akdogan, Ahmad Safari, "Horn Antenna Loaded with Graded Index Dielectric Material," 2004 China-Japan Joint Meeting on Microwaves, Harbin, P. R. China, 2004

Ozgur Ozdemir, Edip Niver, Koray E. Akdogan, Ahmad Safari, "Loading Stepped Horn with Variable Permittivity Dielectric Material," Accepted for publication in Mediterranean Microwave Symposium 2005, Athens, Greece, 2005

To my parents,
Tahsin and Güler Özdemir

ACKNOWLEDGMENT

The preparation of this dissertation was assisted by many people. First of all, I would like to thank my supervisor Dr. Edip Niver who has provided valuable guidance for my life and my research. I would like to express my sincere thanks to Dr. Gerald Whitman for his valuable insight into research issues and his deep interest. I would also like to express my gratitude to Dr. Haim Grebel for his interest in my research. My gratitude is expressed to Dr. Koray E. Akdogan and Dr. Ken Chin for serving as commitee members and for providing useful comments. I would also like to thank to Dr. Ronald Kane for his concern about my graduate studies.

I would like to give my special thanks to Igor Stanojev who has always been such a great friend. His support has meant a lot to me than he could possibly realize. Also I would like to give my special thanks to Nikolaus Lehmann for his unbelievable support by taking care of everything for me from my presentation suit to fixing LaTeX problems. I am really grateful to Jingdi Zeng, Didem Gozupek, Gokhan Erkavun, Jordi Diaz, Zoran Latinovic, Taha Sencar and Chairat Pinthong for their friendship. I would like to thank to Ali Yapar and Funda Akleman for their encouragement from Istanbul. Without Arzu Aysu Gursoy, I would not be able to finish this dissertation.

I will be always grateful to my parents, Tahsin and Güler Özdemir, for their endless love. Their immeasurable devotion and encouragement gave me the strength to push through difficulties all my life. I also feel so lucky to have siblings like my brother Battal Özdemir and my sister Fadime Ergün who both always loved and believed in me. Finally, during the last two years, whenever I felt down, I only had to look at the picture of my gorgeous niece, Ada, to be happy again.

TABLE OF CONTENTS

LIST OF TABLES

LIST OF FIGURES

LIST OF FIGURES
(Continued)

Figure **Page**

LIST OF FIGURES
(Continued)

Figure **Page**

CHAPTER 1

INTRODUCTION

One of the most widely used microwave antennas is the horn antenna. In general, it is a simple radiating aperture used to provide a smooth tapered transition for a wave traveling from a feed waveguide into the free space. Horn antennas are used in satellite communications, as a feed element for radio astronomy reflector antennas and as a standard antenna for calibration and gain measurements in the laboratory. Horn antennas also find use in aperture phase array systems. When used as radiating elements in an array, it is desirable that a horn antenna have higher aperture efficiency in order to achieve favourable gain characteristics. Extensive research work has been made as a goal of improving the cross-polarization level and aperture efficiency of horn antennas. The use of dielectric loading, hybrid modes or multimodes, and corrugations on the walls of the horn are all consequences of such research efforts [1] -[7]. Dielectric loading approach has the advantage over corrugated horns. It has comparable performance to corrugated horns but is much simpler to construct. In the work of Tsandoulas and Fitzgerald [3], dielectric loading was used to enhance the aperture efficiency of a rectangular horn antenna. In that work, dielectric material was only placed along the walls and assuming that only the dominant mode was propagating. Clarricoats et.al. [6] and Lier [8] have proposed inserting a conical dielectric core inside the conical metal horn that is separated from the metal wall by a dielectric layer with lower permittivity rather of the core material.

In this thesis, loading the horn antenna with variable dielectric material is proposed to accomplish to improve cross-polarization, aperture efficiency and gain characteriscs without increasing the size. Dielectric material is assumed to be filling the entire cross-section of the part or the whole of the antenna structure. Multi-mode rectangular horns employ TE_{m0}(m=1,3,5) modes with approximate amplitude $1/m$ to improve the aperture

field uniformity and this results in higher aperture efficiencies than horns with fundamental mode alone. Optimization routine is introduced to implement desired modes at the aperture.

Rigorous theoretical approaches to analyze an empty horn were reported in the literatur [9]-[11]. In Chapter 2, as a mathematical model for dielectric loaded horn analysis, hybrid numerical approach is used. In the analysis, the overall geometry is separated into two parts. The tapered region is divided into a number of rectangular waveguide sections filled with lossless dielectric material. Change in a dielectric permittivity within each step has been included in the mode matching analysis in the tapered region. The method of moments solution is applied across the radiating horn aperture.

Following the standard mode matching technique [12]-[14] all possible TE and TM modes (both propagating and evanescent) in each section are taken in account and the transverse electric and magnetic fields on both sides of junction are matched. A set of simultaneous matrix equations for each junction is obtained by making use of the orthogonality of waveguide modes and the continuity of the transverse fields through an aperture and zero tangential electric field at conducting walls. The elements of these equations are coupled power integrals of all the propagating and evanescent modes on both sides of the junction. The overall scattering matrix of the horn is determined by cascading the scattering matrices of the involved junctions, iteratively.

It is known that significant mode generation and reflection may occur at the aperture. In accurate design of a horn antenna, the effect of the aperture should be included. In the analysis of a junction of a dielectric loaded horn and free space, it is assumed initially that the horn is placed in an infinite metallic ground plane. To facilitate the analysis, equivalent field distributions are assumed for the interior and exterior regions of the horn antenna, by closing the aperture with a perfectly conducting plate having the same size and shape as that of an aperture and introducing unknown surface magnetic currents on either side of the aperture. Next, the magnetic field boundary conditions are imposed at the aperture and the integral equation is obtained with magnetic surface current distribution as an unknown.

The integral equation is solved numerically via the method of moments [15],[16]. The generalized reflection matrix of an aperture is combined with the generalized scattering matrix of the horn. This procedure yields the complex weighting coefficient of each mode at the horn aperture in terms of the power of the incident TE_{10} mode. Furthermore, the results are used to determine the input reflection coefficient of the antenna and radiation patterns.

In Chapter 3, the performance optimization routine is presented. Both, the loaded and the empty horn antenna dimensions, are optimized independently in respect to the cross-polarization and the aperture efficiency. To excite the higher order modes at the aperture with proper amplitude, a stepped-horn antenna design is introduced. Using appropriate step sizes, the desired amplitude of the modes can be implemented. The length of the uniform waveguide between the step and aperture is optimized in order to achieve in phase relation of the propagating modes at the aperture to yield uniform phase distribution. This is important for improving the aperture efficiency and cross-polarization levels. Loading antenna with dielectric material, without increasing the size, leads to an improvement of the gain characteristics. Introducing the different dielectric material in the tapered section and step section of the horn result in additional parameter to control the input reflection coefficient. The characteristics of a horn antenna loaded with dielectric material are compared with those of an empty horn antenna in Chapter 4. The important result of this comparison is that loading the horn antenna with dielectric material increases the gain for the entire bandwidth. In general, dielectric loading increases the reflection from the aperture, therefore the input reflection coefficient increases, too. However, step dielectric loading allows to keep the input reflection coefficient on the same level as the one of the empty horn antenna or even to reduce it to a smaller value in a narrow frequency band. The results for optimized stepped-horn antennas are presented. As expected, the aperture efficiency, cross-polarization and gain characteristics are improved by optimization. Apart

from improving the gain, dielectric loading enables the reduction of the physical size of the stepped-horn antenna.

CHAPTER 2

MATHEMATICAL MODEL

Typical pyramidal horn antenna geometry is shown in Figure 2.1. Analysis of this radiating structure is done by separating the antenna into two parts. The first part is the tapered section of the horn starting at the feed waveguide and ending at the aperture. This section is modelled by a set of N_I cascaded dielectric loaded uniform waveguide sections as shown in Figure 2.2. The mode matching method is performed to obtain the generalized scattering matrix at each step discontinuity. The overall scattering matrix of the tapered region is then computed by cascading the scattering matrices of the junctions involved in the model.

The second part of the problem is an aperture radiating into the half-space assuming the horn to be terminated by an infinite metallic plane as shown in Figure 2.3. The method of moments is then invoked to determine the generalized reflection matrix of this aperture and then the unknown aperture field distribution.

2.1 Mode Matching

The tapered region of the horn antenna is approximated in terms of N_I rectangular waveguide sections each of length $\Delta l = L/N_I$ filled with dielectric material of permittivity, $\varepsilon_i = \varepsilon_{r_i}\varepsilon_o$, $i = 1, 2, \ldots, N_I$. Each section begins at $z_i = (i-1)\Delta l$ where $z = 0$ corresponds to the junction adjacent to the feed waveguide ($i = 1$), and the aperture plane is located at $z = L$. The cross-sectional dimensions of the $i\text{-}th$ waveguide section, a_i and b_i being the waveguide dimensions in the transverse (x, y) plane, are defined as

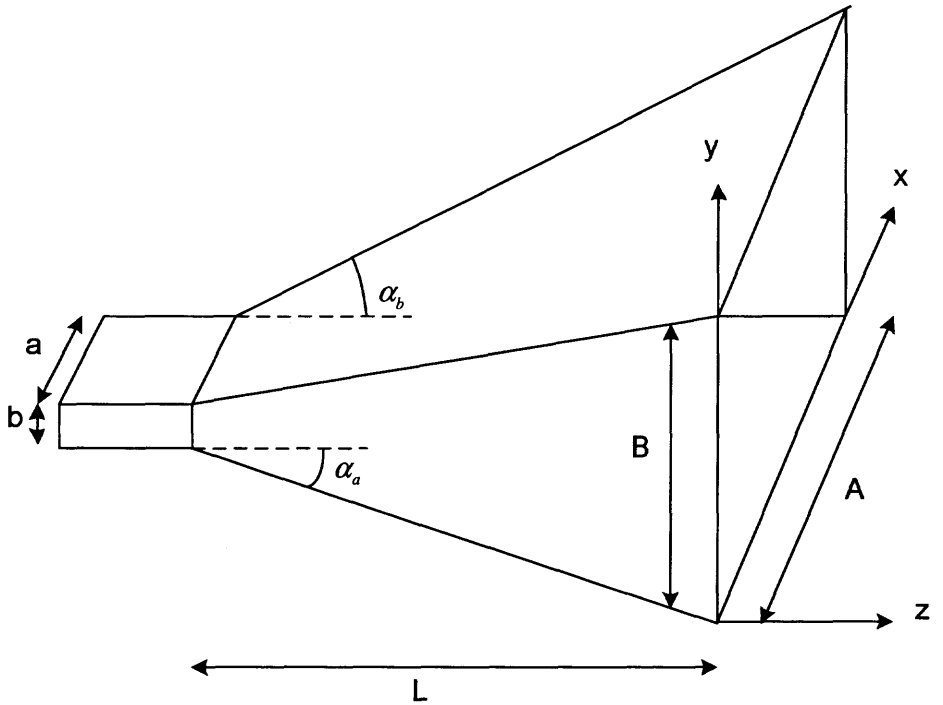

Figure 2.1 Geometry of pyramidal a horn antenna.

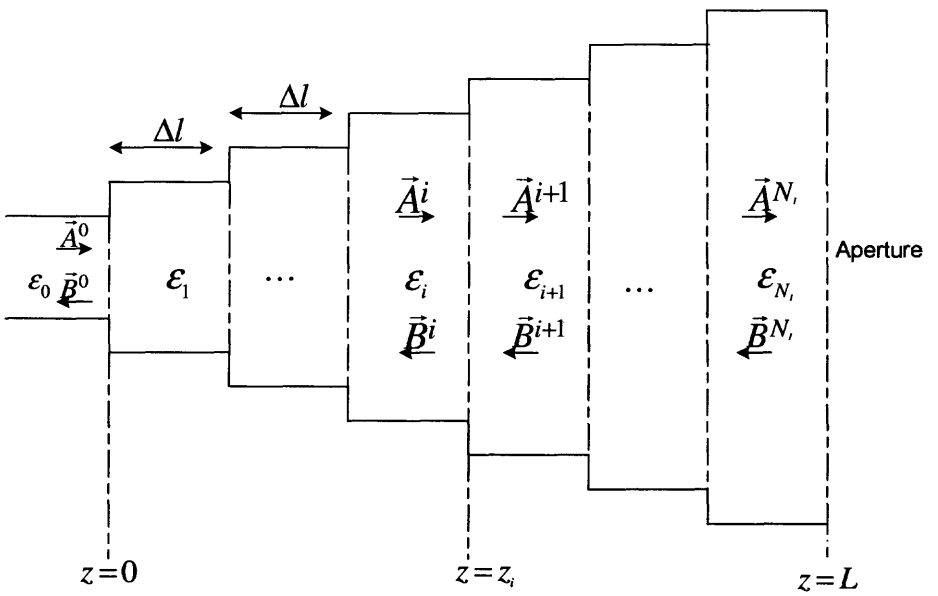

Figure 2.2 Stepped-waveguide model of tapered region of horn antenna.

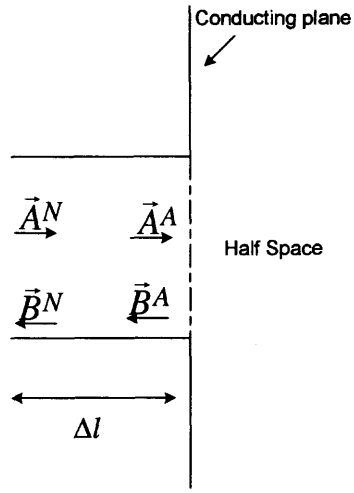

Figure 2.3 Radiating aperture of a horn antenna.

$$a_i = a + 2(i-1)c \tag{2.1}$$
$$b_i = b + 2(i-1)d$$

where c and d are given as

$$c = \Delta l \; tan(\alpha_a) \tag{2.2}$$
$$d = \Delta l \; tan(\alpha_b)$$

and sectoral angles α_a and α_b are given as

$$tan(\alpha_a) = (A-a)/2L \tag{2.3}$$
$$tan(\alpha_b) = (A-b)/2L$$

The presence of an abrupt discontinuity between the i-th and $(i+1)$-th waveguide sections, as shown in Figure 2.4, requires representation of electromagnetic fields in each waveguide sections in terms of the sum of TE and TM modes (propagating and evanescent).

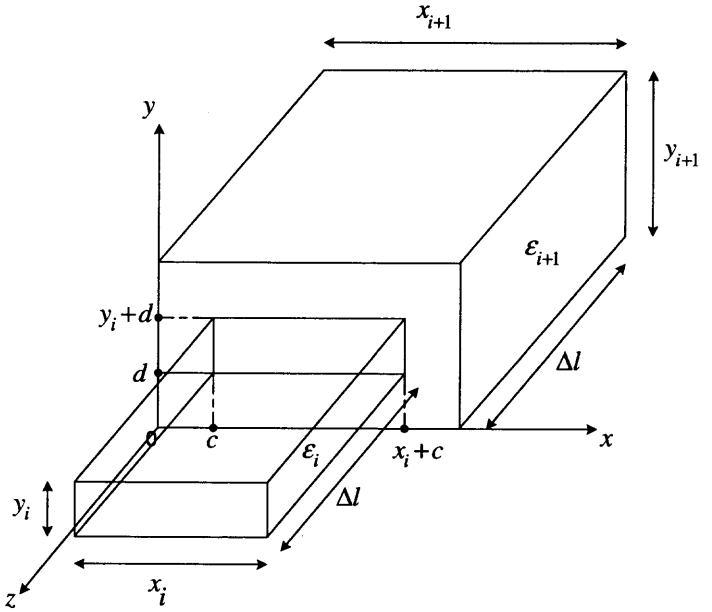

Figure 2.4 Step discontinuity between i-th and $i+1$-th waveguide sections.

TE modes are derived from the axial z-component of the magnetic Hertzian vector potential $\vec{\Pi}_h$ and TM modes are derived from the axial z-component of the electric Hertzian vector potential $\vec{\Pi}_e$. Hence, complete modal field in the i-th waveguide section can be written in form as

$$\begin{aligned} \vec{E}^i &= \nabla \times \vec{\Pi}_h^i + (1/j\omega\varepsilon_i)\nabla \times \nabla \times \vec{\Pi}_e^i \\ \vec{H}^i &= \nabla \times \vec{\Pi}_e^i - (1/j\omega\mu)\nabla \times \nabla \times \vec{\Pi}_h^i \end{aligned} \tag{2.4}$$

Hertzian vector potentials are expressed as sums of the complete set of eigenmodes

$$\begin{aligned} \Pi_{h_z}^i &= \sum_{m,n} \sqrt{Z_{h_{mn}}^i} T_{h_{mn}}^i (a_{h_{mn}}^i e^{-\gamma_{h_{mn}}^i z} + b_{h_{mn}}^i e^{\gamma_{h_{mn}}^i z}) \\ \Pi_{e_z}^i &= \sum_{m,n} \sqrt{Y_{e_{mn}}^i} T_{e_{mn}}^i (a_{e_{mn}}^i e^{-\gamma_{e_{mn}}^i z} + b_{e_{mn}}^i e^{\gamma_{e_{mn}}^i z}) \end{aligned} \tag{2.5}$$

with the wave impedance of TE mode, $Z_{h_{mn}}^i$, and admittance of TM mode, $Y_{e_{mn}}^i$ given by,

$$
\begin{aligned}
Z^i_{h_{mn}} &= j\omega\mu/\gamma^i_{mn} = 1/Y_{h_{mn}} \\
Y^i_{e_{mn}} &= j\omega\varepsilon_i/\gamma^i_{mn} = 1/Z_{e_{mn}}
\end{aligned}
\tag{2.6}
$$

where the propagation constant γ^i_{mn} is expressed as

$$
\begin{aligned}
\gamma^i_{mn} = j\beta^i &= \begin{cases} jk^i\sqrt{1-(k^i_c/k^i)^2} & \textit{propagating modes} \\ k^i\sqrt{(k^i_c/k^i)^2-1} & \textit{evanescent modes} \end{cases} \\
k^i_c &= \sqrt{{k^i_x}^2 + {k^i_y}^2} \\
k^i_x &= m\pi/a_i \qquad k^i_y = n\pi/b_i
\end{aligned}
\tag{2.7}
$$

k^i_c is the cut-off wavenumber of the mn-th mode and $k^i = k_o\sqrt{\varepsilon_i}$ is the wavenumber in the i-th waveguide section. k_o is the free space wavenumber.

$T_{h_{mn}}$ and $T_{e_{mn}}$ are the cross-sectional eigenfunctions for the given boundaries in Figure 2.4

$$
\begin{aligned}
T^i_{h_{mn}} &= 2\cos k^i_x(x-c)\cos k^i_y(y-d)/(N_i\sqrt{1+\delta_{mo}}\sqrt{1+\delta_{on}}\,) \\
T^i_{e_{mn}} &= 2\sin k^i_x(x-c)\sin k^i_y(y-d)/(N_i) \\
T^{i+1}_{h_{mn}} &= 2\cos k^{i+1}_x(x)\cos k^{i+1}_y(y)/(N_{i+1}\sqrt{1+\delta_{mo}}\sqrt{1+\delta_{on}}\,) \\
T^{i+1}_{e_{mn}} &= 2\sin k^{i+1}_x(x)\sin k^i_y(y)/(N_{i+1}) \\
N_i &= \sqrt{a_ib_i}\,k_c
\end{aligned}
\tag{2.8}
$$

where δ_{mn} is the Kronecker delta symbol.

The eigenfunctions are normalized so that for a wave amplitude of unity, the total power carried by the corresponding mode is

$$
\begin{aligned}
S^i_m &= \int_{S^i} (\vec{e}^i_m \times \vec{h^i_m}^*).\vec{z}ds = \sqrt{Z^i_m}\sqrt{Y^{i\,*}_m}\int_{S^i} |\nabla T^i_m|^2 ds \\
&= \begin{cases} 1 & \text{for propagating modes} \\ j & \text{for evanescent TE modes} \\ -j & \text{for evanescent TM modes} \end{cases}
\end{aligned}
\tag{2.9}
$$

From (2.4), the transverse electromagnetic fields are represented in each waveguide section as

$$\begin{aligned}\vec{E}_t^i &= \sum_{m,n} \vec{e}^i_{h_{mn}}(A^i_{h_{mn}} + B^i_{h_{mn}}) + \sum_{m,n} \vec{e}^i_{e_{mn}}(A^i_{e_{mn}} + B^i_{e_{mn}}) \\ \vec{H}_t^i &= \sum_{m,n} \vec{h}^i_{h_{mn}}(A^i_{h_{mn}} - B^i_{h_{mn}}) + \sum_{m,n} \vec{h}^i_{e_{mn}}(A^i_{e_{mn}} - B^i_{e_{mn}})\end{aligned} \tag{2.10}$$

where A^i_{mn} and B^i_{mn} are the complex amplitudes of the incident and reflected waves for the $mn\text{-}th$ mode as

$$A^i_{mn} = a^i_{mn}\, e^{-\gamma^i_{mn} z} \tag{2.11}$$

$$B^i_{mn} = b^i_{mn}\, e^{-\gamma^i_{mn} z} \tag{2.12}$$

Subindices h and e are used to differentiate TE and TM modes, respectively. Mode indices in the summations are $m = 1, 2..., M$ and $n = 0, 1, 2, ..., N$. In the above equations (due to the closed nature of the model), in the $i\text{-}th$ waveguide section, the integers M and N tend to infinity, i.e., $N \to \infty$ and $M \to \infty$. $\vec{e}^i_{h_{mn}}$ and $\vec{h}^i_{h_{mn}}$ are the transverse electric and magnetic fields of the $mn\text{-}th$ TE mode in the $i\text{-}th$ waveguide section and $\vec{e}^i_{e_{mn}}$ and $\vec{h}^i_{e_{mn}}$ are the transverse electric and magnetic fields for the $mn\text{-}th$ TM mode in the $i\text{-}th$ waveguide section

$$\begin{aligned}\vec{e}^i_{h_{mn}} &= \sqrt{Z^i_{h_{mn}}}(\nabla T^i_{h_{mn}} \times \hat{z}) \\ \vec{e}^i_{e_{mn}} &= -\sqrt{Z^i_{e_{mn}}}(\nabla T^i_{e_{mn}}) \\ \vec{h}^i_{h_{mn}} &= \sqrt{Y^i_{h_{mn}}}(\nabla T^i_{h_{mn}}) \\ \vec{h}^i_{e_{mn}} &= \sqrt{Y^i_{e_{mn}}}(\nabla T^i_{e_{mn}} \times \hat{z})\end{aligned} \tag{2.13}$$

At the overlapping aperture regions over the junction, the boundary conditions impose the continuity of the tangential electric and magnetic fields and on non-overlapping region over the larger cross-section, the tangential electric field is assumed to be equal to zero.

The boundary conditions relating the two adjacent waveguides are

$$\vec{E}_t^{i+1} = \begin{cases} \vec{E}_t^i \ on \ S^i \\ 0 \ \ on \ (S^{i+1} - S^i) \end{cases} \tag{2.14}$$

for the electric field, and

$$\vec{H}_t^{i+1} = \vec{H}_t^i \ on \ S^i \tag{2.15}$$

for the magnetic field. In above equations, S^i is the cross-section area of the smaller waveguide section and S^{i+1} is the cross-section area of complimentary larger waveguide section. Mode matching of the tangential electric and magnetic fields at the junction and using the orthogonality property of TE and TM modes [17] yields a matrix equation for the mode amplitude vector for the larger guide in terms of the mode amplitude vector of the smaller waveguide section. Then combined mode-matching with generalized scattering matrix representation, the scattering matrix corresponding to $i\text{-}th$ junction between two neighboring dielectric-loaded waveguides is shown to be equal to

$$\begin{bmatrix} B^i \\ A^{i+1} \end{bmatrix} = \begin{bmatrix} S_{11}^i \ S_{12}^i \\ S_{21}^i \ S_{22}^i \end{bmatrix} \begin{bmatrix} A^i \\ B^{i+1} \end{bmatrix} \tag{2.16}$$

where A^i, A^{i+1} are incident waves and B^i, B^{i+1} are reflected waves represented by the column matrices containing amplitudes of the modes in the $i\text{-}th$ and $(i+1)\text{-}th$ waveguide sections, respectively.

2.2 Generalized Scattering Matrix

Matching the transverse electric and magnetic fields due to imposing the boundary conditions, at the common interface of general waveguide step discontinuity leads to the set of following equations for the electric field

$$\sum_{k=1}^{N_{TE}} \vec{e}^{\,i}_{h_k}(A^i_{h_k} + B^i_{h_k}) + \sum_{k=1}^{N_{TM}} \vec{e}^{\,i}_{e_k}(A^i_{e_k} + B^i_{e_k}) = \sum_{l=1}^{N_{TE}} \vec{e}^{\,i+1}_{h_l}(A^{i+1}_{h_l} + B^{i+1}_{h_l}) + \sum_{l=1}^{N_{TM}} \vec{e}^{\,i+1}_{e_l}(A^{i+1}_{e_l} + B^{i+1}_{e_l}) \qquad (2.17)$$

and for the magnetic field

$$\sum_{k=1}^{N_{TE}} \vec{h}^{\,i}_{h_k}(A^i_{h_k} - B^i_{h_k}) + \sum_{k=1}^{N_{TM}} \vec{h}^{\,i}_{e_k}(A^i_{e_k} - B^i_{e_k}) = \sum_{l=1}^{N_{TE}} \vec{h}^{\,i+1}_{h_l}(A^{i+1}_{h_l} - B^{i+1}_{h_l}) + \sum_{l=1}^{N_{TM}} \vec{h}^{\,i+1}_{e_l}(A^{i+1}_{e_l} - B^{i+1}_{e_l}) \qquad (2.18)$$

In the summation, N_{TE} is the total number of TE modes and N_{TM} is the total number of TM modes. Total number of modes N_T is the sum of N_{TE} and N_{TM}. Here, to reduce the complexity in the notation, in (2.17) and (2.18), $i\text{-}th$ waveguide mode numbers mn are replaced by k and $(i+1)\text{-}th$ waveguide mode numbers mn are replaced by l.

To determine the unknown coefficients, the equation system in (2.17) and (2.18) has to be multiplied by testing functions. The proper choice for the testing functions for enforcing the electric field continuity are the transverse magnetic fields of the larger waveguide and for enforcing the magnetic field continuity are the transverse electric fields of the smaller waveguide [18]. Multiplying each side of the electric field in continuity equation (2.17) by $h^{i+1^*}_{h_l}$ and $h^{i+1^*}_{e_l}$ and integrating over the waveguide cross-section S^i, results in

$$\sum_{k=1}^{N_{TE}} (A^i_{h_k} + B^i_{h_k}) \int_{S^i} (\vec{e}^{\,i}_{h_k} \times \vec{h}^{\,i+1^*}_{h_l})\hat{z}.ds + \sum_{k=1}^{N_{TM}} (A^i_{e_k} + B^i_{e_k}) \int_{S^i} (\vec{e}^{\,i}_{e_k} \times \vec{h}^{\,i+1^*}_{h_l})\hat{z}.ds = \sum_{l=1}^{N_{TE}} (A^{i+1}_{h_l} + B^{i+1}_{h_l}) \int_{S^i} (\vec{e}^{\,i+1}_{h_l} \times \vec{h}^{\,i+1^*}_{h_l})\hat{z}.ds + \sum_{l=1}^{N_{TM}} (A^{i+1}_{e_l} + B^{i+1}_{e_l}) \int_{S^i} (\vec{e}^{\,i+1}_{e_l} \times \vec{h}^{\,i+1^*}_{h_l})\hat{z}.ds \qquad (2.19)$$

$$\sum_{k=1}^{N_{TE}} (A_{h_k}^i + B_{h_k}^i) \int_{S^i} (\vec{e}_{h_k}^i \times \vec{h}_{e_l}^{i+1^*}) \hat{z}.ds + \sum_{k=1}^{N_{TM}} (A_{e_k}^i + B_{e_k}^i) \int_{S^i} (\vec{e}_{e_k}^i \times \vec{h}_{e_l}^{i+1^*}) \hat{z}.ds =$$
$$\sum_{l=1}^{N_{TE}} (A_{h_l}^{i+1} + B_{h_l}^{i+1}) \int_{S^i} (\vec{e}_{h_l}^{i+1} \times \vec{h}_{e_l}^{i+1^*}) \hat{z}.ds + \sum_{l=1}^{N_{TM}} (A_{e_l}^{i+1} + B_{e_l}^{i+1}) \int_{S^i} (\vec{e}_{e_l}^{i+1} \times \vec{h}_{e_l}^{i+1^*}) \hat{z}.ds \tag{2.20}$$

Multiplying each side of magnetic field in equation (2.18) by $e_{h_k}^i$ and $e_{e_k}^i$ and integrating over the waveguide cross-section leads to

$$\sum_{k=1}^{N_{TE}} (A_{h_k}^{i^*} - B_{h_k}^{i^*}) \int_{S^i} (\vec{e}_{h_k}^i \times \vec{h}_{h_k}^{i^*}) \hat{z}.ds + \sum_{k=1}^{N_{TM}} (A_{e_k}^{i^*} - B_{e_k}^{i^*}) \int_{S^i} (\vec{e}_{h_k}^i \times \vec{h}_{e_k}^{i^*}) \hat{z}.ds =$$
$$\sum_{l=1}^{N_{TE}} (A_{h_l}^{i+1^*} - B_{h_l}^{i+1^*}) \int_{S^i} (\vec{e}_{h_k}^i \times \vec{h}_{h_l}^{i+1^*}) \hat{z}.ds + \sum_{l=1}^{N_{TM}} (A_{e_l}^{i+1^*} - B_{e_l}^{i+1^*}) \int_{S^i} (\vec{e}_{h_k}^i \times \vec{h}_{e_l}^{i+1^*}) \hat{z}.ds \tag{2.21}$$

and

$$\sum_{k=1}^{N_{TE}} (A_{h_k}^{i^*} - B_{h_k}^{i^*}) \int_{S^i} (\vec{e}_{e_k}^i \times \vec{h}_{h_k}^{i^*}) \hat{z}.ds + \sum_{k=1}^{N_{TM}} (A_{e_k}^{i^*} - B_{e_k}^{i^*}) \int_{S^i} (\vec{e}_{e_k}^i \times \vec{h}_{e_k}^{i^*}) \hat{z}.ds =$$
$$\sum_{l=1}^{N_{TE}} (A_{h_l}^{i+1^*} - B_{h_l}^{i+1^*}) \int_{S^i} (\vec{e}_{e_k}^i \times \vec{h}_{h_l}^{i+1^*}) \hat{z}.ds + \sum_{l=1}^{N_{TM}} (A_{e_l}^{i+1^*} - B_{e_l}^{i+1^*}) \int_{S^i} (\vec{e}_{e_k}^i \times \vec{h}_{e_l}^{i+1^*}) \hat{z}.ds \tag{2.22}$$

In the $i\text{-}th$ waveguide with perfectly conducting walls, $k\text{-}th$ TE mode and $l\text{-}th$ TM mode are satisfied the following orthogonality properties,

$$\begin{aligned} \int_{S^i} (\vec{e}_{h_k}^i \times \vec{h}_{e_l}^{i^*}) \hat{z}.ds &= 0 \\ \int_{S^i} (\vec{e}_{h_k}^i \times \vec{h}_{h_l}^{i^*}) \hat{z}.ds &= \delta_{kl} \\ \int_{S^i} (\vec{e}_{e_k}^i \times \vec{h}_{e_l}^{i^*}) \hat{z}.ds &= \delta_{kl} \end{aligned} \tag{2.23}$$

Using these orthogonality relations, equation system (2.19)-(2.22) can be rewritten as

$$
\begin{aligned}
A^i_{h_k} - B^i_{h_k} &= \sum_{l=1}^{N_{TE}} (A^{i+1}_{h_l} - B^{i+1}_{h_l}) V^*_{hh_{kl}} + \sum_{l=1}^{N_{TM}} (A^{i+1}_{e_l} - B^{i+1}_{e_l}) V^*_{eh_{kl}} \\
A^i_{e_k} - B^i_{e_k} &= \sum_{l=1}^{N_{TM}} (A^{i+1}_{e_l} - B^{i+1}_{e_l}) V^*_{ee_{kl}} \\
\sum_{k=1}^{N_{TE}} (A^i_{h_k} + B^i_{h_k}) V_{hh_{kl}} &= A^{i+1}_{h_l} + B^{i+1}_{h_l} \\
\sum_{k=1}^{N_{TE}} (A^i_{h_k} + B^i_{h_k}) V_{eh_{kl}} + \sum_{k=1}^{N_{TM}} (A^i_{e_k} + B^i_{e_k}) V_{ee_{kl}} &= A^{i+1}_{e_l} + B^{i+1}_{e_l}
\end{aligned}
\tag{2.24}
$$

where $*$ shows complex conjugate. In equation system (2.24), V_{hh}, V_{eh} and V_{ee} represent the TE to TE, TE to TM and TM to TM mode coupling coefficients, which are evaluated repectively, as

$$
\begin{aligned}
V_{hh_{kl}} &= \int_{S^i} (\vec{e}^{\,i}_{h_k} \times \vec{h}^{\,i+1^*}_{h_l}) \hat{z}.ds \\
V_{eh_{kl}} &= \int_{S^i} (\vec{e}^{\,i}_{h_k} \times \vec{h}^{\,i+1^*}_{e_l}) \hat{z}.ds \\
V_{ee_{kl}} &= \int_{S^i} (\vec{e}^{\,i}_{e_k} \times \vec{h}^{\,i+1^*}_{e_l}) \hat{z}.ds
\end{aligned}
\tag{2.25}
$$

At each junction between two waveguide sections power is coupled between the different modes on either side of the junction, including evanescent modes. This coupling is evaluated by integrating the fields over the surface. These coupling integrals have been evaluated analytically in closed form to reduce the compuational burden. Furthermore, it is assumed that TE waves are coupled with the TM waves; TM waves are not coupled with TE waves ($V_{he} = 0$). This effect is rigorously taken into account in (2.24). The equation system in (2.24) can be expressed in matrix form as

$$
\underbrace{\begin{bmatrix} I_{TE} & 0 & V^*_{hh} & V^*_{eh} \\ 0 & I_{TM} & 0 & V^*_{ee} \\ V_{hh} & 0 & -I_{TE} & 0 \\ V_{eh} & V_{ee} & 0 & -I_{TM} \end{bmatrix}}_{K_2}
\begin{bmatrix} B^i_h \\ B^i_e \\ A^{i+1}_h \\ A^{i+1}_e \end{bmatrix}
=
\underbrace{\begin{bmatrix} I_{TE} & 0 & V^*_{hh} & V^*_{eh} \\ 0 & I_{TM} & 0 & V^*_{ee} \\ -V_{hh} & 0 & I_{TE} & 0 \\ -V_{eh} & -V_{ee} & 0 & I_{TM} \end{bmatrix}}_{K_1}
\begin{bmatrix} A^i_h \\ A^i_e \\ B^{i+1}_h \\ B^{i+1}_e \end{bmatrix}
\tag{2.26}
$$

where I_{TE} and I_{TM} are unit matrices of the size $N_{TE} \times N_{TE}$ and $N_{TM} \times N_{TM}$, respectively.

K_2 and K_1 can be simplified as

$$K_2 = \begin{bmatrix} I & P^* \\ P & -I \end{bmatrix} \tag{2.27}$$

$$K_1 = \begin{bmatrix} I & P^* \\ -P & I \end{bmatrix} \tag{2.28}$$

where I is unit matrix of the size $N_T \times N_T$, P is coupling matrix of the same size $N_T \times N_T$. N_T is the sum of the number of TE modes, N_{TE} and TM modes, N_{TM} in the waveguide. Then, the scattering matrix of the $i\text{-}th$ step discontinuity is obtained as

$$S^i = \begin{bmatrix} S^i_{11} & S^i_{12} \\ S^i_{21} & S^i_{22} \end{bmatrix} = K_2^{-1} \cdot K_1 \tag{2.29}$$

Elements of scattering matrix of the junction can be expressed as

$$\begin{aligned} S^i_{11} &= (I + P^*P)^{-1}(I - P^*P) \\ S^i_{12} &= 2(I + P^*P)^{-1}(P^*) \\ S^i_{21} &= 2(I + P^*P)^{-1}(P) \\ S^i_{22} &= -(I + P^*P)^{-1}(I - PP^*) \end{aligned} \tag{2.30}$$

Once the scattering matrices of the discontinuities are known, the overall scattering matrix of the tapered section S^T is obtained by cascading the generalized scattering matrices corresponding to the discontinuities between the waveguide sections. Overall scattering matrix relates the field in the feed waveguide to the radiating aperture field. The scattering matrices of two adjacent discontinuities are expressed by S^i and S^{i+1}, respectively. They are combined into one overall scattering matrix S^T using the following equations,

$$
\begin{aligned}
S_{11}^T &= S_{11}^i + S_{12}^i F D S_{11}^{i+1} D S_{21}^i \\
S_{12}^T &= S_{12}^i F D S_{12}^{i+1} \\
S_{21}^T &= S_{21}^{i+1} D E S_{21}^i \\
S_{22}^T &= S_{22}^{i+1} + S_{21}^{i+1} D E S_{22}^i D S_{12}^{i+1}
\end{aligned}
\tag{2.31}
$$

where

$$
\begin{aligned}
E &= (I - S_{22}^i D S_{11}^{i+1} D)^{-1} \\
F &= (I - D S_{22}^i D S_{11}^{i+1})^{-1}
\end{aligned}
\tag{2.32}
$$

where D is a diagonal matrix of the size $N_T \times N_T$ whose diagonal elements are given as

$$
D_{jj} = e^{-\gamma_j \Delta l} \tag{2.33}
$$

due to the uniform waveguide sections of length Δl between the steps. The process is repeated iteratively to include all discontinuities into an equivalent taper representation in terms of the input and output ports. The input port corresponds to the feed waveguide while the output port is the radiating aperture of the horn antenna. This permits us to determine the incident fields at the aperture in terms of the complex amplitudes of the modes exciting the horn.

In order to preserve numerical accuracy, the direct combination of the involved scattering matrices at all step discontinuities of the total tapered section are used as opposed to the common treatment by transmission matrices. Although analytically more extensive, such as a need to take the inverse of $2N_T \times 2N_T$ matrix twice, this technique leads to matrix elements only containing exponential functions with negative argument, [13] where evanescent modes decrease relatively quickly with distance between adjacent discontinuities. This direct combination of scattering matrices avoids numerical instabilities caused by the otherwise known situation of interacting discontinuities. There are two important factors which affect the accuracy of the stepped-waveguide aproximation: the size of the step,

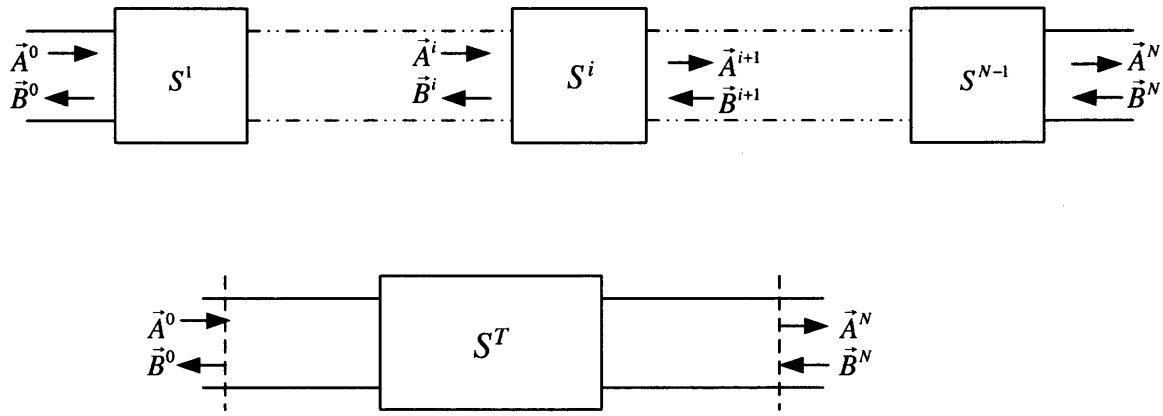

Figure 2.5 Scattering matrix representation of cascaded discontinuities.

Δl, and the number of modes in the expansion, N_T. The number of sections along the horn antenna must be chosen so that the pyramidal tapered section is accurately modeled and modes excited by the artificial steps do not influence the radiating aperture fields. It is important to notice that the elements of the generalized scattering matrix $[S]$ are in the form of infinite series summations. In reality, the series must be truncated with finite number of terms. Selecting the number of terms is very critical from convergence point of view. A simple formula derived for determining M and N for convergence [11], is the nearest higher integer of

$$(M, N) = 3(A, B)/\lambda + 1.5 \tag{2.34}$$

where A and B are the dimensions of the horn aperture.

2.3 Method of Moments

The generalized reflection matrix S_{11}^A of the aperture as shown in Figure 2.6, is formulated by incorporating the mismatch between the aperture section of the horn antenna and the free space.

The approximation of the horn aperture terminated by an infinite ground plane is based on negligible effect of the induced current on the horn metallic walls. For practical

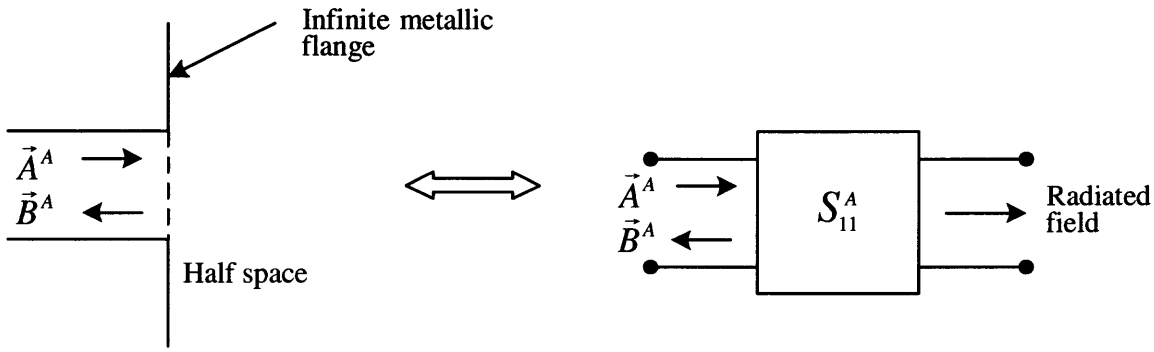

Figure 2.6 Generalized reflection matrix representation of an aperture.

horn sizes the contributions of the outside wall currents to the input reflection coefficient are negligibly small and can be ignored to avoid the complexity of formulation and numerical evaluations.

The equivalence principle is used on the radiating aperture by dividing the original problem into two decoupled parts as waveguide region and half-space region, as shown in Figure 2.7. This is accomplished by closing the aperture with a perfect electric conductor and placing sheets of equivalent magnetic current density. By the equivalence principle, the electromagnetic fields in both regions remain unchanged if the aperture is closed by a conductor, a sheet of magnetic current $\vec{M}$ is placed on the inner side of the aperture and a sheet of $-\vec{M}$ is placed on the outer region. Magnetic current density is given by

$$\vec{M} = \hat{n} \times \vec{E}^A \tag{2.35}$$

In (2.35), $\hat{n}$ is the unit normal vector pointing into free space and $\vec{E}^A$ is the unknown electric field on the aperture plane of the original problem.

Equivalent magnetic current sheet in waveguide is $+\vec{M}$ and that in half-space is $-\vec{M}$ ensures that the tangential component of electric field is continuous across the aperture of the original problem. The other boundary condition is the continuity of the tangential component of the magnetic field across the aperture which is

$$\vec{H}_t^{wg}\Big|_{Aper.} = \vec{H}_t^{hs}(-\vec{M})\Big|_{Aper.} \tag{2.36}$$

where $\vec{H}_t^{wg}$ is the tangential component of the magnetic field in the waveguide over the

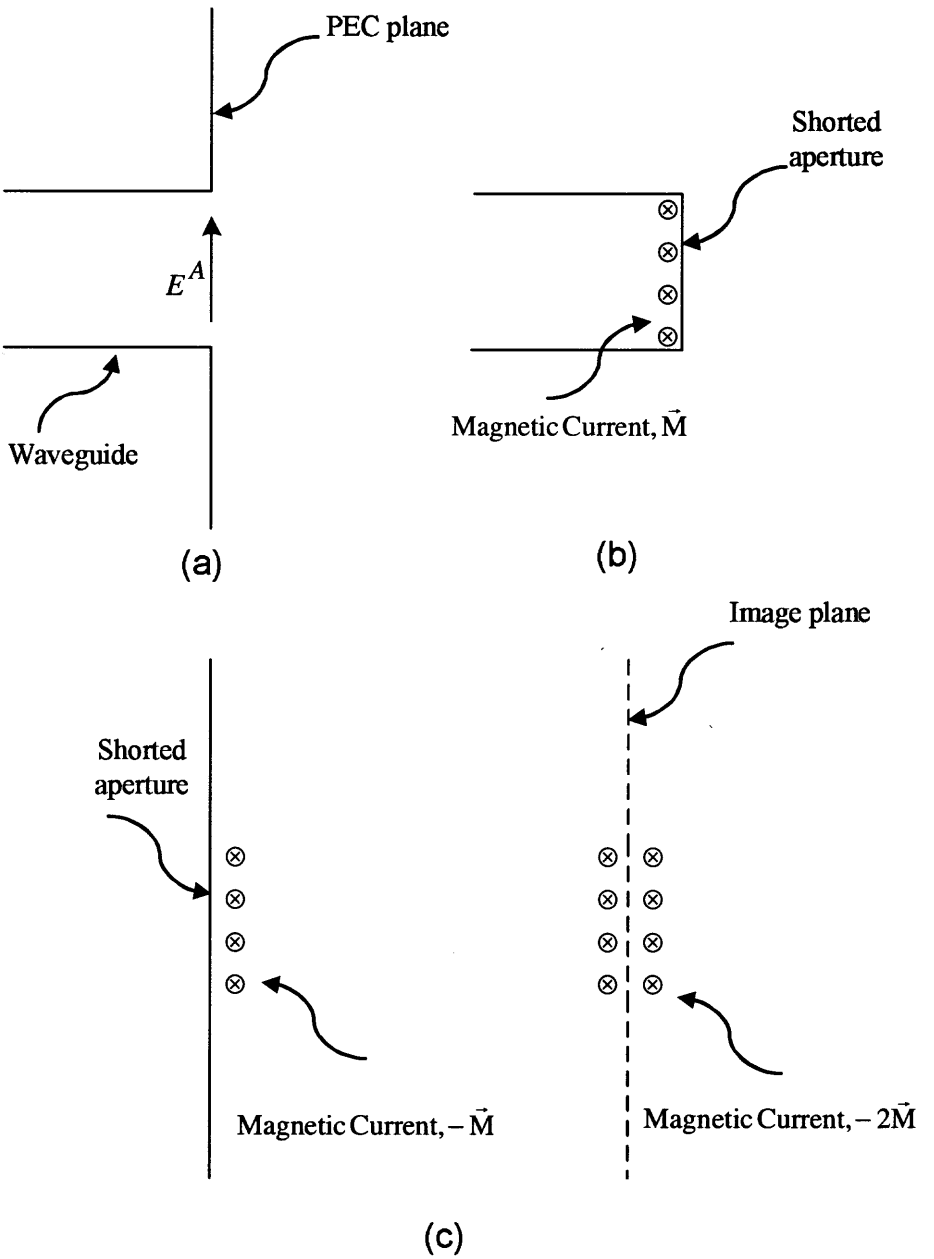

Figure 2.7 (a) Original problem (b) Equivalent problem (valid only in waveguide section) (c) Equivalent problem (valid only in half space section).

aperture region and $\vec{H}_t^{hs}$ is the magnetic field in the half-space. The expression for the magnetic field in the half space $\vec{H}_t^{hs}$ is constructed by means of the electric vector potential and magnetic scalar potential ensuring that Maxwell's equations and the radiation condition are satisfied. Since magnetic field is linearly dependent on the magnetic current density, it can be written as $\vec{H}_t^{hs}(-\vec{M}) = -\vec{H}_t^{hs}(\vec{M})$. $\vec{H}_t^{wg}$ is the superposition of that due to impressed field due to modal fields in the waveguide region radiating in the presence of the closed aperture, $\vec{H}_t^{imp}$, and that due to the equivalent current, denoted as $\vec{H}_t^{wg}(\vec{M})$

$$\vec{H}_t^{wg} = \vec{H}_t^{imp} + \vec{H}_t^{wg}(\vec{M}) \tag{2.37}$$

If (2.36) is rewritten using (2.37)

$$\vec{H}_t^{wg}(\vec{M}) + \vec{H}_t^{imp} = -\vec{H}_t^{hs}(\vec{M}) \tag{2.38}$$

To apply the method of moments, the unknown magnetic current density $\vec{M}$ is expanded in terms of a set of linearly independent basis functions, M_n

$$\vec{M} = \sum_{n=1}^{N_M} V_n \vec{M}_n \tag{2.39}$$

where V_n are unknown expansion coefficients. Here, N_M is the number of unknown coefficients V_n to be determined by using the subdomain basis function. Substituting (2.39) into (2.38) leads to

$$\sum_{n=1}^{N_M} V_n \vec{H}_t^{wg}(\vec{M}_n) + \sum_{n=1}^{N_M} V_n \vec{H}_t^{hs}(\vec{M}_n) = -\vec{H}_t^{i} \tag{2.40}$$

Enforcement of the continuity equation of magnetic fields by linearly independent testing functions W_m leads to the set of linear equations system. Solution of this system of linear equations determines the set of unknown coefficients V_n, leading to determination of $\vec{M}$. Linear equations system obtained from (2.40) can be written in a matrix form as

$$[Y^{wg} + Y^{hs}]\,\vec{V} = \vec{I}^{i} \tag{2.41}$$

where Y^{wg} is the admittance matrix for waveguide region and its size is $N_M \times N_M$, with elements defined as

$$Y_{mn}^{wg} = \int\int_{Aper.} \vec{H}_t^{wg}(M_n) \cdot \vec{W}_m ds \tag{2.42}$$

and Y^{hs} is the admittance matrix for half-space region and its size is $N_M \times N_M$ and its elements are

$$Y_{mn}^{hs} = \int\int_{Aper.} \vec{H}_t^{hs}(M_n) \cdot \vec{W}_m ds \tag{2.43}$$

and $\vec{I}_m^i$ is an excitation vector with size $N_M \times 1$. Its elements are

$$\vec{I}_m^i = \int\int_{Aper.} \vec{H}_t^i \cdot \vec{W}_m ds \tag{2.44}$$

In the method of moments solution, the aperture is subdivided into L_x and L_y segments in the x and y directions, respectively, resulting in patches of size $\Delta x \Delta y$. Two orthogonally polarized sets of overlapping rooftop basis functions $\vec{M}_n^x$ and $\vec{M}_n^y$ are used to model the magnetic surface currents across the aperture (2.39), as shown in Figure 2.8. The total number of expansion functions is $N_M = (L_x - 1)L_y + (L_y - 1)L_x$.The set of x directed magnetic current basis functions $\vec{M}_n^x$ and the set of y directed magnetic current basis function $\vec{M}_n^y$ are defined by

$$\begin{aligned} \vec{M}_{n_x}^{x} = \hat{x}\, T_p^x(x) P_q^y(y), \qquad & n_x = p + (q-1)(L_x - 1) \\ & p = 1, 2, \ldots, L_x - 1, \\ & q = 1, 2, \ldots, L_y \end{aligned} \tag{2.45}$$

$$\begin{aligned} \vec{M}_{n_y}^{y} = \hat{y}\, T_q^y(y) P_p^x(x), \qquad & n_y = p + (q-1)L_x \\ & p = 1, 2, \ldots, L_x, \\ & q = 1, 2, \ldots, L_y - 1 \end{aligned} \tag{2.46}$$

where $T_p^x(x)$ and $T_q^y(y)$ are triangular functions defined by

$$T_p^x(x) = \begin{cases} \frac{x-(p-1)\Delta x}{\Delta x}, & (p-1)\Delta x \le x \le p\Delta x \\ \frac{(p+1)\Delta x - x}{\Delta x}, & p\Delta x \le x \le (p+1)\Delta x \\ 0, & |x - p\Delta x| \ge \Delta x \end{cases} \tag{2.47}$$

$$T_q^y(y) = \begin{cases} \frac{y-(q-1)\Delta y}{\Delta y}, & (q-1)\Delta y \le y \le q\Delta y \\ \frac{(q+1)\Delta y - y}{\Delta y}, & q\Delta y \le y \le (q+1)\Delta y \\ 0, & |y - q\Delta y| \ge \Delta y \end{cases} \tag{2.48}$$

and $P_p^x(x)$ and $P_q^y(y)$ are pulse functions defined by

$$P_p^x(x) = \begin{cases} 1, & (p-1)\Delta x \le x \le p\Delta x \\ 0, & elsewhere \end{cases} \tag{2.49}$$

$$P_q^y(y) = \begin{cases} 1, & (q-1)\Delta y \le y \le q\Delta y \\ 0, & elsewhere \end{cases} \tag{2.50}$$

In the original problem, unknown aperture fields can be expressed as a sum of all possible modes, including evanescent modes

$$\vec{E}^A = \sum_k^{N_{TE}} \vec{e}_{h_k}^A (A_{h_k}^A + B_{h_k}^A) + \sum_k^{N_{TM}} \vec{e}_{e_k}^A (A_{e_k}^A + B_{e_k}^A) \tag{2.51}$$

$$\vec{H}^A = \sum_k^{N_{TE}} \vec{h}_{h_k}^A (A_{h_k}^A - B_{h_k}^A) + \sum_k^{N_{TM}} \vec{h}_{e_k}^A (A_{e_k}^A - B_{e_k}^A) \tag{2.52}$$

where $\vec{e}_{h_k}^A$, $\vec{e}_{e_k}^A$ and $\vec{h}_{h_k}^A$, $\vec{h}_{e_k}^A$ are the transverse electric and magnetic fields for the $k\text{-}th$ TE and $k\text{-}th$ TM mode across the aperture. $A_{h_k}^A$ and $A_{e_k}^A$ are the complex amplitudes of incident $k\text{-}th$ mode to the aperture and $B_{h_k}^A$ and $B_{e_k}^A$ are the complex amplitudes of reflected $k\text{-}th$ mode from the aperture. Same as in mode matching method calculation, indices h and e represent TE and TM modes, respectively.

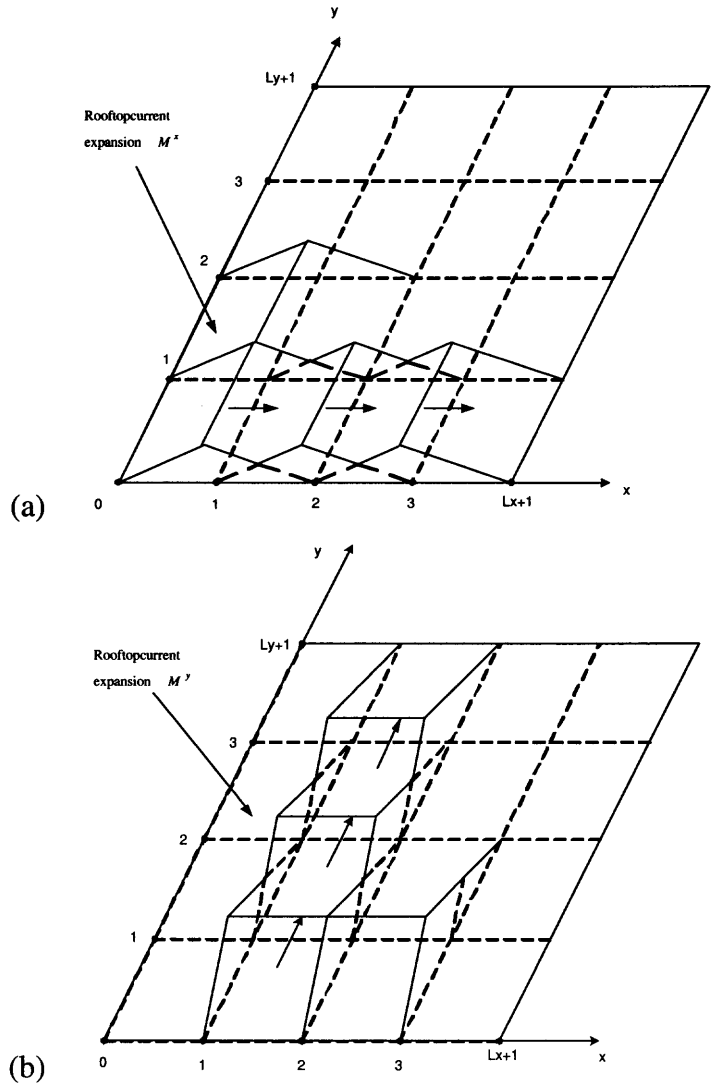

Figure 2.8 Rooftop expansion function for M^x and M^y.

To evaluate elements of the aperture admittance for the waveguide region, Y_{mn}^{wg}, a single expansion function $\vec{M}_n$ is considered on the aperture plane in the waveguide region. The tangential field produced by $\vec{M}_n$ will be of the same form as (2.51) and (2.52) except only reflected waves are present on the aperture. Therefore, the fields are decomposed into corresponding TE and TM parts as,

$$\vec{E}_t^{wg}(\vec{M}_n) = \sum_k^{N_{TE}} \vec{e}_{h_k}^A \Gamma_{h_{nk}}^{wg} + \sum_k^{N_{TM}} \vec{e}_{e_k}^A \Gamma_{e_{nk}}^{wg} \tag{2.53}$$

$$\vec{H}_t^{wg}(\vec{M}_n) = -\sum_k^{N_{TE}} \vec{h}_{h_k}^A \Gamma_{h_{nk}}^{wg} - \sum_k^{N_{TM}} \vec{h}_{e_k}^A \Gamma_{e_{nk}}^{wg} \tag{2.54}$$

where $\Gamma^{wg}_{h_{nk}}$ and $\Gamma^{wg}_{e_{nk}}$ are the complex modal amplitudes of the k-th reflected mode produced by M_n, for TE and TM modes, respectively.

Using (2.35) and (2.51), a single element of the magnetic current density on the aperture plane is expressed as,

$$\vec{M}_n\Big|_{Aper.} = \sum_{k}^{N_{TE}} (\hat{n} \times \vec{e}^{A}_{h_k})\Gamma^{wg}_{h_{nk}} + \sum_{k}^{N_{TM}} (\hat{n} \times \vec{e}^{A}_{e_k})\Gamma^{wg}_{e_{nk}}\Big|_{Aper.} \tag{2.55}$$

Multiplying each side of (2.55) by $(\hat{n} \times \vec{e}_{h_l})$ and $(\hat{n} \times \vec{e}_{e_l})$ and integrating over the aperture cross section and from orthogonality, all terms in the summation are zero except $k = l$ term, leads to

$$\Gamma^{wg}_{h_{nk}} = \int\int_{Aper.} Y_{h_k} (\hat{n} \times \vec{e}^{A}_{h_k})\vec{M}_n ds \tag{2.56}$$

$$\Gamma^{wg}_{e_{nk}} = \int\int_{Aper.} Y_{e_k} (\hat{n} \times \vec{e}^{A}_{e_k})\vec{M}_n ds \tag{2.57}$$

Admittance matrix of waveguide region Y^{wg}_{mn} (2.42)is then expressed as

$$Y^{wg}_{mn} = \sum_{k}^{N_{TE}} \Gamma^{wg}_{h_{nk}} \int\int_{Aper.} \vec{W}_m Y_h (\hat{n} \times \vec{e}^{A}_{h_k}) + \sum_{k}^{N_{TM}} \Gamma^{wg}_{e_{nk}} \int\int_{Aper.} \vec{W}_m Y_e (\hat{n} \times \vec{e}^{A}_{e_k}) \tag{2.58}$$

If testing function is chosen as the same as expansion function (also called Galerkin method), $\vec{W}_m = \vec{M}_n$, aperture admittance can be expressed as

$$Y^{wg}_{mn} = \sum_{k}^{N_{TE}} \Gamma^{wg}_{h_{nk}} \Gamma^{wg}_{h_{mk}} + \sum_{k}^{N_{TM}} \Gamma^{wg}_{e_{nk}} \Gamma^{wg}_{e_{mk}} \tag{2.59}$$

Utilizing the image theory, the tangential magnetic field of incident wave on the conducting surface that replaces the aperture is twice of the tangential component of the incident magnetic field

$$\vec{H}_t^i = 2\{\sum_k^{N_{TE}} \vec{h}_{h_k}^A A_{h_k}^A + \sum_k^{N_{TM}} \vec{h}_{e_k}^A A_{e_k}^A\} \tag{2.60}$$

Therefore, using (2.60), the components of the excitation vector can be expressed as

$$\begin{aligned} \vec{I}_m^i &= 2\{\sum_k^{N_{TE}} A_{h_k}^A \int\int_{Aper.} \vec{W}_m Y_h (\vec{n} \times \vec{e}_{h_k}^A) - \sum_k^{N_{TM}} A_{e_k}^A \int\int_{Aper.} \vec{W}_m Y_e (\vec{n} \times \vec{e}_{e_k}^A)\} \\ \vec{I}_m^i &= 2\{\sum_k^{N_T} A_{h_k}^A \Gamma_{h_{mk}}^{wg} + \sum_k^{N_T} A_{e_k}^A \Gamma_{e_{mk}}^{wg}\} \end{aligned} \tag{2.61}$$

From (2.41), coefficient vector $\vec{V}$ can be expressed as

$$\vec{V} = (Y^{wg} + Y^{hs})^{-1} \vec{I}^i \tag{2.62}$$

Incident vector in the matrix form is given as

$$\vec{I}^i = 2 \begin{bmatrix} \Gamma_h^{wg} \\ \Gamma_e^{wg} \end{bmatrix} \begin{bmatrix} A_h^A \\ A_e^A \end{bmatrix} \tag{2.63}$$

Since, magnetic current distribution on aperture is known in terms of the modal amplitudes of incident field A^A, one can calculate the reflection matrix of the aperture. Magnetic current density on the aperture plane is expressed by using (2.35)

$$\vec{M}\Big|_{Aper.} = \sum_k^{N_{TE}} (\hat{n} \times \vec{e}_{h_k}^A)(A_{h_k}^A + B_{h_k}^A) + \sum_k^{N_{TM}} (\hat{n} \times \vec{e}_{e_k}^A)(A_{e_k}^A + B_{e_k}^A)\Big|_{Aper.} \tag{2.64}$$

Substitution of (2.39) into (2.64) yields

$$\sum_{n=1}^{N_M} V_n \vec{M}_n = \sum_k^{N_{TE}} (\hat{n} \times \vec{e}_{h_k}^A)(A_{h_k}^A + B_{h_k}^A) + \sum_k^{N_{TM}} (\hat{n} \times \vec{e}_{e_k}^A)(A_{e_k}^A + B_{e_k}^A)\Big|_{Aper.} \tag{2.65}$$

To determine the unknown coefficients V_n, multiply each side of (2.65) by $\vec{h}_{h_l}$ and $\vec{h}_{e_l}$ and integrate over the waveguide cross section, resulting in

$$\sum_{n=1}^{N_M} V_n \Gamma^{wg}_{h_{nk}} = (A^A_{h_k} + B^A_{h_k}) \tag{2.66}$$

$$\sum_{n=1}^{N_M} V_n \Gamma^{wg}_{e_{nk}} = (A^A_{e_k} + B^A_{e_k}) \tag{2.67}$$

Using equations (2.67), (2.62) in the matrix format, leads to

$$\begin{bmatrix} A^A_h \\ A^A_e \end{bmatrix}_{N_T \times 1} + \begin{bmatrix} B^A_h \\ B^A_e \end{bmatrix}_{N_T \times 1} = \begin{bmatrix} \Gamma^{wg}_h \\ \Gamma^{wg}_e \end{bmatrix}_{N_T \times N_M} [V]_{N_M \times 1} \tag{2.68}$$

$$[V]_{N_M \times 1} = (Y^{wg} + Y^{hs})^{-1} 2 \begin{bmatrix} \Gamma^{wg}_h \\ \Gamma^{wg}_e \end{bmatrix} \begin{bmatrix} A^A_h \\ A^A_e \end{bmatrix} \tag{2.69}$$

Since $B^A = S^A_{11} A^A$, one can express B^A as a function of A^A in (2.68),

$$[I + S^A_{11}] \begin{bmatrix} A^A_h \\ A^A_e \end{bmatrix}_{N_T \times 1} = \begin{bmatrix} \Gamma^{wg}_h \\ \Gamma^{wg}_e \end{bmatrix}_{N_T \times N_M} [Y^{wg} + Y^{hs}]^{-1} 2 \begin{bmatrix} \Gamma^{wg}_h \\ \Gamma^{wg}_e \end{bmatrix} \begin{bmatrix} A^A_h \\ A^A_e \end{bmatrix} \tag{2.70}$$

From (2.70), the reflection matrix of aperture S^A_{11} can be written as

$$[S^A_{11}] = 2 \begin{bmatrix} \Gamma^{wg}_h \\ \Gamma^{wg}_e \end{bmatrix} [Y^{wg} + Y^{hs}]^{-1} \begin{bmatrix} \Gamma^{wg}_h \\ \Gamma^{wg}_e \end{bmatrix} - I \tag{2.71}$$

where I is a unit matrix of size $N_T \times N_T$. The tapered section and the aperture are connected through a uniform waveguide section of length Δl, as shown in Figure 2.3.

In the previous section, the generalized scattering matrix, S^T, of the tapered section and diagonal matrix of last uniform waveguide section of the horn antenna were presented using mode matching technique. Combining S^T and D with S^A_{11}, the amplitudes of the incident and reflected modes in the aperture A^A and B^A, and the reflected modes at the

input of the horn B^0 are obtained for any incident field A^0 using following formulas

$$\begin{aligned} B^0 &= [S_{11}^T + (S_{21}^T D S_{11}^A)(I - D S_{22}^T D S_{11}^A)^{-1} D S_{21}^T] A^0 \\ A^A &= [(I - D S_{22}^T D S_{11}^A)^{-1} D S_{21}^T] A^0 \\ B^A &= S_{11}^A A^A \end{aligned} \tag{2.72}$$

Equation (2.72) uniquely determines the aperture field. Since we know the aperture fields, exact solution of magnetic current distributions on the aperture can be found using either (2.62) or (2.64). Antenna characteristics then can be calculated using the equivalent magnetic current density.

2.4 Half-Space Admittance

The expressions for the magnetic field are constructed by means of the electric vector potential and magnetic scalar potential which ensures that Maxwell's equations and the radiation condition are satistified. Also, image theory is invoked, thereby causing the field expressions to satisfy the boundary conditions on the screen. Half-space magnetic field can be obtained from

$$\vec{H}_t^{hs}(\vec{M}) = -j\omega\vec{F} - \nabla\Phi \tag{2.73}$$

If we expand the x and y components of the magnetic field,

$$H_x^{hs} = -j\omega F_x - \frac{\partial \Phi}{\partial x} \tag{2.74}$$

$$H_y^{hs} = -j\omega F_y - \frac{\partial \Phi}{\partial y} \tag{2.75}$$

An electric vector potential $\vec{F}$ and magnetic scalar potential Φ are given by,

$$\vec{F} = \varepsilon_o \iint \vec{M} \frac{e^{-jk_o|\vec{r}-\vec{r}'|}}{4\pi|\vec{r}-\vec{r}'|} ds'$$
$$\Phi(r) = \frac{1}{\mu} \iint \rho \frac{e^{-jk_o|\vec{r}-\vec{r}'|}}{4\pi|\vec{r}-\vec{r}'|} ds' \tag{2.76}$$

where $\vec{r}$ and $\vec{r}'$ are respectively the vectors to the field and source points on the aperture, ω is the angular frequency, ε_o is the electric permittivity of the free space.

Using (2.43), the admittance of half-space region isexpressed as,

$$Y_{mn}^{hs} = \iint_{Aper} \vec{W}_m \cdot (j\omega \vec{F}_n + \nabla \Phi_n) ds. \tag{2.77}$$

If we expand the x and the y components of the electric vector potential and substitute magnetic current expansion (2.39) in (2.76),

$$F_x = \sum_{q=1}^{Ly} \sum_{p=1}^{Lx-1} V_{n_x} \iint_{Aper} M_{n_x}(\vec{r}') \frac{e^{-jk_o|\vec{r}-\vec{r}'|}}{4\pi|\vec{r}-\vec{r}'|} dx'dy' \tag{2.78}$$

$$F_y = \sum_{q=1}^{Ly-1} \sum_{p=1}^{Lx} V_{n_y} \iint_{Aper} M_{n_y}(\vec{r}') \frac{e^{-jk_o|\vec{r}-\vec{r}'|}}{4\pi|\vec{r}-\vec{r}'|} dx'dy' \tag{2.79}$$

where

$$n_x = p + (q-1)(Lx-1)$$
$$n_y = p + (q-1)Lx \tag{2.80}$$

The magnetic charge and current are related through the continuity equation as

$$-j\omega\rho = \nabla \cdot \vec{M} = \frac{\partial M_x}{\partial x} + \frac{\partial M_y}{\partial y} \tag{2.81}$$

Finite difference approximations can be applied to take derivatives in the continuity equation (2.81). This approximation produces

$$\rho = \sum_{q=1}^{Ly}\sum_{p=1}^{Lx-1} V_{n_x}\frac{(P_p^x(x) - P_{p+1}^x(x))P_q^y(y)}{-j\omega\Delta x} + \sum_{q=1}^{Ly-1}\sum_{p=1}^{Lx} V_{n_y}\frac{(P_q^y(y) - P_{q+1}^y(y))P_p^x(x)}{-j\omega\Delta y} \tag{2.82}$$

Using (2.82), scalar magnetic potential Φ will be expressed in the following form as,

$$\begin{aligned}\Phi(r) = \frac{j}{4\pi\mu\omega}\Bigg\{ &\sum_{q=1}^{Ly}\sum_{p=1}^{Lx-1} V_{n_x}\frac{1}{dx}\{\int_{x_{p-1}y_{q-1}}^{x_p y_q} G(\vec{r},\vec{r}')\,dx'dy' - \int_{x_p\ y_{q-1}}^{x_{p+1} y_q} G(\vec{r},\vec{r}')\,dx'dy'\} \\ &\sum_{q=1}^{Ly-1}\sum_{p=1}^{Lx} V_{n_y}\frac{1}{dy}\{\int_{x_{p-1}y_{q-1}}^{x_p y_q} G(\vec{r},\vec{r}')\,dx'dy' - \int_{x_{p-1}\ y_q}^{x_p y_{q+1}} G(\vec{r},\vec{r}')\,dx'dy'\}\Bigg\}\end{aligned} \tag{2.83}$$

where $G(\vec{r},\vec{r}^{\,'})$ is the free space Green function given by

$$G(\vec{r},\vec{r}^{\,'}) = \frac{e^{-jk_o|\vec{r}-\vec{r}^{\,'}|}}{4\,\pi|\vec{r}-\vec{r}^{\,'}|} \tag{2.84}$$

Testing function, W_m is chosen same as the expansion function, $W_m = M_n$

$$\iint_{Aper} H_x.W_{m_x}dx\,dy = j\omega\int_{x_{s-1}}^{x_{s+1}}\int_{y_{t-1}}^{y_t} F_x.W_{m_x}dx\,dy + \int_{x_{s-1}}^{x_{s+1}}\int_{y_{t-1}}^{y_t}\frac{\partial\Phi}{\partial x}.W_{m_x}dx\,dy \tag{2.85}$$

$$\iint_{Aper} H_y.W_{m_y}dx\,dy = j\,\omega\int_{x_{s-1}}^{x_s}\int_{y_{t-1}}^{y_{t+1}} F_y.W_{m_y}dx\,dy + \int_{x_{s-1}}^{x_s}\int_{y_{t-1}}^{y_{t+1}}\frac{\partial\Phi}{\partial y}.W_{m_y}dx\,dy \tag{2.86}$$

where

$$\begin{aligned} m_x &= s + (t-1)(Lx-1) \\ m_y &= s + (t-1)Lx \end{aligned} \tag{2.87}$$

Using midpoint rule to evaluate integrals over the electric vector potential and magnetic scalar potential results in

$$\begin{aligned}\int\int_{Aper} H_x.W_{m_x}dx\,dy &= j\,\omega\,\Delta x\Delta y\{1/2\,F_x(x_{s-1/2},y_{t-1/2})+1/2\,F_x(x_{s+1/2},y_{t-1/2})\}\\ &\quad +\Delta y\{\Phi(x_{s+1/2},y_{t-1/2})-\Phi(x_{s-1/2},y_{t-1/2})\} \qquad (2.88)\\ \int\int_{Aper} H_y.W_{m_y}dx\,dy &= j\omega\,\Delta x\Delta y\{1/2\,F_y(x_{s-1/2},y_{t-1/2})+1/2\,F_y(x_{s-1/2},y_{t+1/2})\}\\ &\quad +\Delta x\{\Phi(x_{s-1/2},y_{t+1/2})-\Phi(x_{s-1/2},y_{t-1/2})\} \qquad (2.89)\end{aligned}$$

If we rewrite (2.89), using (2.79), (2.79), (2.83) bla

$$\begin{aligned}&\int\int_{Aper} H_x.W_{m_x}dx\,dy =\\ &j\omega\,\Delta x\Delta y\left\{\frac{\varepsilon_o}{8\,\pi}\sum_{q=1}^{Ly}\sum_{p=1}^{Lx-1}V_{n_x}\{\int_{x_{p-1}y_{q-1}}^{x_{p+1}\,y_q}M_{n_x}(\vec{r}\,')G(x_{s-1/2},y_{t-1/2},\vec{r}\,')\,dx'dy'\right.\\ &\left.+\int_{x_{p-1}y_{q-1}}^{x_{p+1}\,y_q}M_{n_x}(\vec{r}\,')G(x_{s+1/2},y_{t-1/2},\vec{r}\,')\,dx'dy'\}\right\}\\ &-\Delta y\left\{\frac{j}{4\pi\mu\omega}\{\sum_{q=1}^{Ly}\sum_{p=1}^{Lx-1}V_{n_x}\frac{1}{\Delta x}\{\int_{x_{p-1}y_{q-1}}^{x_p\,y_q}G(x_{s+1/2},y_{t-1/2},\vec{r}\,')\,dx'dy'\right.\\ &-\int_{x_p\,y_{q-1}}^{x_{p+1}\,y_q}G(x_{s+1/2},y_{t-1/2},\vec{r}\,')\,dx'dy'\}-\int_{x_{p-1}y_{q-1}}^{x_p\,y_q}G(x_{s-1/2},y_{t-1/2},\vec{r}\,')\,dx'dy'\\ &+\int_{x_p\,y_{q-1}}^{x_{p+1}\,y_q}G(x_{s-1/2},y_{t-1/2},\vec{r}\,')\,dx'dy'\}+\{\sum_{q=1}^{Ly-1}\sum_{p=1}^{Lx}V_{n_y}\frac{1}{\Delta y}\{\int_{x_{p-1}y_{q-1}}^{x_p\,y_q}G(x_{s+1/2},y_{t-1/2},\vec{r}\,')\,dx'dy'\\ &-\int_{x_{p-1}\,y_q}^{x_p\,y_{q+1}}G(x_{s+1/2},y_{t-1/2},\vec{r}\,')\,dx'dy'\}-\int_{x_{p-1}y_{q-1}}^{x_p\,y_q}G(x_{s-1/2},y_{t-1/2},\vec{r}\,')\,dx'dy'\\ &\left.+\int_{x_{p-1}\,y_q}^{x_p\,y_{q+1}}G(x_{s-1/2},y_{t-1/2},\vec{r}\,')\,dx'dy'\}\right\} \qquad (2.90)\end{aligned}$$

Similiar procedure applied to H_y, results in

$$\iint\limits_{Aper} H_y.W_{m_y}dx\,dy =$$

$$j\omega\,\Delta x\Delta y\left\{\frac{\varepsilon_o}{8\,\pi}\sum_{q=1}^{Ly-1}\sum_{p=1}^{Lx}V_{n_y}\{\int\limits_{x_{p-1}y_{q-1}}^{x_p\ y_{q+1}}M_{n_y}(r')G(x_{s-1/2},y_{t-1/2},\vec{r}')\,dx'dy'\right.$$

$$\left.+\int\limits_{x_{p-1}y_{q-1}}^{x_p\ y_{q+1}}M_{n_y}(\vec{r}')G(x_{s-1/2},y_{t+1/2},\vec{r}')\,dx'dy'\}\right\}$$

$$-\Delta x\left\{\frac{j}{4\pi\mu\omega}\{\sum_{q=1}^{Ly}\sum_{p=1}^{Lx-1}V_{n_x}\frac{1}{\Delta x}\{\int\limits_{x_{p-1}y_{q-1}}^{x_p\ y_q}G(x_{s-1/2},y_{t+1/2},\vec{r}')\,dx'dy'\right.$$

$$-\int\limits_{x_p\ y_{q-1}}^{x_{p+1}\ y_q}G(x_{s-1/2},y_{t+1/2},\vec{r}')\,dx'dy'\}-\int\limits_{x_{p-1}y_{q-1}}^{x_p\ y_q}G(x_{s-1/2},y_{t-1/2},\vec{r}')\,dx'dy'$$

$$+\int\limits_{x_p\ y_{q-1}}^{x_{p+1}\ y_q}G(x_{s-1/2},y_{t-1/2},\vec{r}')\,dx'dy'\}$$

$$+\{\sum_{q=1}^{Ly-1}\sum_{p=1}^{Lx}V_{n_y}\frac{1}{\Delta y}\{\int\limits_{x_{p-1}y_{q-1}}^{x_p\ y_q}G(x_{s-1/2},y_{t+1/2},\vec{r}')\,dx'dy'$$

$$-\int\limits_{x_{p-1}\ y_q}^{x_p\ y_{q+1}}G(x_{s-1/2},y_{t+1/2},\vec{r}')\,dx'dy'\}-\int\limits_{x_{p-1}y_{q-1}}^{x_p\ y_q}G(x_{s-1/2},y_{t-1/2},\vec{r}')\,dx'dy'$$

$$\left.+\int\limits_{x_{p-1}\ y_q}^{x_p\ y_{q+1}}G(x_{s-1/2},y_{t-1/2},\vec{r}')\,dx'dy'\}\right\} \tag{2.91}$$

If one can arrange (2.90) and (2.91)

$$\begin{aligned}\iint\limits_{Aper} H_x.W_{m_x}dx\,dy &= \sum_{q=1}^{Ly}\sum_{p=1}^{Lx-1}V_{n_x}Y_{m_xn_x}+\sum_{q=1}^{Ly-1}\sum_{p=1}^{Lx}V_{n_y}Y_{m_xn_y}\\ \iint\limits_{Aper} H_y.W_{m_y}dx\,dy &= \sum_{q=1}^{Ly-1}\sum_{p=1}^{Lx}V_{n_y}Y_{m_yn_y}+\sum_{q=1}^{Ly}\sum_{p=1}^{Lx-1}V_{n_x}Y_{m_yn_x}\end{aligned} \tag{2.92}$$

where

$$Y_{m_x n_x} =$$
$$\frac{j\Delta x\Delta y}{\pi\mu}[\frac{1}{2}I_g(s-p,t-q) - \frac{1}{2}I_x(s-p+1,t+q) + \frac{(s-p+3/2)}{2}I_g(s-p+1,t-q)$$
$$+ \frac{1}{2}I_x(s-p-1,t-q) - \frac{(s-p-3/2)}{2}I_g(s-p-1,t-q)$$
$$+ \frac{1}{{k_o}^2\Delta x^2}(I_g(s-p+1,t-q) - 2I_g(s-p,t-q) + I_g(s-p-1,t-q)] \quad (2.93)$$

$$Y_{m_x n_y} =$$
$$\frac{j}{\pi\eta_o {k_o}^2}[-I_g(s-p,t-q) + I_g(s-p+1,t-q)$$
$$I_g(s-p,t-q-1) - I_g(s-p+1,t-q-1)] \quad (2.94)$$

$$Y_{m_y n_x} =$$
$$\frac{j}{\pi\eta_o {k_o}^2}[-I_g(s-p,t-q) + I_g(s-p,t-q+1)$$
$$I_g(s-p-1,t-q) - I_g(s-p-1,t-q+1)] \quad (2.95)$$

$$Y_{m_y n_y} =$$
$$\frac{j\Delta x\Delta y}{\pi\mu}[\frac{1}{2}I_g(s-p,t-q) - \frac{1}{2}I_y(s-p,t+q+1) + \frac{(t-q+3/2)}{2}I_g(s-p,t-q+1)$$
$$+ \frac{1}{2}I_y(s-p,t-q-1) - (t-q-3/2)/2I_g(s-p,t-q-1)$$
$$+ 1/{k_o}^2\Delta y^2(I_g(s-p,t-q+1) - 2I_g(s-p,t-q) + I_g(s-p,t-q-1)] \quad (2.96)$$

Green function integrals, I_g, I_x, I_y, are evaluated using Taylor expansions as shown in the APPENDIX.

2.5 Antenna Characteristics

Antenna characteristics are determined based on the solution for the magnetic current density across the aperture and the aperture field coefficients. Far field pattern computation is done using electric vector potential with the knowledge of magnetic current density across the aperture.

The input reflection matrix at the feed waveguide including the aperture discontinuity is given by

$$S_{11} = S_{11}^T + (S_{21}^T D^N S_{11}^A)(I - D^N S_{22}^T D^N S_{11}^A)^{-1} D^N S_{21}^T \tag{2.97}$$

Reflection coefficient due to the incident TE_{10} mode is defined as

$$\Gamma = S_{11}(1,1) \tag{2.98}$$

The radiation intensity in normalized form is calculated using far field components of electric field as following

$$U(\theta,\phi) = |E_\theta(\theta,\phi)|^2 + |E_\phi(\theta,\phi)|^2 \tag{2.99}$$

Gain is defined as

$$G(\theta,\phi) = \frac{4\pi U(\theta,\phi)}{P_{in}} \tag{2.100}$$

where P_{in} is the incident power at the input section of the horn.

The directive gain of the antenna is

$$D(\theta,\phi) = \frac{4\pi U(\theta,\phi)}{P_{rad}} \tag{2.101}$$

where P_{rad} is radiated power. The aperture efficiency is a figure-of-merit which indicates how efficiently the physical area of the antenna is utilized. The aperture efficieny is a function of many factors. Among them is the most prominent parameters are the amplitude

taper and the phase distribution across the aperture. Aperture efficiency, ϵ_{ap} is defined as

$$\epsilon_{ap} = \frac{\lambda^2}{4\pi}\frac{D_o}{A} \tag{2.102}$$

where A is the physical area of the aperture and D_o is the directivitiy.

The maximum radiation intensity (U_{max}) occurs at $\theta = 0$, therefore directivity of the aperture

$$D_o = \frac{4\pi U_{max}}{P_{rad}} \tag{2.103}$$

The cross-polar radiation characteristics are dependent on the difference between the E- and H- plane patterns. The co- and cross-polarization pattern components $E_{co}(\theta, \phi)$ and $E_{cross}(\theta, \phi)$ are given by the relations, with a definition of cross-polarization based on ' *Ludwig's third definition*' [19],

$$\begin{bmatrix} E_{co}(\theta,\phi) \\ E_{cross}(\theta,\phi) \end{bmatrix} = \begin{bmatrix} sin(\phi) & cos(\phi) \\ cos(\phi) & -sin(\phi) \end{bmatrix} \begin{bmatrix} E_\theta \\ E_\phi \end{bmatrix} \tag{2.104}$$

CHAPTER 3

PERFORMANCE OPTIMIZATION

The optimization objective is to reduce cross-polarization and improve aperture efficiency characteristics of a horn antenna. Figure 3.1 shows the proposed stepped-horn antenna configurations subjected to optimization. Stepped-horn antenna consists of three major sections:

- Tapered region of length L_1,
- Symmetrical step on the horn wall,
- Uniform waveguide region of length L_2 between step and the aperture.

The cross-polarization characteristics depend on the difference between the $E-$ and $H-$ plane patterns. If identical $E-$ and $H-$ plane aperture field distributions can be realized, it would result in minimized cross-polarization level. Aperture efficiency is a measure how efficiently the physical area of the aperture is utilized. Since gain linearly depends on the aperture efficiency, improving the aperture efficiency implies an increase in gain, too. Aperture efficiency is mainly a function of the aperture field amplitude taper and phase distributions. Maximum efficiency can be achieved by excitation of uniform amplitude and phase distribution over the aperture. Therefore, if identical uniform field distributions along the E- and H- plane can be implemented, both cross-polarization level and aperture efficiency characteristics can be improved simultaneoulsy. For uniform aperture field distribution across the aperture, TM modes should not be present and also TE_{mn} modes where $n \neq 0$ should not be exited. TE_{m0} modes should have an approximate amplitude relation of $1/m$ to satisfy the uniform aperture field distributions as

$$TE_{10} : TE_{30} : TE_{50} \ldots = 1 : \frac{1}{3} : \frac{1}{5} \ldots \tag{3.1}$$

Even though, TE_{10} mode is an incident wave at the feed waveguide, higher order modes are generated along the horn taper. The amplitude and phase of these induced modes depend on the size of the aperture and flare angle of the antenna. But amplitude of higher order modes usually remain small compared to a dominant mode if flare angle is not so large. To excite the higher order modes in desired amplitude levels as given in (3.1), there should be proper adjustment in the size of the symmetrical step on the horn wall. Since symmetrical H-plane step is used in this study, only $TE_{m0}, m = 1, 3, 5...$ modes are excited at the step and $TE_{mn}, n \neq 0$ and TM_{mn} modes are not excited. The step should be located at the horn wall where its cross-section size should be about $\frac{m}{2}\lambda$ to allow the higher order TE_{m0} mode to propagate.

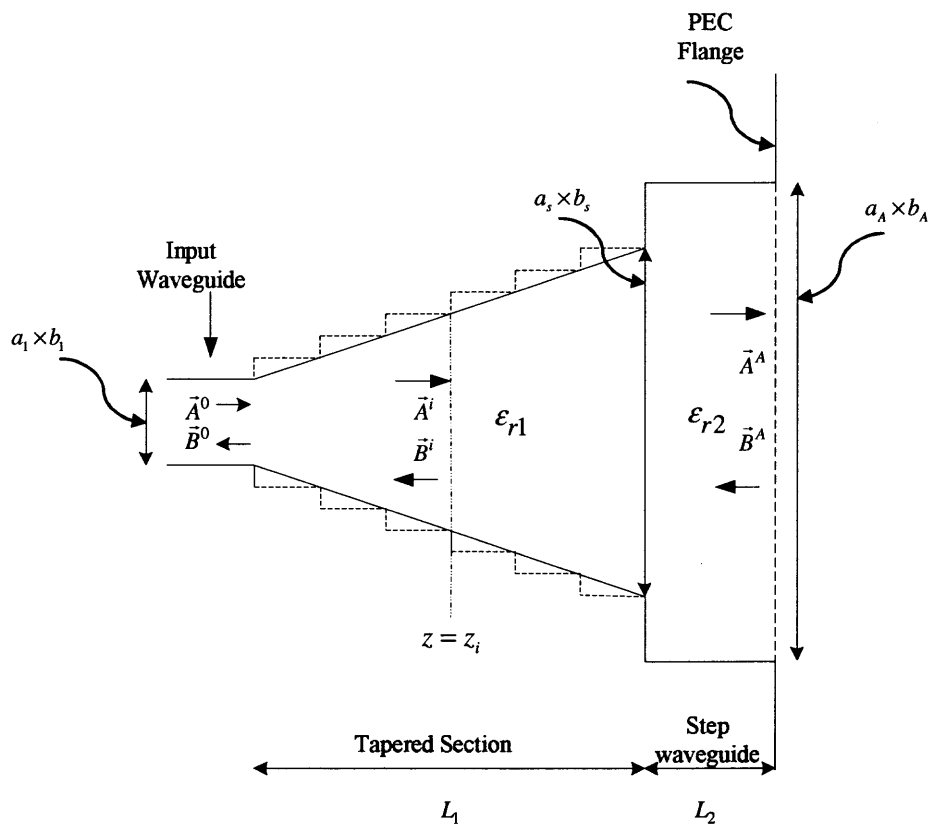

Figure 3.1 Stepped-horn antenna with variable dielectric loading for excitation of TE_{30} mode at the aperture with $1/3$ amplitude ratio of TE_{10} mode

It should be mentioned that even though the step does not excite $TE_{mn}, n \neq 0$ and TM modes, they might be still present at the aperture if the size of aperture is large enough to support these modes, because of reflection from aperture and the presence of the tapered section of the horn antenna.

The H-plane step dimension for TE_{n0} mode excitation is determined as a function of the step ratio, α, which is defined as $\alpha = a_s/a_A$. a_s is the vertical dimension of the last section of the tapered region and a_A is the vertical dimension of the step waveguide adjacent to the aperture as shown in Figure 3.1. Using continuity of the electromagnetic fields across the aperture of step, the coupling integral of TE_{m0} mode with unit amplitude in the smaller waveguide, last section of the tapered part, to TE_{n0} mode amplitude in step waveguide is evaluated analytically as a function of α, ε_{r1} and ε_{r2} as

$$|A_{mn}| = \sqrt{\frac{Z_{h_{m0}}}{Z_{h_{n0}}}}\sqrt{\frac{b_s}{b_A}}\frac{\sqrt{\alpha}}{(m^2 - n^2\alpha^2)\pi} sin(n\pi(\frac{1-\alpha}{2})) \tag{3.2}$$

where b_s is the y-dimension of the smaller waveguide, and b_A is the y-dimension of the step-waveguide. Since in this study of H-plane step, only x dimension is changed symmetrically, $b_s = b_A$. $Z_{h_{n0}}$ is the wave impedance of the TE_{n0}-th mode in the step waveguide (aperture) and $Z_{h_{m0}}$ is the wave impedance of the TE_{m0}-th mode at the smaller waveguide (tapered section) as

$$Z_{h_{j0}} = \frac{k_o Z_o}{\sqrt{k^2 - k_{c_j}^2}} \tag{3.3}$$

where $j = m, n$ and k is the wave number in the step waveguide as $k = k_o\sqrt{\varepsilon_{r1}}$ for smaller waveguide, $j = n$, and $k = k_o\sqrt{\varepsilon_{r2}}$ for step waveguide, $j = m$. k_0 is the free space wavenumber. $k_{c_{j0}}$ is the cut-off wavenumber of the TE_{j0}-th mode.

The formula given above is valid for all TE_{n0} mode excitations from the incident TE_{m0} mode. In this study, only TE_{30} mode optimization is considered. The goal is to

satisfy the amplitude ratio of $1/3$ for TE_{30} mode to TE_{10} mode at the aperture. Here, it is assumed that aperture size is large enough so that the TE_{30} mode propagates and only TE_{10} mode is incident to the step waveguide. To evaluate the ratio of the amplitude of TE_{30} to TE_{10} mode, the coupling coefficient from TE_{10} to TE_{10} mode and TE_{10} to TE_{30} mode across the step discontinuity was evaluated analytically. Then, the ratio of this coupling coefficient is determined as

$$\frac{|A_{30}|}{|A_{10}|} = \sqrt{\frac{Z_{h_{10}}}{Z_{h_{30}}}} \frac{1-\alpha^2}{1-9\alpha^2} \frac{sin(3\pi\frac{1-\alpha}{2})}{sin(\pi\frac{1-\alpha}{2})} \tag{3.4}$$

By equating this ratio to $1/3$, (3.4) is solved numerically to obtain step ratio α. Since aperture size, a_A is known, step size can be calculated by $\alpha = a_s/a_A$. Figure 3.2 shows the relation of sizes a_s and a_A in wavelength to excite the amplitude of TE_{30} mode in ratio $1/3$ of amplitude of TE_{10} mode. Figure 3.2 depicts typical relation between a_s and a_A, independent from dielectric constant of the smaller waveguide. Also notice that, even though coupling coefficient depends on the dielectric constant of both smaller and step waveguide, when the ratio of the coupling coeffients is taken, $Z_{h_{10}}$ which is a function of ε_{r1} will not be used anymore. Hence, smaller waveguide dielectric constant does not affect the ratio of the mode amplitudes. As a summary, smaller waveguide dielectric constant changes the amplitude of the aperture modes but does not affect their ratio.

Length of stepped-waveguide section, L_2, is used to adjust TE_{10} and TE_{30} modes in phase relation at the aperture which is important for reducing cross-polarization level and increasing the aperture efficiency. Input reflection coefficient significantly affected by reflection from the aperture and the reflection from the flare cross-section at the input waveguide to. Here, the length of the tapered section, L_1 is used to minimize the input reflection coefficient by making the aperture reflection coefficient and the feed-flare section reflection contributions to yield coefficient out of phase realtions. The phase of each mode

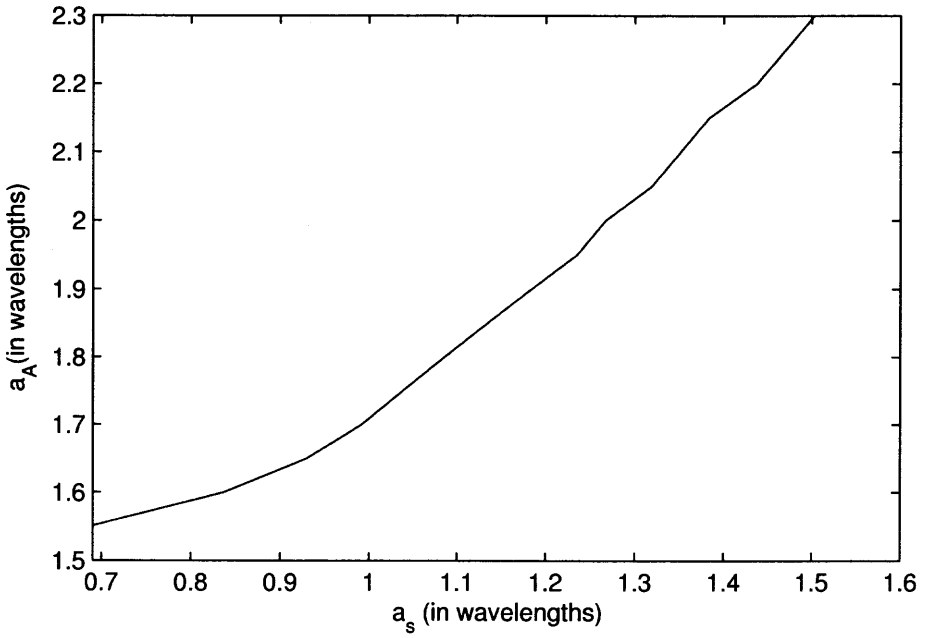

Figure 3.2 a_s and a_A width of H -plane step for TE_{30} mode amplitude in the ratio $1/3$ to the TE_{10} mode excitation.

along the tapered section can be determined by

$$\begin{aligned} \Phi^{mn} &= \frac{2\pi}{\lambda}\int_0^{L_1} \beta_{mn}(z)dz \\ \Phi^{mn} &= \frac{2\pi}{\lambda}\int_0^{L_1} (1-\frac{\lambda^2}{4}((\frac{m}{a(z)})^2+(\frac{n}{b(z)})^2)^{1/2}dz \end{aligned} \tag{3.5}$$

where β_{mn} is phase change coefficient of the TE_{mn} mode, L_1 is the length of the tapered section, $\lambda = \lambda_o/\sqrt{\varepsilon_{r1}}$ is the wavelength. The physical dimensions, $a(z)$ and $b(z)$ are

$$\begin{aligned} a(z) &= \frac{a_s - a1}{L_1}z + a_1 \\ b(z) &= \frac{b_s - b1}{L_1}z + b_1 \end{aligned} \tag{3.6}$$

It should be mentioned that (3.5) is not a rigorous relation since the multiple reflections between the step and the feed were not included. Also, amplitude ratio of modes is not implemented exactly by $1/3$ using (3.4), due to the presence of multiple reflections, there

would be slight deviation from this value, but it has been checked that this difference is small enough to not to change the overall design procedure.

The complete optimization steps are:

- Define the input waveguide dimensions a_1,b_1 and the aperture dimensions a_A and b_A,
- Define dielectric constants, ε_1 and ε_2,
- To determine step dimension a_s, calculate step ratio α from (3.5), Since H-plane step is used in this example, b_s remains same as b_A
- Calculate the length L_2 so that TE_{10} and TE_{30} modal coefficients are in phase. Note that at the step discontinuity, TE_{10} mode excites TE_{30} mode out of phase 180°,
- Determine the length L_1 so that overall reflection of the TE_{10} mode along the tapered section includes step discontinuity and reflection of TE_{10} mode from the aperture should be 180° out of phase at the feed waveguide plane to minimize the input return loss.

Since formulas used in the optimization routine are quite simple, it is very fast to obtain results unlike the commercial optimization software tools. However, numerical electromagnetic simulators can be exploited to optimze overall solutions which may include higher order modes higher than the TE_{30} mode.

CHAPTER 4

NUMERICAL RESULTS

In Chapter 2, the hybrid numerical technique is presented to analyze stepped-horn antenna loaded with variable permittivity dielectric material. In this model, mode matching technique is used in step approximated tapered section of the horn modeled with N_I uniform rectangular waveguide sections. Hence, it is very important to choose the size of each waveguide section, $\Delta l = L/N_I$ properly so that the pyramidal tapered section is accurately modeled. Choice of 30 steps per wavelength has been found to work well in numerical evaluations.

As a first example, empty pyramidal horn antenna with input waveguide section size $a_1 = 0.675\lambda$, $b_1 = 0.3\lambda$ and aperture size $a_A = 1.25\lambda, b_A = 0.5\lambda$, length of the tapered section, $L = 2.5\lambda$ is considered. It is assumed that TE_{10} mode in an incident wave at the input of the feed waveguide has a power density of 1 $Watt/m^2$. Table 4.1 shows amplitude and phase of reflection and transmission coefficient of TE_{10} mode and the total power P_{tot}, $P_{tot} = P_{rad} + P_{ref}$ where P_{rad} and P_{ref} are radiated and reflected power densities, respectively. Total number of modes used in this example were 3. As it seen from Table 4.1, $\lambda/30$ waveguide section size is enough for convergence to until fifth significant digit. Notice that power conservation check is also satisfied for every waveguide section size. Same study is repeated for dielectric loaded horn antenna and the similiar results were obtained as seen in Table 4.2. Notice that the wavelength, λ inside the dielectric medium is smaller than the wavelength of the empty horn, the number of waveguide section, N_I should be bigger compared to the empty one. As it was expected, power conservation is also satisfied for dielectric loaded horn antenna. However, there is a small difference compared to the the empty horn antenna, decrease in the wavelengths necessitated to include higher order modes which were excited at the aperture. Hence, the chosen total mode number

increased to 15. Scattering matrix size became 30×30 which is much larger than 6×6 used in the case of an empty horn.

$\lvert\Delta_l\rvert$	$\lvert\Gamma\rvert$	Γ_{pha}	$\lvert\tau\rvert$	τ_{pha}	P_{tot}
$\lambda/3$	0.0094418	135.68826	0.9999554	55.9931946	1
$\lambda/10$	0.0072330	109.85862	0.9999738	13.3108120	1
$\lambda/20$	0.0070830	99.7516022	0.9999749	-0.8616687	1
$\lambda/30$	0.0070799	96.1675339	0.9999750	-5.5772729	1
$\lambda/40$	0.0070870	94.3311768	0.9999749	-7.9332714	1

Table 4.1 Amplitude and Phase of Reflection and Transmission Coefficients of TE_{10} Mode in an Empty Horn of Length $L = 2.5\lambda$ and Free Space Wavelength $\lambda = 0.03$m.

$\lvert\Delta_l\rvert$	$\lvert\Gamma\rvert$	Γ_{pha}	$\lvert\tau\rvert$	τ_{pha}	P_{tot}
$\lambda/3$	0.0272985	66.3099976	0.9992032	-1.1458129	1.000052
$\lambda/10$	0.0096992	-17.3840485	0.9997759	166.73718	1.000035
$\lambda/20$	0.0086497	-44.055122	0.9998208	140.42763	1.000005
$\lambda/30$	0.0084742	-52.8015099	0.9998305	131.66652	1.000002
$\lambda/40$	0.0084134	-57.1421928	0.9998346	127.88453	1.000001

Table 4.2 Amplitude and Phase of Reflection and Transmission Coefficient of a TE_{10} mode in a Dielectric ($\varepsilon_r = 2.5$) Loaded Horn Antenna of Length $L = 2.5\lambda$. λ is the Wavelength Inside the Dielectric Medium.

The magnitude and phase of the reflection and transmission coefficients of the dominant TE_{10} mode at the feed section are checked to examine the overall convergence of the mode matching technique versus the total mode number, N_T. Consider horn antenna with the input feed section dimensions of $x1 = 0.75\lambda$ and $y1 = 0.3\lambda$ and aperture dimensions of $a2 = 2.7\lambda$ and $b2 = 1.2\lambda$ and the length of the tapered section $L = 2.5\lambda$. Number of steps are chosen as $N_I = 75$. Power density carried by the incident TE_{10} mode is assumed

to be equaled to 1 $Watt/m^2$. Table 4.3 shows convergence of the magnitude of the input reflection coefficent, its dependence on the total mode number used in calculations for an empty and $\varepsilon_r = 3$ dielectric loaded horn antennas. As seen from Table 4.3 and Table 4.4, 10 modes for the empty horn and 20 modes for the dielectric loaded horn antenna are enough to observe convergence. Total number of modes, N_T in each waveguide depend on the physical dimensions and the permittivity of loading dielectric material. Total number of sections, N_I and number of modes, N_T used in all the subsequent calculations, were determined based on above mentioned criteria.

Mode	$\lvert\Gamma\rvert$	Γ_{pha}	$\lvert\tau\rvert$	τ_{pha}	P_{tot}
5	0.0331535	-134.7404	0.9994033	-103.1375	1.000000
10	0.0303541	-136.6471	0.9608723	-106.8663	1.000000
15	0.0294986	-138.4952	0.9596686	-106.7556	1.000000
20	0.0289968	-138.8472	0.9564262	-106.6965	1.000001
25	0.0285240	-139.0114	0.9596345	-106.6353	1.000001
28	0.0288328	-138.8160	0.9596605	-106.6704	1.000001
35	0.0283598	-138.9811	0.9596487	-106.6092	1.000001
45	0.0282123	-138.9438	0.9596625	-106.5849	1.000001

Table 4.3 Amplitude and Phase of Reflection and Transmission Coefficient of TE_{10} Mode in an Empty Horn Antenna of Length $L = 2.5\,\lambda$. λ is a Free Space Wavelength.

The entire analysis were coded in MATLAB. The validity of the code developed in this dissertation has been verified using experimental data available in the literature. Since there is no study available pertaining to a dielectric loaded horn antenna, verification is carried out in two phases. First, 20 dB standard gain horn antenna gain and VSWR are compared with the experimental results [11]. It can be seen from Table 4.5 that the theory and measured results agreed well.

Mode	$\|\Gamma\|$	Γ_{pha}	$\|\tau\|$	τ_{pha}	P_{tot}
5	0.0322685	-65.9037	0.9990225	-62.2632	1.000000
10	0.0306700	-68.1207	0.9413418	-73.8805	1.000000
15	0.0297606	-67.2730	0.9060044	-74.9057	1.000001
20	0.0297213	-67.1719	0.8999104	-74.8256	1.000002
25	0.0295998	-66.7879	0.8997418	-74.7871	1.000021
28	0.0297143	-67.0907	0.8999757	-74.9057	1.000013
35	0.0295930	-66.7067	0.8998064	-74.7706	1.000029
45	0.0295890	-66.6328	0.8998724	-74.7553	1.000042

Table 4.4 Amplitude and Phase of Reflection and Transmission Coefficient of a TE_{10} Mode in a Dielectric ($\varepsilon_r = 3$) Loaded Horn Antenna of Length $L = 2.5\lambda$. λ is the Wavelength Inside the Dielectric Medium.

	9 GHz		10 GHz		11 GHz	
	VSWR	Gain	VSWR	Gain	VSWR	Gain
Experiment	1.100	19.72 dB	1.060	20.46 dB	1.040	21.24 dB
Calculated	1.086	19.76 dB	1.050	20.75 dB	1.025	21.46 dB

Table 4.5 Comparison of VSWR's and Gains of the 20 dB Standard Gain Horn Antenna.

Numerical validation of the developed code was carried out also on a dielectric loaded waveguide [20]. Numerical simulations for the input reflection coefficient corresponding to an open-ended loaded waveguide with dielectric material $\varepsilon_r = 2.63$, the length of waveguide $L = 9.51$mm, are compared with experimental results. Figure 4.1 shows excellent agreement between the computed model and measured results.

The presence of a dielectric material loading in a 10dB standard gain antenna is chosen as a test antenna to study the proposed method. Input waveguide section sizes are chosen as $a_1 = 22.86$ mm and $b_1 = 10.16$ mm. Aperture sizes are $a_A = 40.13$ mm

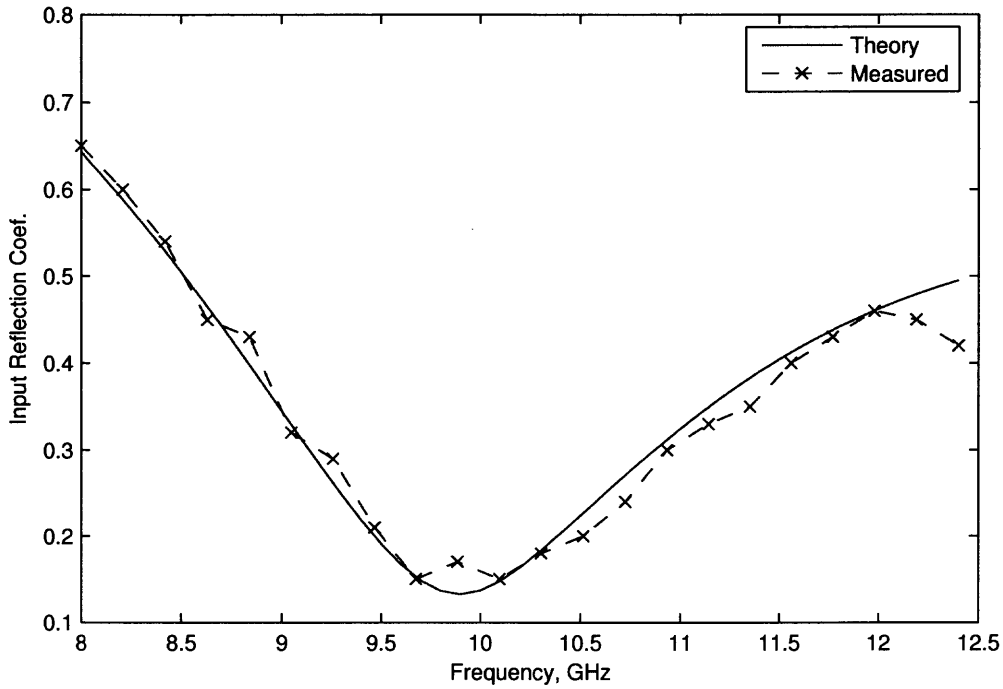

Figure 4.1 Input reflection coefficient versus frequency for dielectric ($\varepsilon_r = 2.63$) loaded open-ended waveguide radiator with length of $L = 9.51$mm

and $b_A = 29.21$ mm and length of the horn is $L = 51$ mm. Three different dielectric loading configurations are compared. First uniform dielectric loading is applied. In this configuration, both feed waveguide and tapered section of the horn are loaded with the same dielectric material, ε_r. Then step loading is applied. This configuration leaves the feed waveguide empty and loads the tapered section with dielectric medium (ε_r). And last configuration that was tested is a linear profile configuration. From feed waveguide toward the aperture, dielectric constant ε_r changes linearly from 1 to pre-determined value of ε_r. The value of a dielectric constant $\varepsilon_r = 1.5$ is chosen to load the 10 dB standard gain horn antenna.

Results presented in Figure 4.3 to Figure 4.6 depict comparison for input reflection coefficient, gain, aperture efficiency and cross-polarization characteristics between these three configurations and an empty horn antenna. From input reflection coefficient comparisons

Figure 4.3, it is obvious that the empty horn has better characteristics for entire bandwidth. Reason for the observed increase in the reflection coefficient at the input due to loading is that the increase in aperture reflection coeficient. Dielectric loading increases the contrast between the aperture (modes) and free space impedance and resulted in higher aperture reflection coefficient. Step loading might improve the input reflection coefficient within a narrow bandwidth. The other two configuration have no advantage over the empty horn for this comparison. However, Figure 4.4 shows any kind of loading has better gain characteristics values compared to the empty horn antenna. This is mainly due to increase in an electrical size of the aperture because of dielectric loading. It is observed from Figure 4.5 that aperture efficiencies exhibit similiar increases for step and uniform dielectric loading. The extreme change in aperture efficiency can be explained due to excition of higher order modes in these particular frequencies and/or resonance effects of higher order excited modes. Cross-polarization level observed to improve with dielectric loading forrealtively narrow bands as seen. It can be concluded from these results that better loading configuration is a step configuration.

As a next example, step loading is applied to a 10 dB standard gain horn antenna with relative dielectric constants, $\varepsilon_r = 1.2, ,\varepsilon_r = 1.5$ and $\varepsilon_r = 1.7$. Results in Figure 4.7 to Figure 4.10 depict comparisons for input reflection coefficient, gain, aperture efficiency and cross-polarization characteristics between three different dielectric constant loading and of the empty horn antenna. As it expected, bigger the dielectric constant, fluctuations tend to show increase in the input reflection coefficient. Gain increase is proportional to a dielectric constant. From Figure 4.9 and Figure 4.10, $\varepsilon_r = 1.5$ and $\varepsilon_r = 1.7$ dielectric constant loading, cross-polarization levels yield better characteristics for relatvely narrow bandwidth. However, $\varepsilon_r = 1.2$ does not have better cross-polarization and aperture efficieny compare to the empty horn antenna. This is due to that dielectric constant, $\varepsilon_r = 1.2$ dielectric constant loading for this particular horn antenna can not excite the higher order modes. Figure 4.11 and Figure 4.12 shows E- and H-plane pattern comparisons of different

dielectric loaded and emtpy horn antenna at $f = 10$ GHz. Notice that in both plane, relative beamwidth show slight shrinkage with increased permittivity. Dielectric loading also cause the increase in sidelobe levels in E-plane patterns.

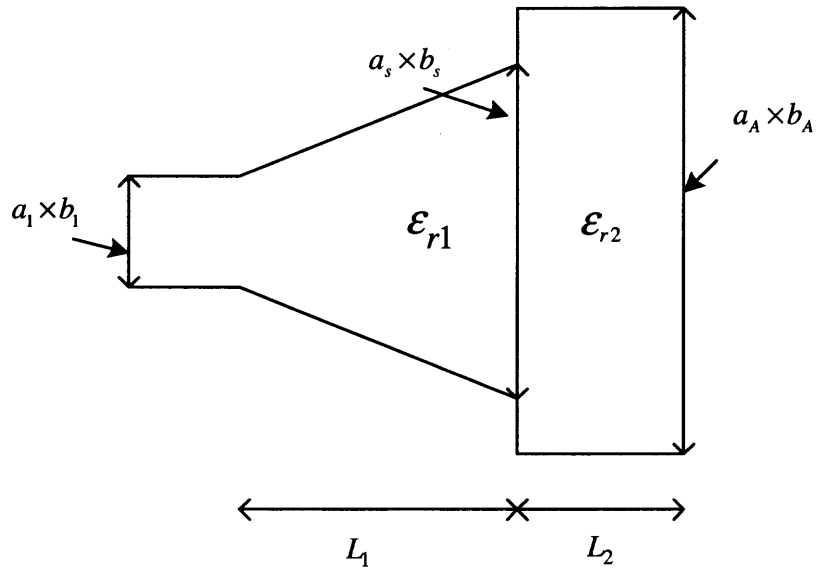

Figure 4.2 Stepped-horn antenna model.

In Chapter 3, optimization routine is presented. Stepped-horn antenna under consideration is shown in Figure 4.2. As a first example of optimization, input waveguide section of the stepped-horn antenna is chosen as $a_1 = 0.73\lambda$, $b_1 = 0.34\lambda$ and aperture size is $a_A = 1.8\lambda$, $b_A = 0.77\lambda$.The optimization is done at $f = 10$ Ghz. Four different optimization routine were run to compare the effect of dielectric loading, ($\varepsilon_{r1} = 1.0$ and $\varepsilon_{r2} = 1.0$), ($\varepsilon_{r1} = 1.2$ and $\varepsilon_{r2} = 1.2$), ($\varepsilon_{r1} = 1.2$ and $\varepsilon_{r2} = 1.0$), ($\varepsilon_{r1} = 1.0$ and $\varepsilon_{r1} = 1.2$). Length of tapered section ,L_1, length of step waveguide section, L_2, step size a_s and b_s, according the optimization results are presented in Table 4.6. It can be seen from Table 4.6 that smallest length of the overall stepped-horn antenna can accomplished by using ($\varepsilon_{r1} = 1.2$ and $\varepsilon_{r2} = 1.2$) as expected due to the highest value of the realative dielectric constant. Optimize stepped-horn antennas are compared with empty test horn antenna. Test horn antenna is chosen such has the same aperture, same input waveguide size and same overall length of ($\varepsilon_{r1} = 1.0$ and $\varepsilon_{r2} = 1.0$) as an optimized antenna. Therefore, its input waveguide size is

$a_1 = 0.73\lambda$, $b_1 = 0.34\lambda$ and aperture size is $a_A = 1.8\lambda$, $b_A = 0.77\lambda$ and lengths,$L = 80.2$ mm.

$\varepsilon_{r1}/\varepsilon_{r2}$	1.0/1.0	1.0/1.2	1.2/1.2	1.2/1.0
a_s (mm)	34.1	29.7	29.7	28.6
b_s(mm)	23.0	23.0	23.0	23.0
L_1 (mm)	36.8	41.2	30.0	39.8
L_2 (mm)	43.4	43.0	43.0	40.1
$L_1 + L2$ (mm)	80.2	84.2	73.0	79.9

Table 4.6 Optimization Values of Stepped-horn Antenna for Input Waveguide Size, $a_1 = 0.73\lambda$, $b_1 = 0.34\lambda$ and Aperture Size $a_A = 1.8\lambda$, $b_A = 0.77\lambda$.

Figure 4.13-Figure 4.16 show the comparison results of the input reflection coefficient, gain, aperture efficieny and cross-polarization level for optimized dielectric loaded horn antennas and the empty horn antenna. It can seen that from Figure 4.13, optimized dielectric loading of the step region with $\varepsilon_{r2} = 1.2$ leads to improved input reflection coefficient $|\Gamma| < 0.03$ in a relatively wide band(9.6 to 10.35 GHz) compared to an empty horn $|\Gamma| < 0.1$ throughout the band of 9.0-11.0 GHz. It is possible to get even further reduction of $|\Gamma| < 0.02$ within a very narrow band around 9.2 GHz. Figure 4.14 shows that inclusion of a step region to an empty horn results of an increase of gain by 1 dB over the entire band. However further increase by additional 1 dB (2 dB overall) is observed in the presence of dielectric loading. It was observed that gain performance of a fully loaded step-horn versus step region only dielectric loaded horn were identical. Presence of a dielectric can be attributed to an increase in gain due to enhancement of the equivalent aperture size in terms of electrical dimensions.

One of the goals for optimization was to reduce the cross-polarization characteristics. The presence of a step region helps to reduce cross-polarization by almost 5 dB, Figure 4.15. Further, inclusion of a dielectric can be used to tune cross-polarization to desired

-30 dB at the expense of significant narrowing of the frequency band. Similiar effect was observed in Figure 4.16 in the aperture efficiency enhancement from 40% to 50% in average over the band. Figure 4.17 shows the co- and cross-polarziation levels of test horn antenna and ($\varepsilon_{r1} = 1.2$ $\varepsilon_{r2} = 1.2$) loaded stepped-horn antenna are presented at $f = 10$ GHz.

To show the effect of optimization, amplitudes of x-component of aperture magnetic field and y-component of aperture electric field for test horn antenna and stepped-horn antenna are presented in Figure 4.18 to Figure4.21. It can be seen from Figure 4.18 and Figure 4.19that aperture field distributions of test horn antenna exhibits tapered nature of the aperture fields along x-direction due to TE_{10} mode. As the step region included in the horn antenna, tapered nature of the aperture fields tend to smooth out leading to more uniform characteristics in x-direction, as seen in Figure 4.20 and Figure 4.21.

As a second example in optimization, input waveguide section of the stepped-horn antenna is chosen as $a_1 = 0.73\lambda$, $b_1 = 0.34\lambda$ and aperture size is $a_A = 2\lambda$, $b_A = 0.82\lambda$.The optimization is carried out at $f = 10$ Ghz. Four different optimization schemes were executed to compare the effect of dielectric loading, ($\varepsilon_{r1} = 1.0$ and $\varepsilon_{r2} = 1.0$), ($\varepsilon_{r1} = 1.4$ and $\varepsilon_{r2} = 1.4$), ($\varepsilon_{r1} = 1.4$ and $\varepsilon_{r2} = 1.2$), ($\varepsilon_{r1} = 1.2$ and $\varepsilon_{r1} = 1.4$). Notice that for this optimization, both aperture size and dielectric constants, ε_{r1} and ε_{r2} are chosen larger than the first example. Optimized length of tapered section L_1, length of step waveguide section L_2, step dimensions a_s and b_s, according the optimization results are presented in Table 4.7. It can be seen from Table 4.7 that smallest length of the overall stepped-horn antenna can accomplished by using ($\varepsilon_{r1} = 1.4$ $\varepsilon_{r2} = 1.4$)) as expected. Optimized stepped-horn antennas are compared with empty test horn antenna. Test horn antenna is chosen such that has the same aperture, same input waveguide size and same overall length of by optimized antenna ($\varepsilon_{r1} = 1.0$ $\varepsilon_{r2} = 1.0$). Therefore, its input waveguide dimensions are $a_1 = 0.73\lambda$, $b_1 = 0.34\lambda$ and aperture size is $a_A = 2\lambda$, $b_A = 0.82\lambda$ and has a of length $L = 91.1$ mm.

$\varepsilon_{r1}/\varepsilon_{r2}$	1.0/1.0	1.2/1.4	1.4/1.2	1.4/1.4
a_s(mm)	36.1	38.3	36.0	38.3
b_s(mm)	24.0	24.0	24.0	24.0
L_1 (mm)	42.2	38.2	26.1	26.1
L_2(mm)	48.9	62.1	55.9	62.1
$L_1 + L2$ (mm)	91.1	100.3	82.0	88.2

Table 4.7 Optimization Values of Stepped-horn Antenna Input Waveguide Size, $a_1 = 0.73\lambda$, $b_1 = 0.34\lambda$ and Aperture Size, $a_A = 2\lambda$, $b_A = 0.82\lambda$.

Figure 4.22 - Figure 4.25 show the comparison of results for input reflection coefficient, gain, aperture efficieny and cross-polarization level for optimized stepped-horn antennas and the empty horn antenna.

Loading the taper with a dielectric while keeping the feed waveguide empty results in increased input reflection coefficient as seen in Figure 4.22 due to the creation of a mismatched boundary at the feed. Simultaneously, the mismatch on the aperture plane due to dielectric loading also contributes to this increase. However, interference effects due to mistmached both boundaries could produce standing wave effects and thereby may result in a reduced input reflection coefficient in a narrow frequency band. The dielectric loaded stepped-horn antenna produced increased gain as seen Figure 4.23 From Figure 4.24 and Figure 4.25, it can be seen that cross-polarization level was reduced and aperture efficiency was increased. Notice that at $f = 10.6$ GHz, there is anamalous increase in cross-polarization and similiar decrease in aperture efficiency. Reason for this is excitation of TE_{12}/TM_{12} modes at this frequency across the aperture as shown in Figure 4.26. Optimization was focused not to excite these modes at the aperture. It is worth to remember that optimization was done at $f = 10$ GHz. As aperture dimensiona and dielectric constant ε_{r2} is getting larger, bandwidth of optimized region is getting smaller. Figure 4.27 and Figure 4.28 depict aperture field distributions of test horn antenna and Figure 4.27 and

Figure 4.28 depict aperture field distributions of stepped-horn antenna are exhibit that aperture distributions tend to become more uniform.

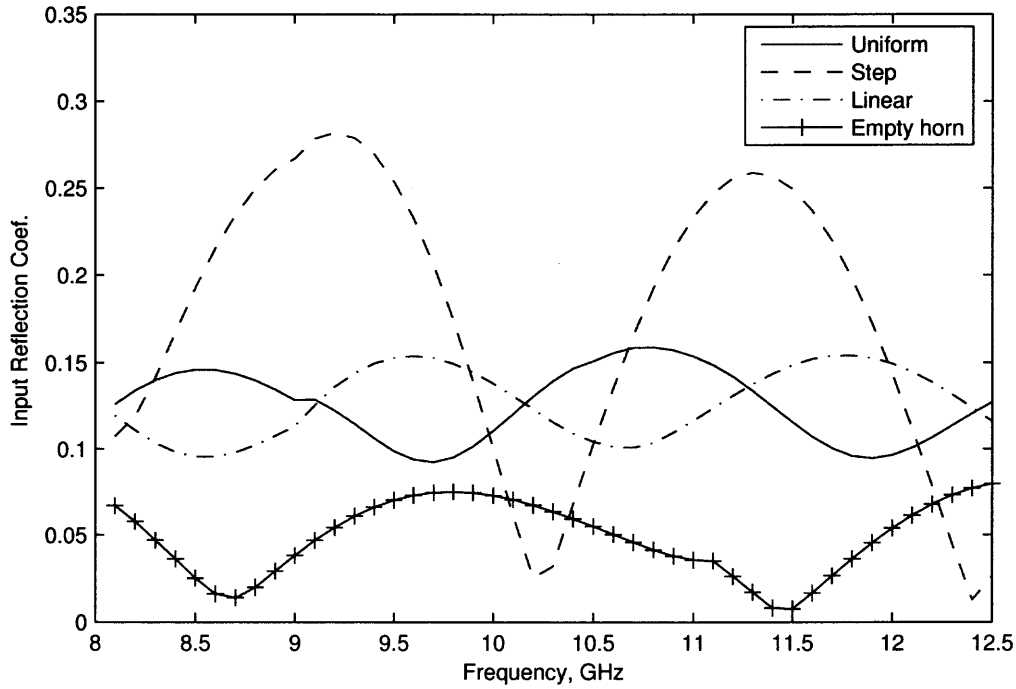

Figure 4.3 Input reflection coefficient versus frequency of $\varepsilon_r = 1.5$ dielectric loading of horn antennas with uniform loading, step loading, linear loading and empty horn antenna.

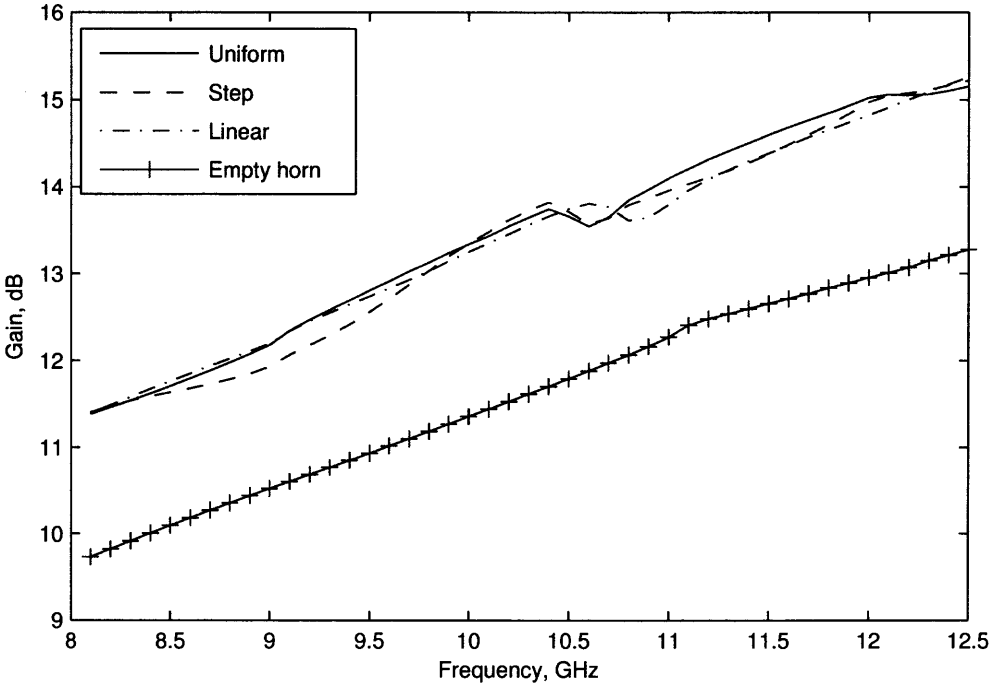

Figure 4.4 Gain versus frequency of dielectric ($\varepsilon_r = 1.5$) loaded horn antennas with uniform loading, step loading, linear loading and empty horn antenna.

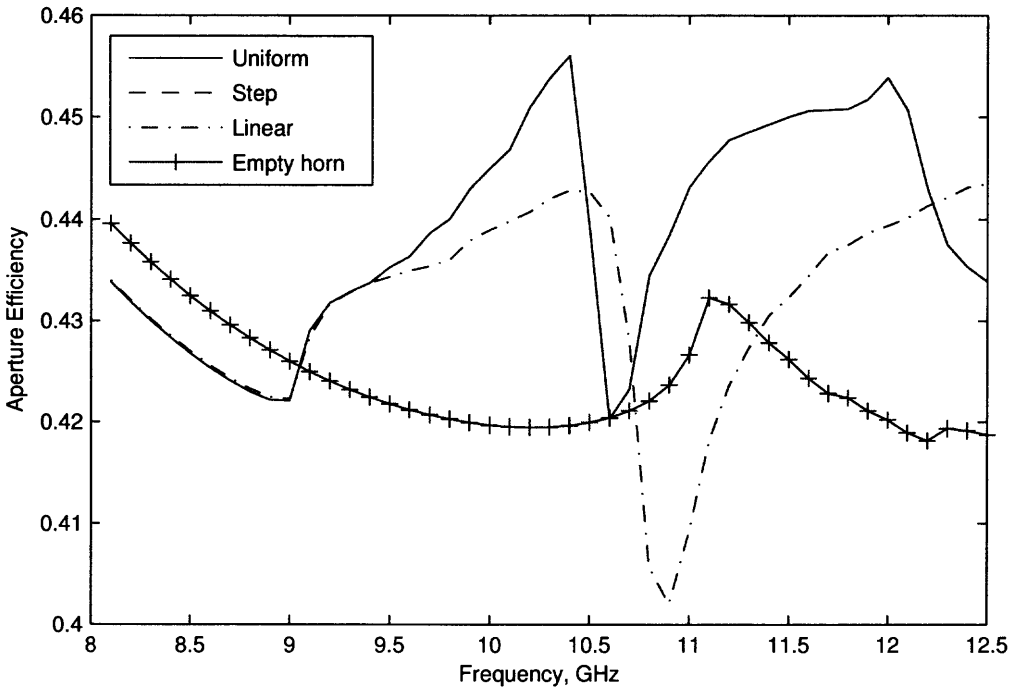

Figure 4.5 Aperture efficiency versus frequency of dielectric ($\varepsilon_r = 1.5$) loaded horn antennas with uniform loading, step loading, linear loading and empty horn antenna.

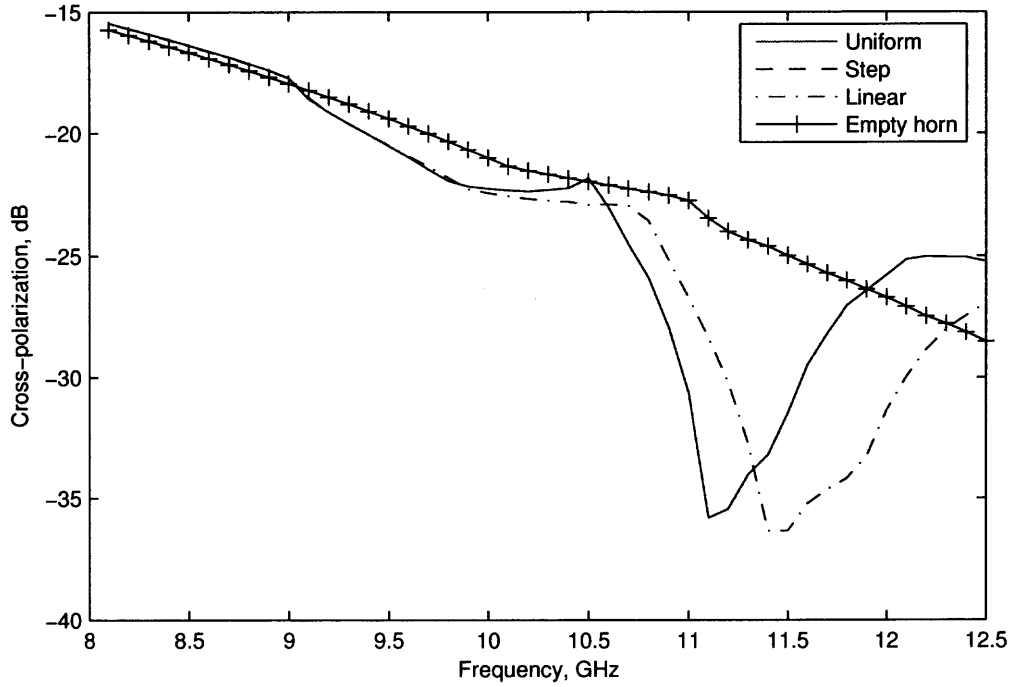

Figure 4.6 Cross-polarization level versus frequency of dielectric ($\varepsilon_r = 1.5$) loaded antennas with uniform loading, step loading, linear loading and empty horn antenna.

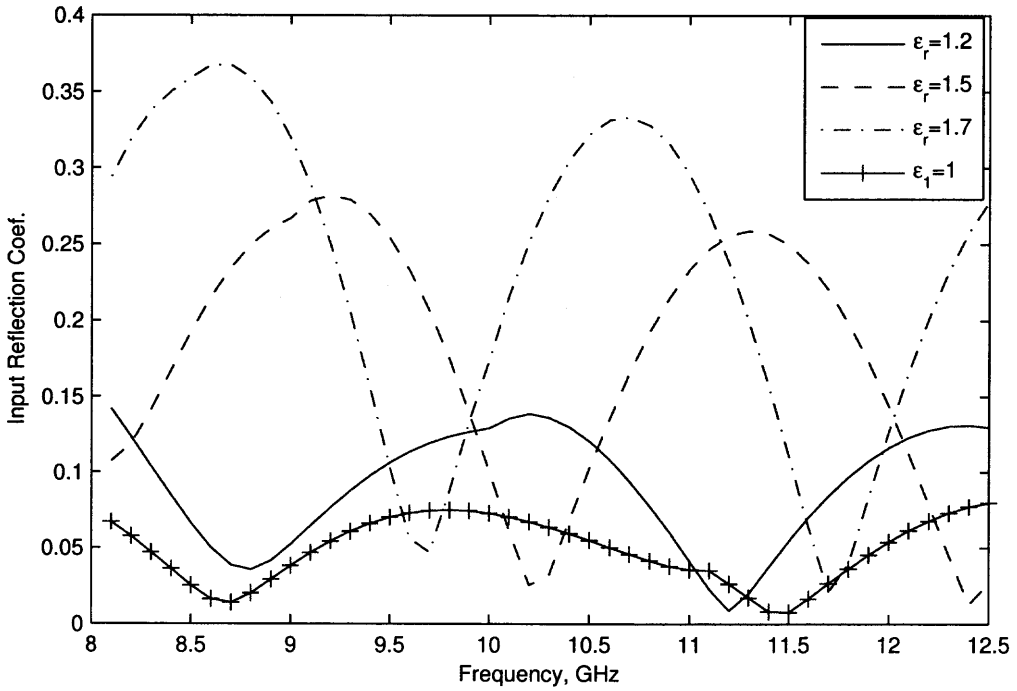

Figure 4.7 Input reflection coefficient versus frequency of the dielectric ($\varepsilon_r = 1.2, \varepsilon_r = 1.5, \varepsilon_r = 1.7$) loaded horn antennas and empty horn antenna.

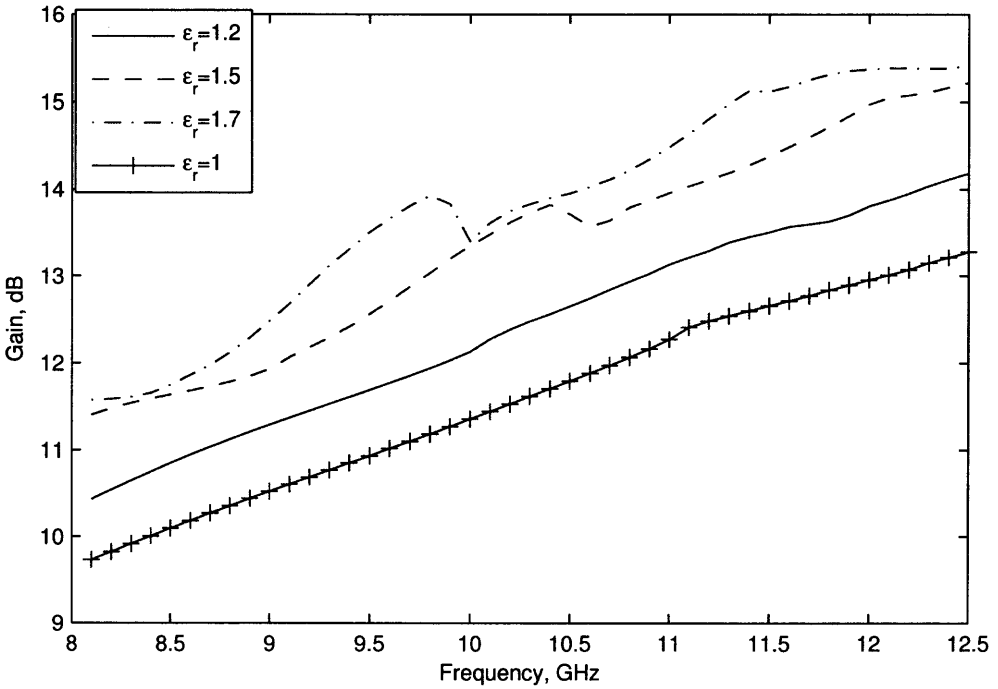

Figure 4.8 Gain versus frequency of the dielectric ($\varepsilon_r = 1.2,\ \varepsilon_r = 1.5, \varepsilon_r = 1.7$) loaded horn antennas and empty horn antenna.

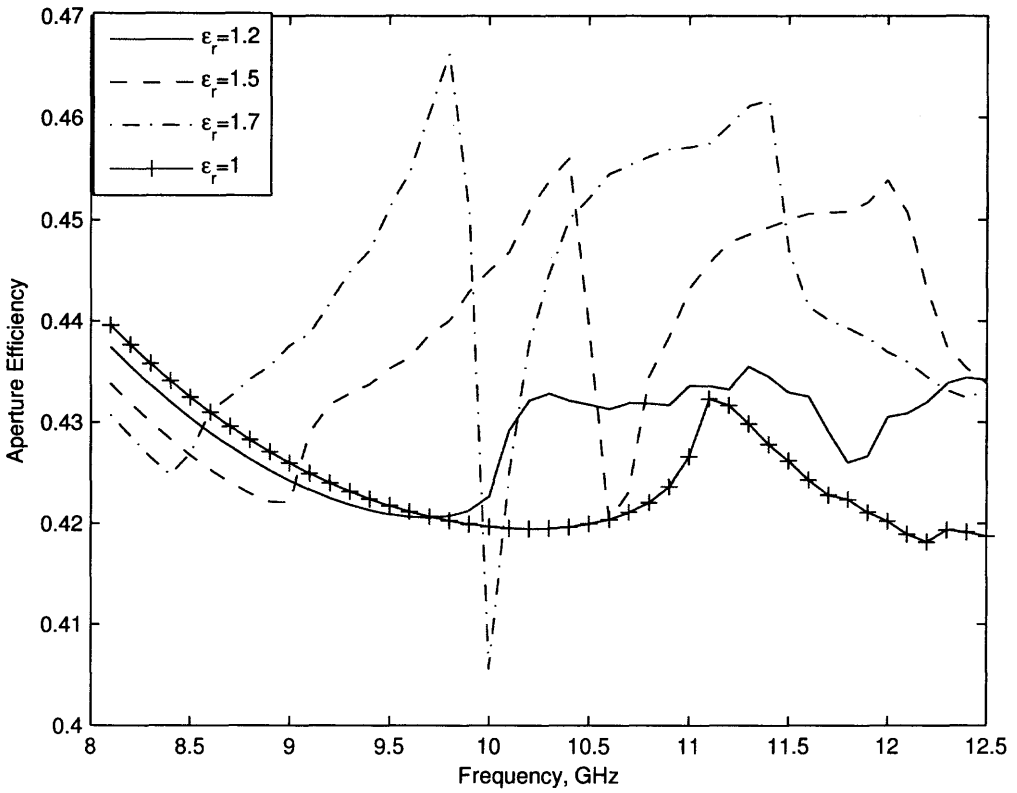

Figure 4.9 Aperture efficiency versus frequency of the dielectric ($\varepsilon_r = 1.2$, $\varepsilon_r = 1.5$ and $\varepsilon_r = 1.7$) loaded horn antennas and empty horn antenna.

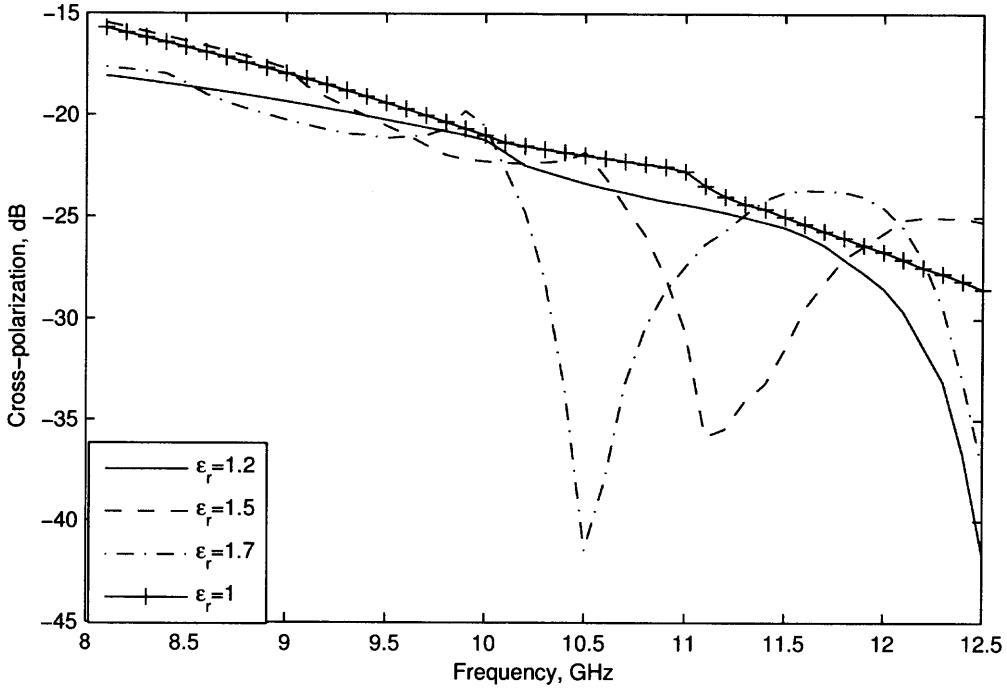

Figure 4.10 Cross-polarization level versus frequency of the dielectric ($\varepsilon_r = 1.2$, $\varepsilon_r = 1.5$, $\varepsilon_r = 1.7$) loaded horn antennas and empty horn antenna.

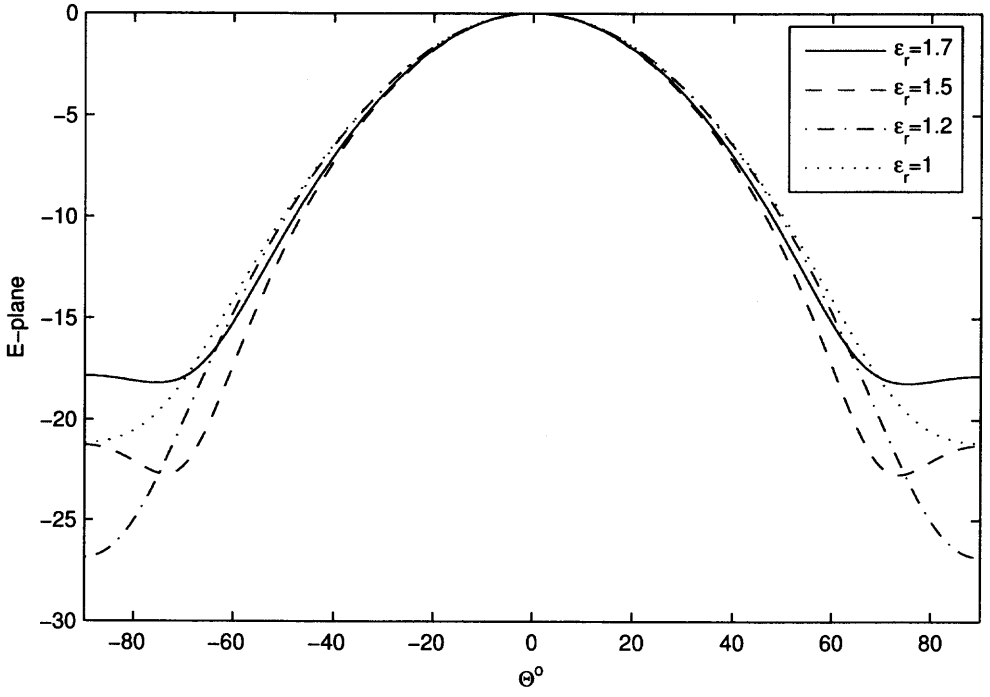

Figure 4.11 E-plane pattern versus Θ^o of the dielectric ($\varepsilon_r = 1.2$, $\varepsilon_r = 1.5$, $\varepsilon_r = 1.7$) loaded horn antennas and empty horn antenna.

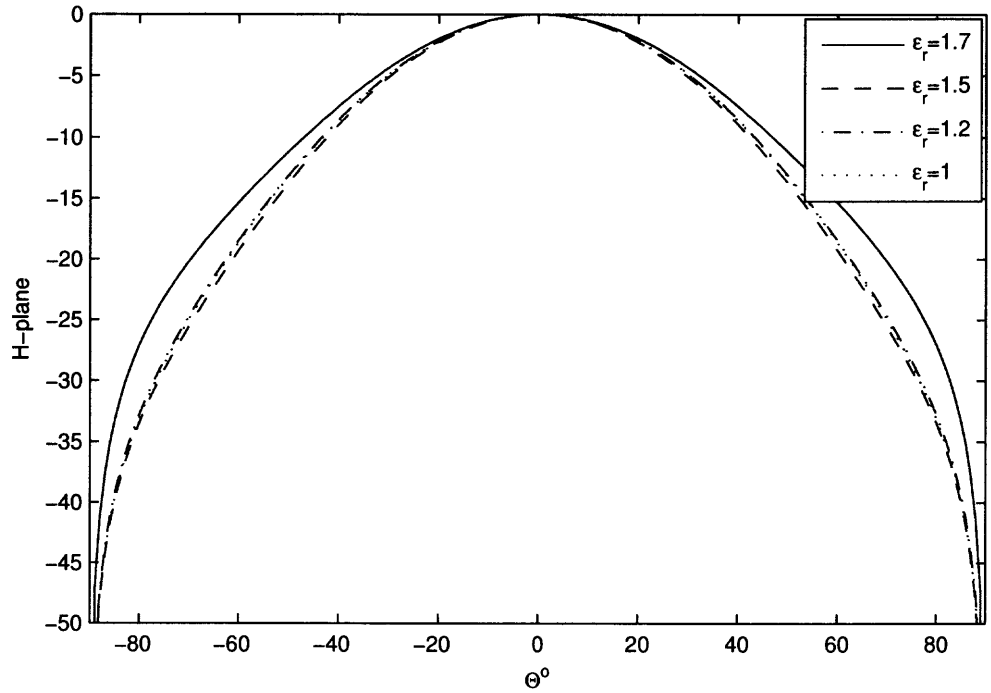

Figure 4.12 H-plane pattern versus Θ^o of the dielectric ($\varepsilon_r = 1.2, \varepsilon_r = 1.5,\ \varepsilon_r = 1.7$) loaded horn antennas and empty horn antenna.

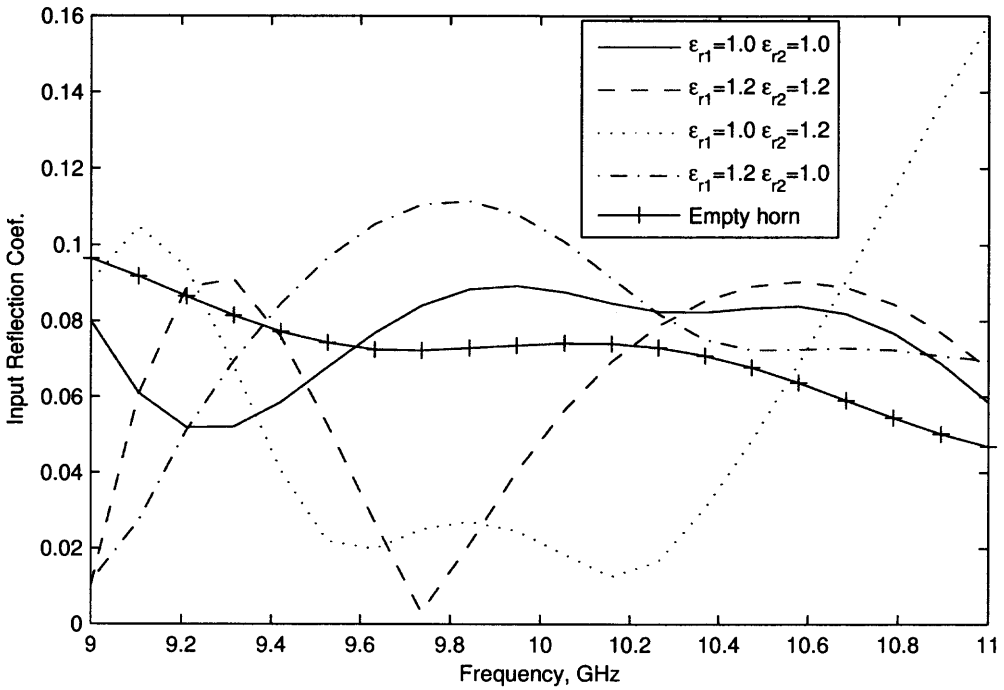

Figure 4.13 Input reflection coefficient versus frequency of the stepped-horn antennas for ($\varepsilon_{r1} = 1.0$ $\varepsilon_{r2} = 1.0$), ($\varepsilon_{r1} = 1.2$ $\varepsilon_{r2} = 1.2$), ($\varepsilon_{r1} = 1.0$ $\varepsilon_{r2} = 1.2$), ($\varepsilon_{r1} = 1.2\varepsilon_{r2} = 1.0$), and empty horn antenna with length $L = 80.2$ mm.

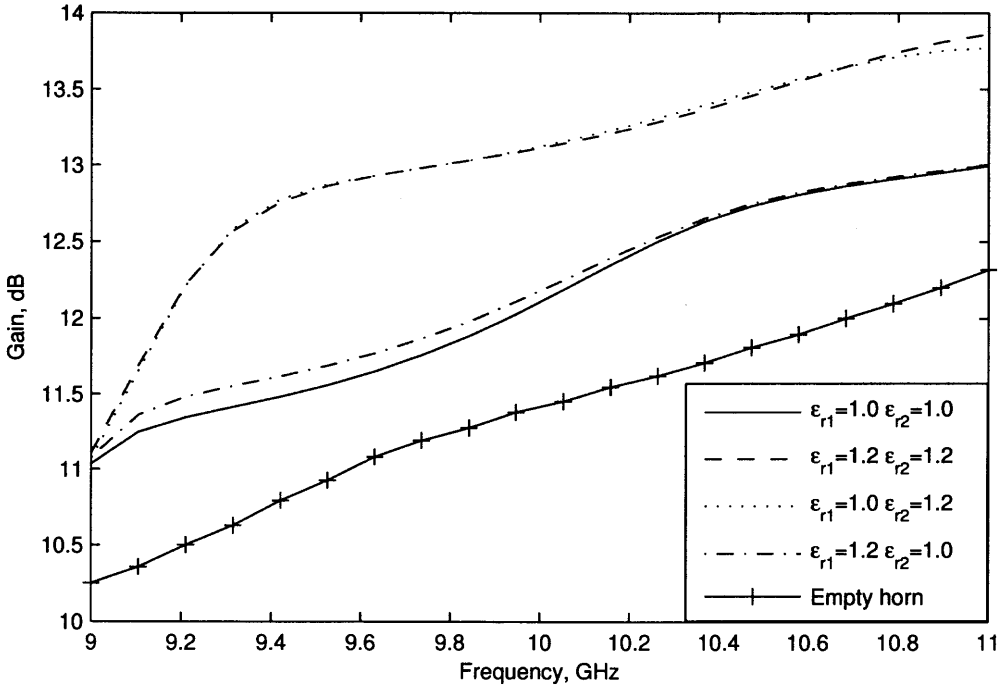

Figure 4.14 Gain versus frequency of the stepped-horn antennas for ($\varepsilon_{r1} = 1.0\,\varepsilon_{r2} = 1.0$), ($\varepsilon_{r1} = 1.2\,\varepsilon_{r2} = 1.2$), ($\varepsilon_{r1} = 1.0\ \varepsilon_{r2} = 1.2$), ($\varepsilon_{r1} = 1.2\,\varepsilon_{r2} = 1.0$) and empty horn antenna with $L = 80.2$ mm.

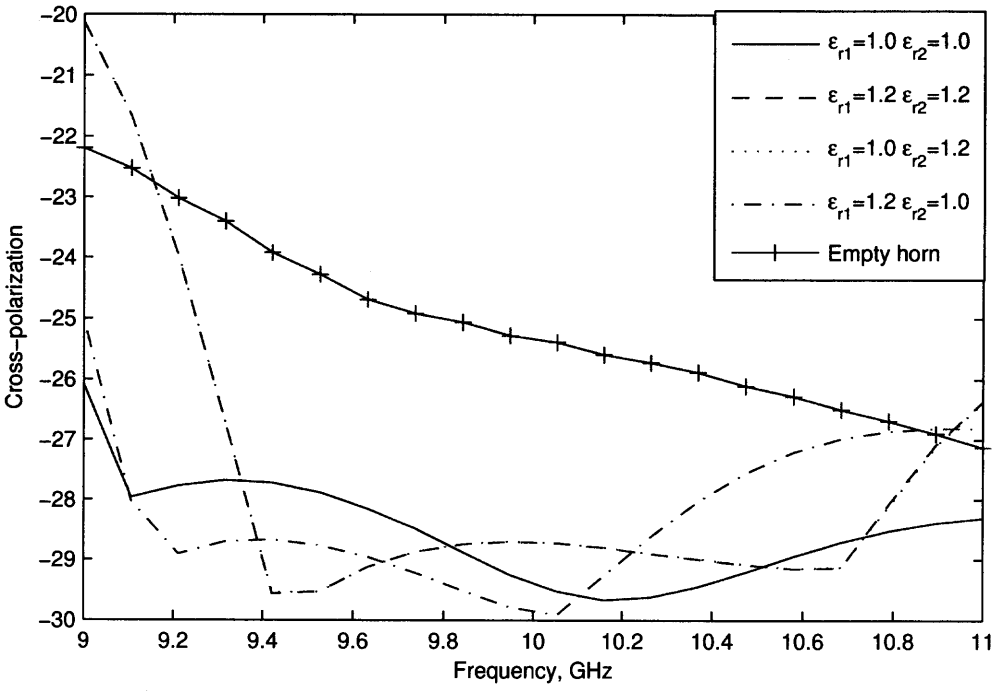

Figure 4.15 Cross-polarization level versus frequency of the stepped-horn antennas for ($\varepsilon_{r1} = 1.0$ $\varepsilon_{r2} = 1.0$), ($\varepsilon_{r1} = 1.2$ $\varepsilon_{r2} = 1.2$), ($\varepsilon_{r1} = 1.0$ $\varepsilon_{r2} = 1.2$), ($\varepsilon_{r1} = 1.2 \varepsilon_{r2} = 1.0$) and empty horn antenna with $L = 80.2$ mm.

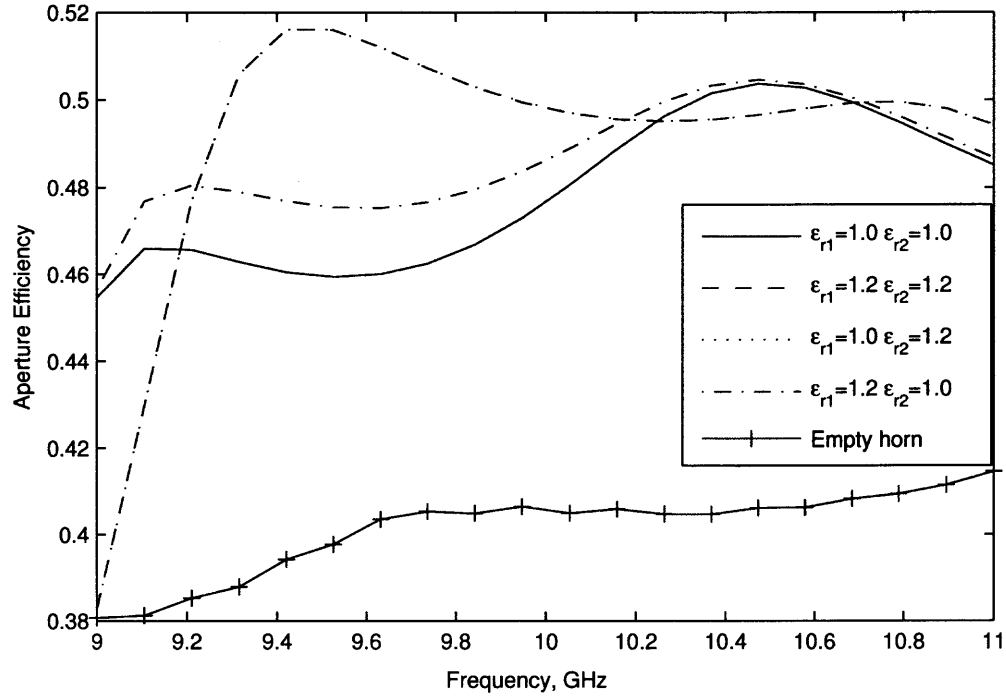

Figure 4.16 Aperture efficiency versus frequency of the stepped-horn antennas for ($\varepsilon_{r1} = 1.0$ $\varepsilon_{r2} = 1.0$), ($\varepsilon_{r1} = 1.2$ $\varepsilon_{r2} = 1.2$), ($\varepsilon_{r1} = 1.0\,\varepsilon_{r2} = 1.2$), ($\varepsilon_{r1} = 1.2$ $\varepsilon_{r2} = 1.0$) and empty horn antenna with $L = 80.2$ mm.

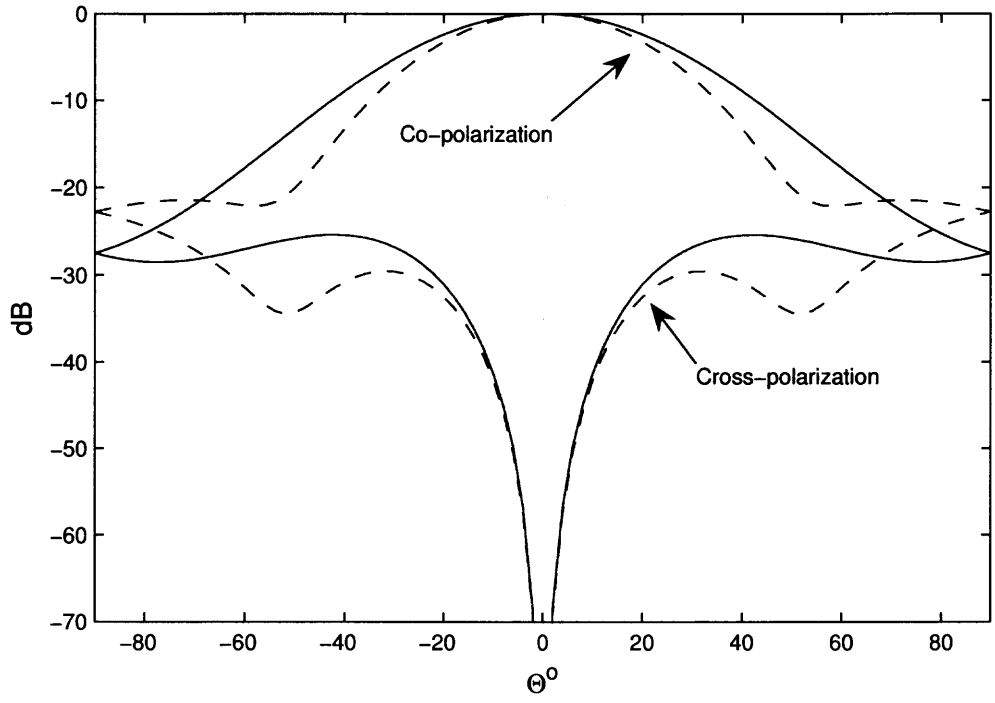

Figure 4.17 Co- and Cross-polarization patterns for stepped-horn antenna ($\varepsilon_{r1} = 1.2$ $\varepsilon_{r2} = 1.2$) and empty horn antenna with $L = 80.2$ mm at $f = 10$ GHz.
—- Empty horn antenna,
– – Stepped-horn antenna

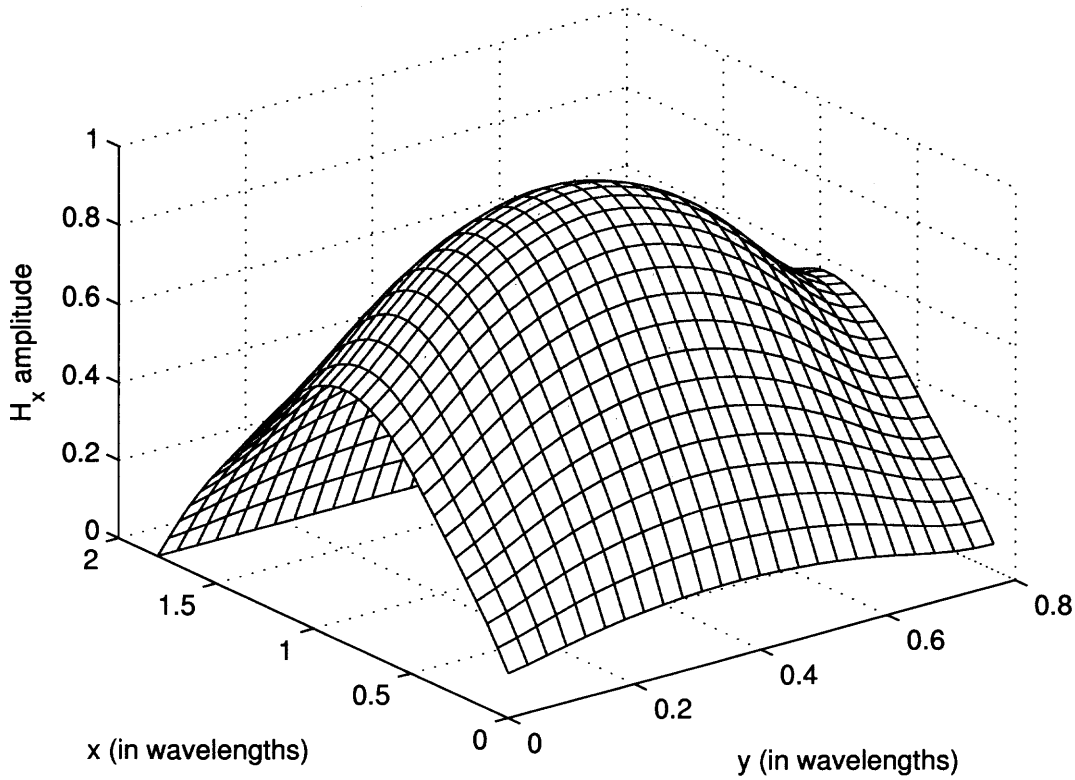

Figure 4.18 Amplitude of aperture magnetic field distribution,H_x versus x and y for empty horn antenna with $L = 80.2$ mm at $f = 10$ GHz.

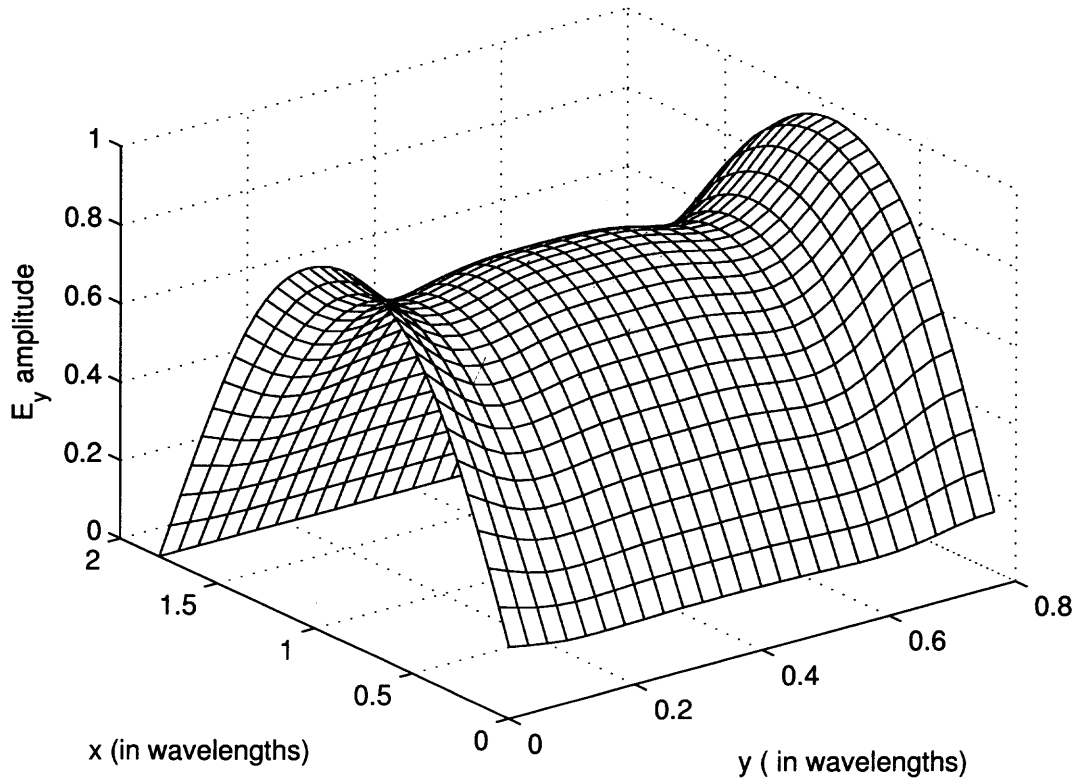

Figure 4.19 Amplitude of aperture electric field distribution, E_y versus x and y for empty horn antenna with $L = 80.2$ mm at $f = 10$ GHz.

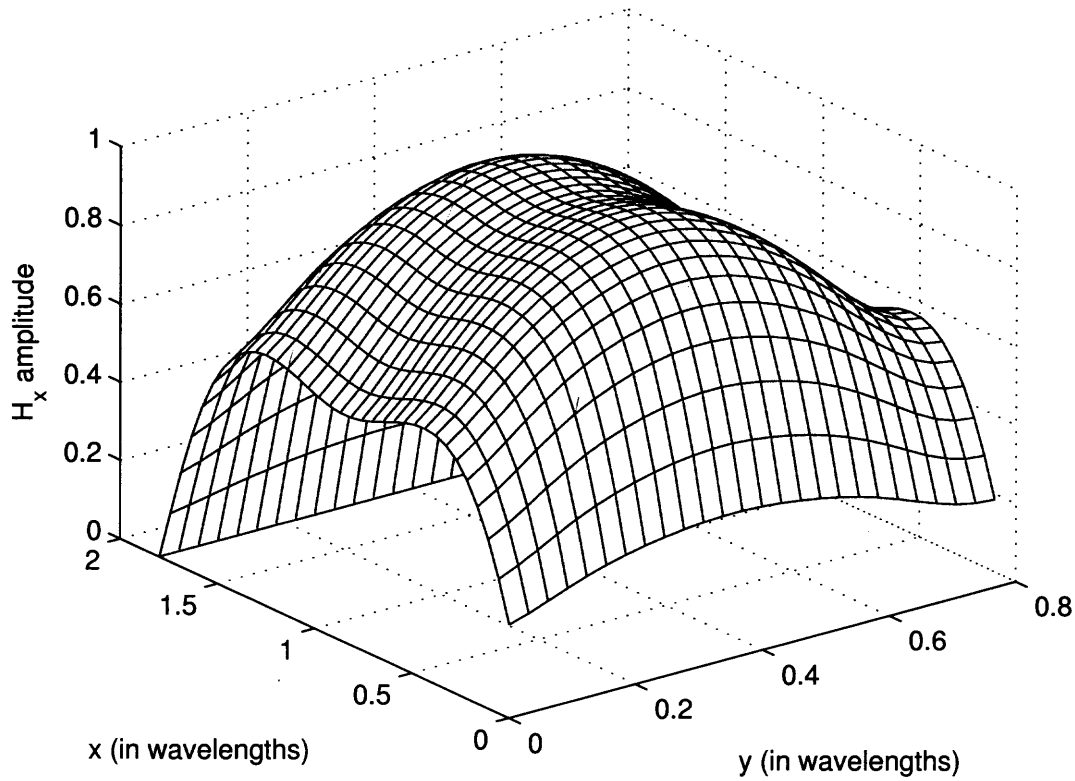

Figure 4.20 Amplitude of aperture magnetic field distribution,H_x versus x and y for ($\varepsilon_{r1} = 1.0$ $\varepsilon_{r2} = 1.0$)stepped-horn antenna at $f = 10$ GHz.

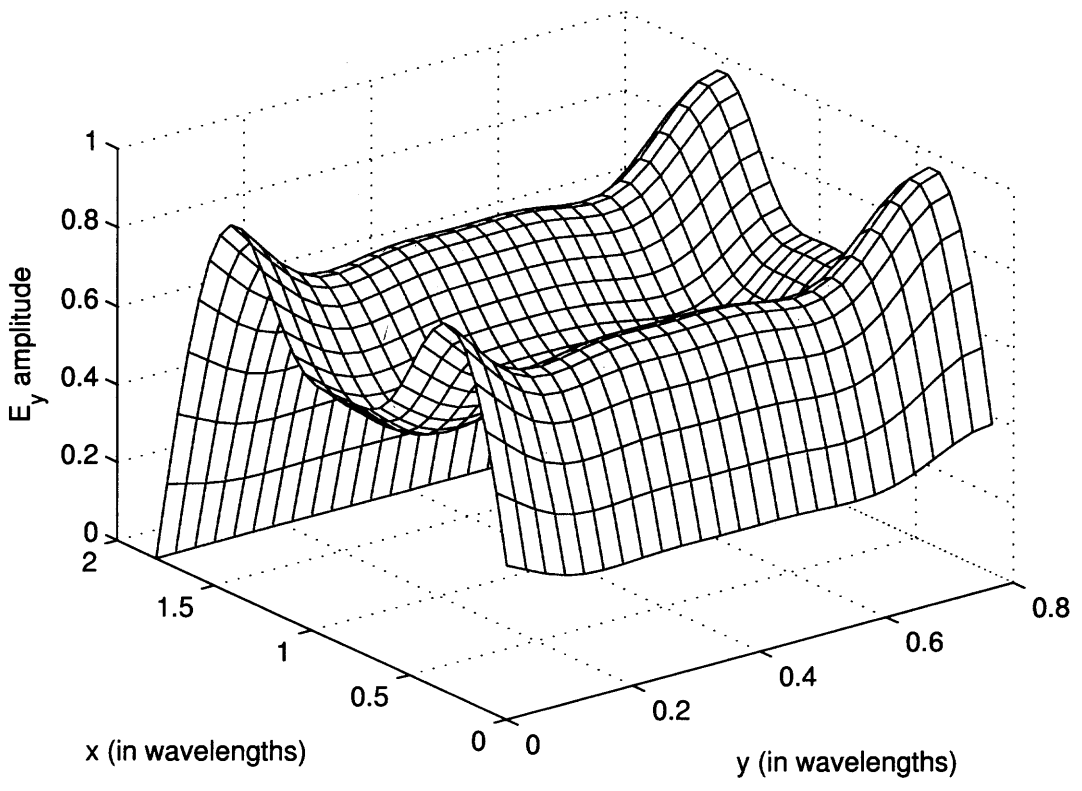

Figure 4.21 Amplitude of aperture electric field distribution, E_y versus x and y for ($\varepsilon_{r1} = 1.0$ $\varepsilon_{r2} = 1.0$) stepped-horn antenna at $f = 10$ GHz.

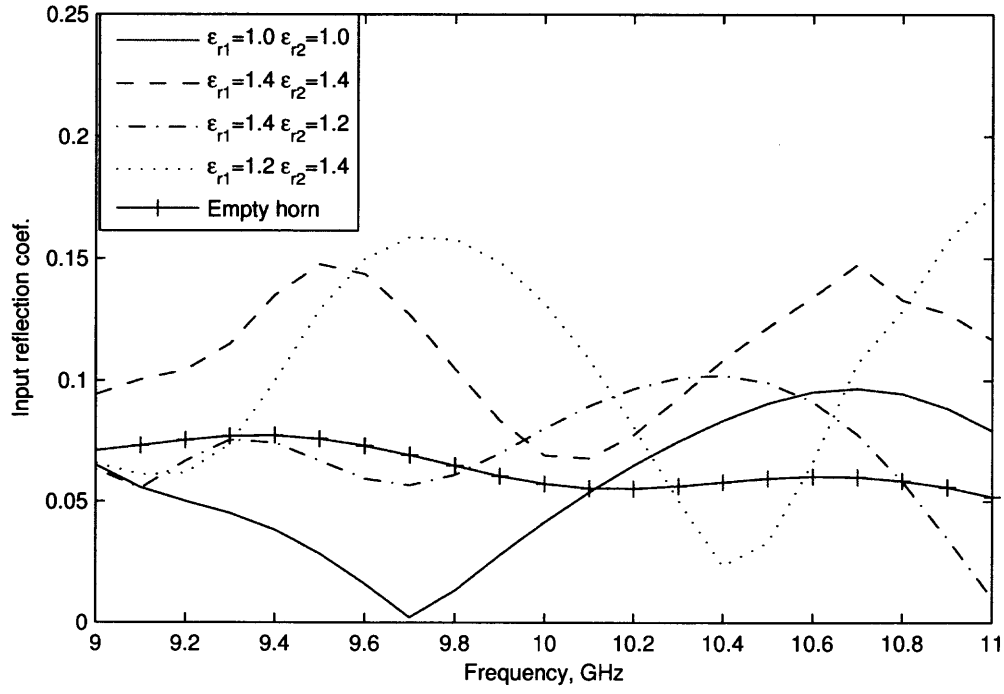

Figure 4.22 Input reflection coefficient versus frequency of the stepped-horn antennas for ($\varepsilon_{r1} = 1.0$ $\varepsilon_{r2} = 1.0$), ($\varepsilon_{r1} = 1.4$ $\varepsilon_{r2} = 1.4$), ($\varepsilon_{r1} = 1.2$ $\varepsilon_{r2} = 1.4$), ($\varepsilon_{r1} = 1.4$ $\varepsilon_{r2} = 1.2$) and empty horn antenna with $L = 91.1$ mm.

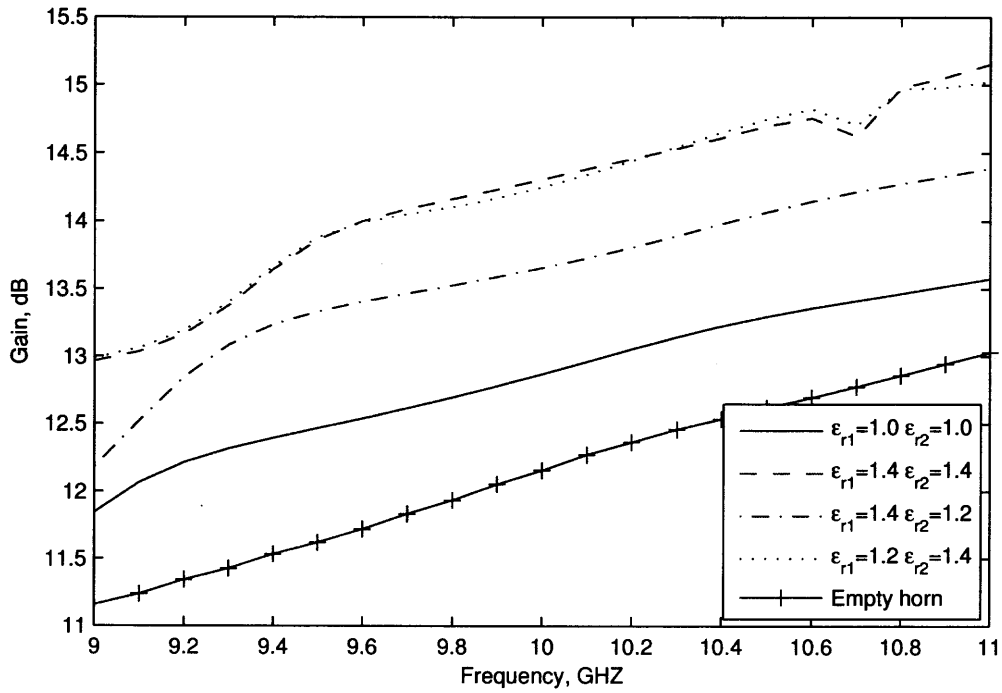

Figure 4.23 Gain versus frequency of the stepped-horn antennas for ($\varepsilon_{r1} = 1.0$ $\varepsilon_{r2} = 1.0$), ($\varepsilon_{r1} = 1.4$ $\varepsilon_{r2} = 1.4$), ($\varepsilon_{r1} = 1.2$ $\varepsilon_{r2} = 1.4$), ($\varepsilon_{r1} = 1.4$ $\varepsilon_{r2} = 1.2$) and empty horn antenna with $L = 91.1$ mm.

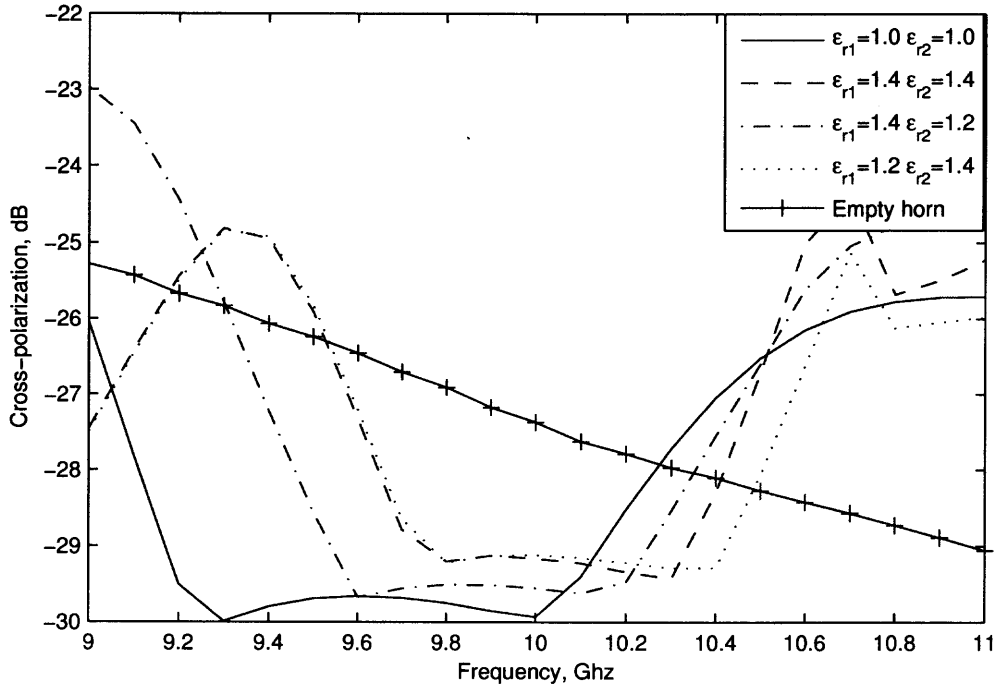

Figure 4.24 Cross-polarization level versus frequency of the stepped-horn antennas for ($\varepsilon_{r1} = 1.0$ $\varepsilon_{r2} = 1.0$), ($\varepsilon_{r1} = 1.4$ $\varepsilon_{r2} = 1.4$), ($\varepsilon_{r1} = 1.2$ $\varepsilon_{r2} = 1.4$), ($\varepsilon_{r1} = 1.4$ $\varepsilon_{r2} = 1.2$) and empty horn antenna with $L = 91.1$ mm.

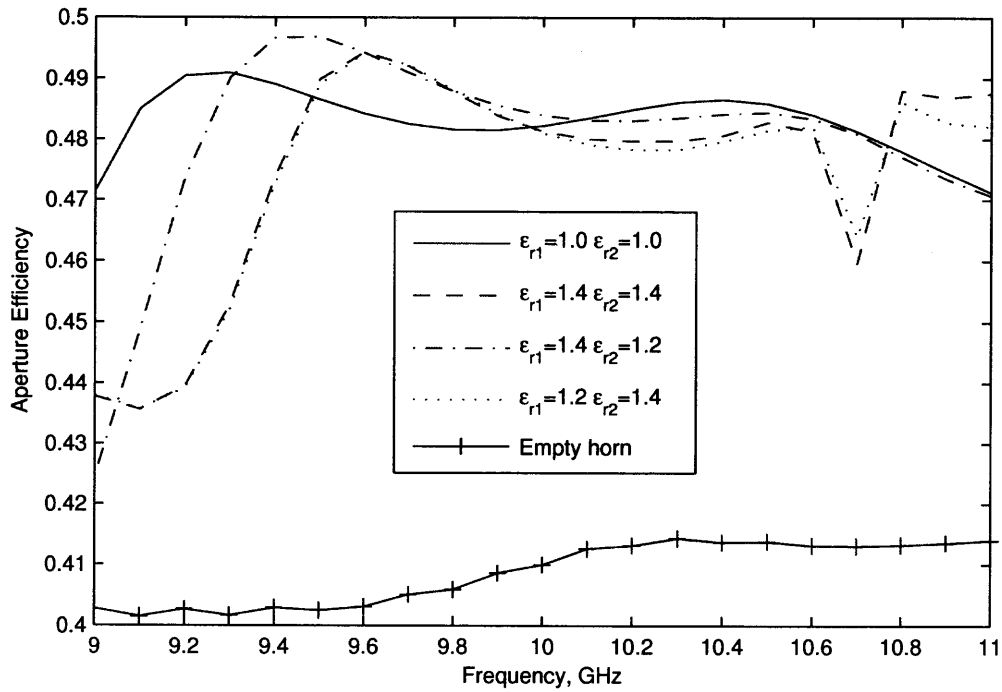

Figure 4.25 Aperture efficiency versus frequency of the stepped-horn antennas for ($\varepsilon_{r1} = 1.0$ $\varepsilon_{r2} = 1.0$), ($\varepsilon_{r1} = 1.4$ $\varepsilon_{r2} = 1.4$), ($\varepsilon_{r1} = 1.2$ $\varepsilon_{r2} = 1.4$), ($\varepsilon_{r1} = 1.4$ $\varepsilon_{r2} = 1.2$) and empty horn antenna with $L = 91.1$ mm.

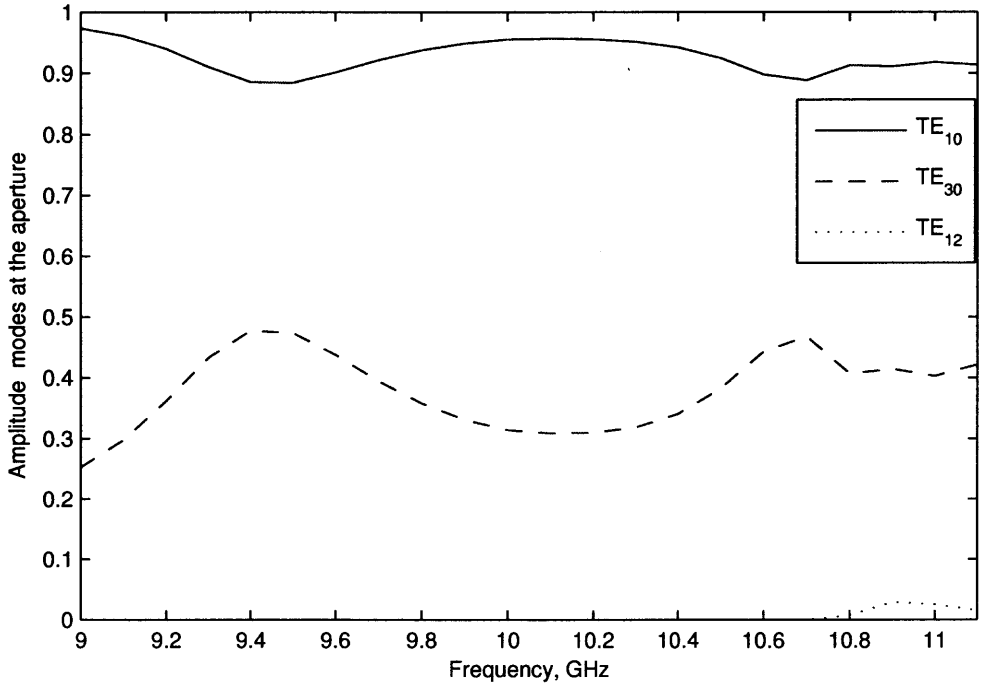

Figure 4.26 Amplitude of aperture modes versus frequency, for ($\varepsilon_{r1} = 1.4$ $\varepsilon_{r2} = 1.4$) stepped-horn antenna.

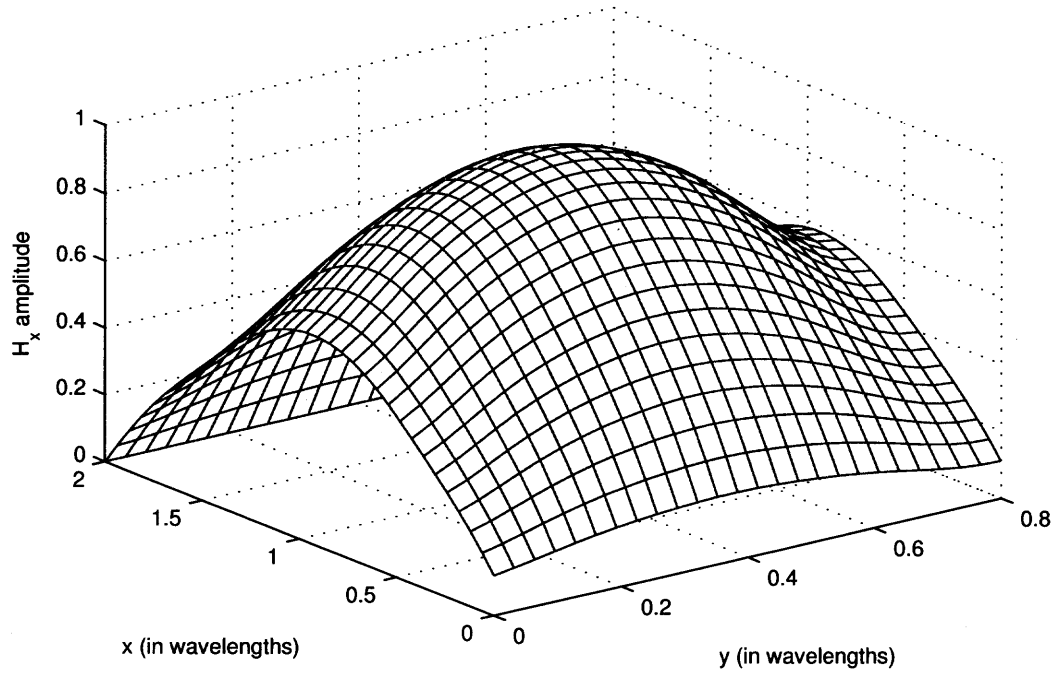

Figure 4.27 Amplitude of aperture magnetic field distribution,H_x versus x and y for empty horn antenna with length $L = 91.1$ mm at $f = 10$GHz.

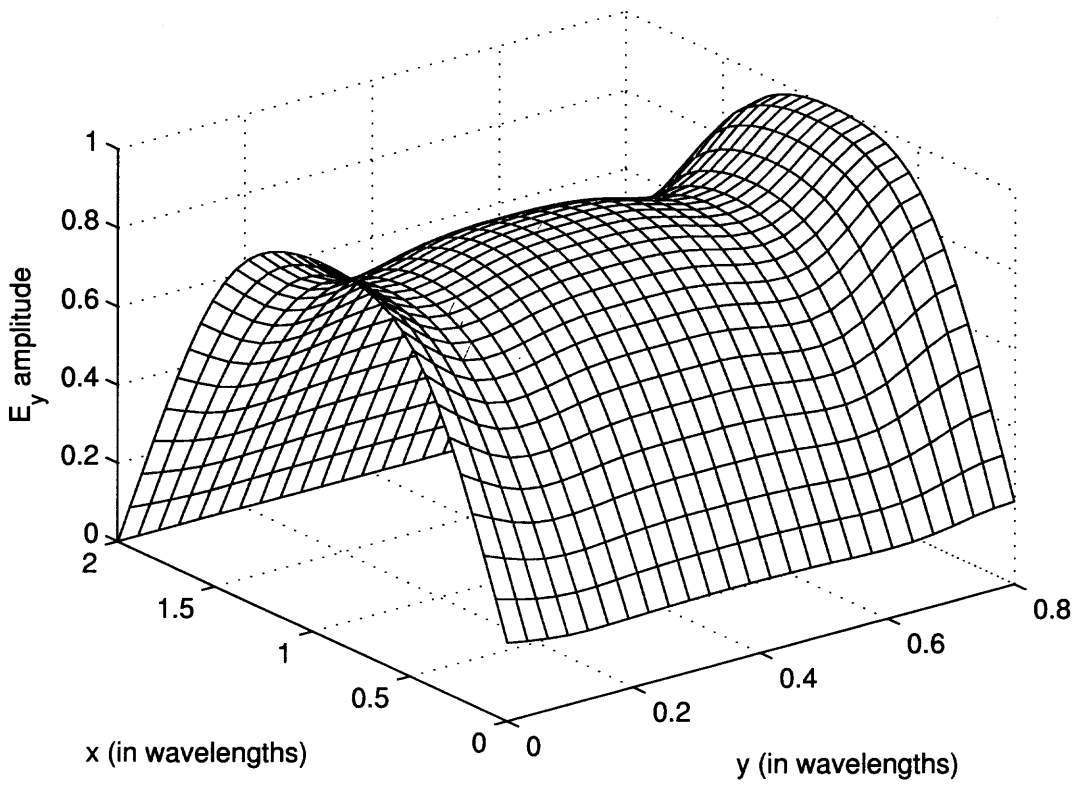

Figure 4.28 Amplitude of aperture electric field distribution, E_y versus x and y for empty horn antenna with length $L = 91.1$ mm at $f = 10$ GHz.

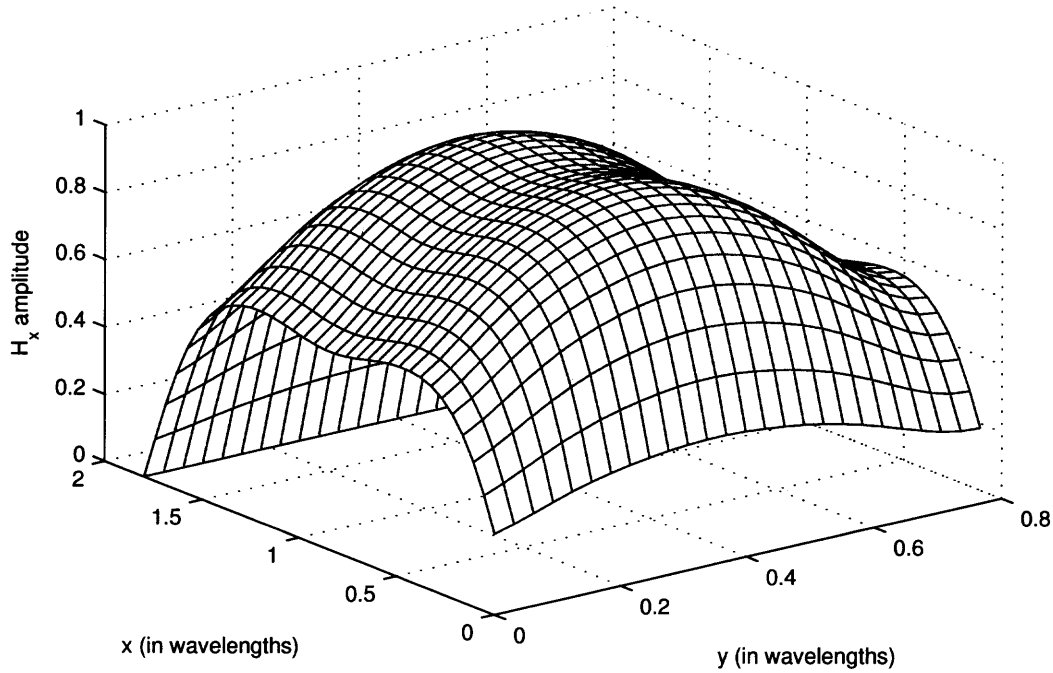

Figure 4.29 Amplitude of aperture magnetic field distribution, H_x versus x and y for ($\varepsilon_{r1} = 1.0\, \varepsilon_{r2} = 1.0$) stepped-horn antenna at $f = 10$ GHz.

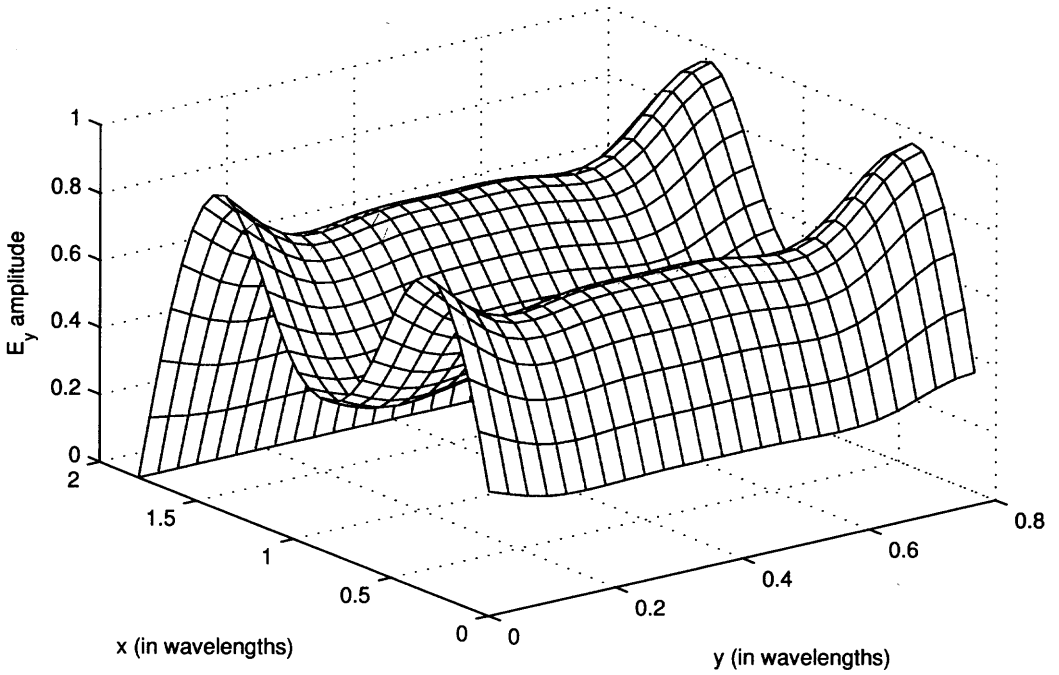

Figure 4.30 Amplitude of aperture electric field distribution, E_y versus x and y for ($\varepsilon_{r1} = 1.0$ $\varepsilon_{r2} = 1.0$) stepped-horn antenna at $f = 10$ GHz.

CHAPTER 5

CONCLUSIONS AND FUTURE WORK

Stepped-horn antenna with variable permittivity dielectric material loading is proposed and analyzed using hybrid numerical method. In the analysis, tapered region including stepped waveguide section is divided into a number of rectangular waveguide sections filled with the lossless dielectric material. Following the standard mode matching, a set of generalized scattering matrix equations in each junction are obtained. The overall scattering matrix of the horn is evaluated by cascading the scattering matrices of individual steps. The generalized reflection matrix of the aperture is determined using the method of moments. Then the generalized scattering matrix of the horn is combined with reflection matrix of the aperture. This analysis extended to determine yields the complex weighting coefficient of each mode at the horn aperture in terms of the power of the incident TE_{10} mode. Finally, the results are used to determine the input reflection coefficient of the antenna including the radiation patterns. Different dielectric materials are applied to achieve better performance characteristics. It was observed that the dielectric material loading improves gain characteristics. Due to the optimization of stepped-horn antennas, aperture efficiency, cross-polarization and gain characteristics were improved. Dielectric material loading to stepped-horn antenna reduced of physical dimensions of the antenna and also improved gain level. It is observed that for higher dielectric constant material and larger apertures, higher TE_{m0} modes are needed to be included into the optimization. However, undesired modes would also be excited at the aperture. For future work, multi-stepped horn antenna loaded with dielectric materials has to be investigated to excite the higher order TE_{m0} modes and to cancel the undesired modes at the aperture.

Dielectric materials of various permittivities based on TiO_2 has been fabricated and are currently being characterized. These materials will be used in optimum horn antenna design to validate numerical results with the experimental measurements.

APPENDIX

TAYLOR EXPANSION OF GREEN FUNCTION INTEGRALS

The integrals (I_g, I_x, I_y) are evaluated by using the following four term Taylor expansion approximation of the Green function,

$$e^{-jk_o r} \approx e^{-jk_o r_o}[1 - jk_o(r - r_o) - \frac{k_o^2}{2}(r - r_o)^2 + \frac{jk_o^3}{6}(r - r_o)^3] \tag{1}$$

where

$$r = \sqrt{x^2 + y^2} \tag{2}$$

$$r_o = \sqrt{(s\Delta x)^2 + (t\Delta y)^2} \tag{3}$$

$$\begin{aligned} I_g(s,t) &= \int_{y=(t-1/2)dy}^{(t+1/2)dy} \int_{x=(s-1/2)dx}^{(s+1/2)dx} \frac{e^{-jk_o r}}{r}\, dxdy \\ &= e^{-jk_o r_o}\{(1 + jk_o r_o - k_o^2\frac{r_o^2}{2} - j\frac{k_o^3}{6}r_o^3)\iint \frac{dxdy}{r} \\ &\quad +(-jk_o + k_o^2 r_o + j\frac{k_o^3}{2}r_o^2)\iint dxdy \\ &\quad +(-\frac{k_o^2}{2} - j\frac{k_o^3}{2}r_o)\iint r\, dxdy \\ &\quad +j\frac{k_o^3}{6}\iint r^2\, dxdy\} \end{aligned}$$

$$
\begin{aligned}
I_x(s,t) &= \frac{1}{\Delta x} \int_{y=(t-1/2)dy}^{(t+1/2)dy} \int_{x=(s-1/2)dx}^{(s+1/2)dx} \frac{e^{-jk_o r}}{r}\, x\, dxdy \\
&= \frac{e^{-jk_o r_o}}{\Delta x}\{(1 + jk_o r_o - k_o^2 \frac{r_o^2}{2} - j\frac{k_o^3}{6} r_o^3) \iint \frac{x\, dxdy}{r} \\
&\quad +(-jk_o + k_o^2 r_o + j\frac{k_o^3}{2} r_o^2) \iint x\, dxdy \\
&\quad +(-\frac{k_o^2}{2} - j\frac{k_o^3}{2} r_o) \iint x\, r\, dxdy \\
&\quad +j\frac{k_o^3}{6} \iint x\, r^2\, dxdy\}
\end{aligned}
$$

$$
\begin{aligned}
I_y(s,t) &= \frac{1}{\Delta y} \int_{y=(t-1/2)dy}^{(t+1/2)dy} \int_{x=(s-1/2)dx}^{(s+1/2)dx} \frac{e^{-jk_o r}}{r}\, y\, dxdy \\
&= \frac{e^{-jk_o r_o}}{\Delta y}\{(1 + jk_o r_o - k_o^2 \frac{r_o^2}{2} - j\frac{k_o^3}{6} r_o^3) \iint \frac{y\, dxdy}{r} \\
&\quad +(-jk_o + k_o^2 r_o + j\frac{k_o^3}{2} r_o^2) \iint y\, dxdy \\
&\quad +(-\frac{k_o^2}{2} - j\frac{k_o^3}{2} r_o) \iint y\, r\, dxdy \\
&\quad +j\frac{k_o^3}{6} \iint y\, r^2\, dxdy\}
\end{aligned}
$$

The indefinite integrals associated with the rest of the required integrals are

$$\iint \frac{dxdy}{r} = x\,log(y+r) + y\,log(x+r) \tag{4}$$

$$\iint \frac{dxdy}{r} = \frac{xyr}{3} + \frac{x^3}{6}\,log(y+r) + \frac{y^3}{6}\,log(x+r) \tag{5}$$

$$\iint r^2\,dxdy = \frac{xyr^2}{3} \tag{6}$$

$$\iint \frac{xdxdy}{r} = \frac{yr}{2} + \frac{x^2}{2}\,log(y+r) \tag{7}$$

$$\iint xrdxdy = yr(\frac{r^2}{12} + \frac{x^2}{8}) + \frac{x^4}{8}\,log(y+r) \tag{8}$$

$$\iint xr^2dxdy = x^2y(\frac{x^2}{4} + \frac{y^2}{6}) \tag{9}$$

$$\iint \frac{ydxdy}{r} = \frac{xr}{2} + \frac{y^2}{2}\,log(x+r) \tag{10}$$

$$\iint yrdxdy = xr(\frac{r^2}{12} + \frac{y^2}{8}) + \frac{y^4}{8}\,log(x+r) \tag{11}$$

$$\iint yr^2dxdy = y^2x(\frac{y^2}{4} + \frac{x^2}{6}) \tag{12}$$

The definite integral is obtained from the indefinite integral by adding the indefinite integral evaluated at the upper limits to that at both lower limits and subtracting both evaluations of the indefinite integral at the mixed (one upper,one lower) limits.

BIBLIOGRAPHY

[1] P. Clarricoats, A. Olver, and B. Ok, "Broadband low-crosspolarization horn," *Electronic Letters*, vol. 30, pp. 2085–2086, December 1994.

[2] P. Clarricoats, A. Olver, and K.Raghavan, "Mode conversion in dielectric loaded horns," *Antennas and Propagation Society International Symposium,AP-S. Digest*, vol. 1, pp. 362–365, 6-10 June 1988.

[3] G.N.Tsandoulas and W. Fitzgerald, "Aperture efficiency enhancement in dielectric loaded rectangular horns," *IEEE Trans. Antennas Propagat.*, vol. 20, pp. 69–74, March 1972.

[4] L. Oh, S. Peng, and C. Lunden, "Effects of dielectrics on the radiation patterns of an electromagnetic horn," *IEEE Trans. Antennas Propagat.*, vol. 18, pp. 553–556, July 1970.

[5] T. Satoh, "Dielectric-loaded horn antenna," *IEEE Trans. Antennas Propagat.*, vol. 20, pp. 199–201, March 1972.

[6] P. Clarricoats, A. D. Olver, and M. Rizk, "A dielectric loaded conical feed with low crosspolar radiation," *Proc. URSI Symp. Electromagnetic Theory, Santiago, Spain*, pp. 351–354, 1983.

[7] F. Dubrovka, O. Krupnov, and Y. Rospopa, "Analysis of partially dielctric loaded coaxial horn antennas," *International Conference on Antenna Theory and Techniques*, pp. 229–232, 2003.

[8] E. Lier, "A dielectric hybrid mode antenna feed: a simple alternative to the corrugated horn," *IEEE Trans. Antennas Propagat.*, vol. 34, pp. 21 – 29, 1986.

[9] T. Wriedt, K. H. Wolff, F. Arndt, and U. Tucholke, "Rigorous hybrid field theoretic design of stepped rectangular waveguide mode converters including the horn transitions into half-space," *IEEE Trans. Antennas Propagat.*, vol. 37, pp. 780–790, June 1989.

[10] A. K. Bhattacharyya and G. Rollins, "Accurate radiation and impedance characteristics of horn antennas-a moment-method model," *IEEE Trans. Antennas Propagat.*, vol. 44, pp. 523–531, April 1996.

[11] K. Liu, C. A. Balanis, C. R. Birtcher, and G. C. Barber, "Analysis of pyramidal horn antennas using moment methods," *IEEE Trans. Antennas Propagat.*, vol. 41, pp. 1379–1389, June 1993.

[12] P. J. B. Clarricoats and K. R. Slinn, "Computer solution of waveguide discontinuity problems," *Microwave Symposium Digest, G-MTT International*, vol. 67, pp. 23–27, May 1967.

[13] H. Patzelt and F. Arndt, "Double-plane steps in rectangular waveguides and their application for transformers, irises, and filters," *IEEE Trans. Microwave Theory Tech.*, vol. 30, pp. 771–776, May 1982.

[14] J. A. Encinar and J. M. Rebollar, "A hybrid technique for analyzing corrugated and noncorrugated rectangular horns," *IEEE Trans. Antennas Propagat.*, vol. 34, pp. 961–968, August 1986.

[15] J. R. Mautz and R. F. Harrington, "Electromagnetic transmission through a rectangular aperture in a perfectly conducting plane," Technical report TR-76-1, Syracuse University, Department of Electrical and Computer Engineering, Syracuse,New York 13210, 1976.

[16] R.H.McPhie and A.I.Zaghloul, "Radiation from a rectangular waveguide with infinite flange–exact solution by the correlation matrix method," *IEEE Trans. Antennas Propagat.*, vol. 28, pp. 497– 503, July 1980.

[17] R. E. Collin, *Field Theory of Guided Waves*. IEEE Press, 2nd ed., 1991.

[18] G. V. Eleftheriades, A. S. Omar, L. P. B. Katehi, and G. M. Rebeiz, "Some important properties of waveguide junction generalized scattering matrices in the context of the mode matching technique," *IEEE Trans. Microwave Theory Tech.*, vol. 42, pp. 1896–1903, October 1994.

[19] A. Ludwig, "The definition of cross-polarization," *IEEE Trans. Antennas Propagat.*, vol. 21, pp. 116–119, January 1973.

[20] S. Gupta, A. K. Bhattacharyya, and A. Chakraborty, "Analsis of an open-ended waveguide radiator with dielectric plug," *IEE Proc.-Microw. Antennas Propag.*,, vol. 44, pp. 126–130, April 1997.

[21] A. K. Bhattacharyya, "Multimode moment method formulation for waveguide discontinuties," *IEEE Trans. Microwave Theory Tech.*, vol. 42, pp. 1567–1571, August 1994.

[22] J. M. Reiter and F. Arndt, "Rigorous analysis of arbitrarily shaped h- and e-plane discontinuities in rectangular waveguides by a full-wave boundary contour mode-matching method," *IEEE Trans. Microwave Theory Tech.*, vol. 43, pp. 780–790, April 1995.

[23] W. Wessel, T. Siverding, and F. Arndt, "Mode-matching analysis of general waveguide multiport junctions," *IEEE MTT-S Digest*, vol. 28, pp. 45–48, 1999.

[24] R. F. Harrington and J. R. Mautz, "A generalized network formulation for aperture problems," *IEEE Trans. Antennas Propagat.*, vol. 24, pp. 870–873, November 1976.

[25] C. A. Balanis, *Antenna Theory: Analysis and Design*. New York: Wiley, 1982.

[26] T. Bird and S. Hay, "Mismatch in dielectric-loaded rectangular waveguide antenna," *Electronic Letters*, vol. 26, pp. 59–61, January 1990.

[27] V. Teodoridis, T. Sphicopoulos, and F. Gardiol, "The reflection from an open-ended rectangular waveguide terminated by a layered dielectric medium," *IEEE Trans. Microwave Theory Tech.*, vol. 33, pp. 359–366, May 1985.

[28] T. Bird, "Mode matching analysis of arrays of stepped rectangular horns and application to satellite antenna design," *ICAP 91*, vol. 2, pp. 849 – 852, 15-18 Apr 1991.

[29] N. Amitay and M. Gans, "Design of rectangular horn arrays with oversized aperture elements.," *IEEE Trans. Antennas Propagat.*, vol. 29, pp. 871–884, November 1981.

[30] S. Gupta, A. Bhattacharya, and A. Chakraborty, "Analysis of an open-ended waveguide radiator with dielectric plug," *Microwaves, Antennas and Propagation, IEE Proceedings*, vol. 144, pp. 126 – 130, 1997.

[31] T. Itoh, *Numerical Techniques for Microwave and Milimeter Wave Passive Structures*. New York: Wiley-Interscience, 1989.

[32] R. Mittra and R.S.Lee, *Analytical Techniques in the Theory of Guided Waves*. The MacMillan company, 1971.

[33] E. Lier, "Hybrid-mode horn antenna with design-specific aperture distribution and gain," *Antennas and Propagation Society International Symposium*, vol. 4, pp. 502–505, 2003.

[34] A. D. Olver and B. Philips, "Profiled dielectric loaded horns," *Eighth International Conference on Antennas and Propagation*, vol. 2, pp. 788–791, 1993.

[35] A. D. Olver, R. A. Pearson, G. Peake, and B. Philips, "Metallised dual dielectric loaded horn," *Seventh International Conference on IEE, ICAP 91*, vol. 1, pp. 121 – 124, 1991.

[36] M. Hamid, S. Towaij, and G. Martens, "A dielectric loaded circular waveguide antenna," *IEEE Trans. Antennas Propagat.*, vol. 20, pp. 96–97, 1972.

[37] D. Vital and J. Descardeci, "Parametric analysis of the pyramidal horn partially filled," *MIKA 2002, 14th International Conference on*, vol. 3, pp. 930 – 933, 2002.

[38] O. Ata, T. Benson, and A. Marincic, "Application of optical ray technique to the design of short microwave horn antennas with low side lobe levels," *IEE Proc.*, vol. 137, pp. 81–88, 1990.

[39] O. Ata and T. Benson, "Novel phase-corrected horn antenna of short length," *Electronic Letters*, vol. 24, pp. 292 – 293, 1988.

[40] E. Kuhn and V. Hombach, "Analysis of partially dielctric loaded coaxial horn antennas," *3rd International Conference on Antenna Theory and Techniques*, pp. 127–131, 1983.

[41] R. C. Johnson and H. Jasik, *Antenna Engineering Handbook.* McGraw-Hill Book Company, 2nd ed., 1984.

[42] F. Arndt, U. Tucholke, and T. Wriedt, "Computer-optimized multisection transformers between rectangular waveguides of adjacent frequency bands," *IEEE Trans. Antennas Propagat.*, vol. 32, pp. 1479–1484, November 1984.

[43] S. P. Skobelev, B. Ku, A. V. Shishlov, and D. Ahn, "Optimum geometry and performance of a dual-mode horn modification," *IEEE Antennas and Propagation Magazine*, vol. 43, pp. 90–93, February 2001.

[44] C. C. Han and A. N. Wickert, "A new multimode rectangular horn antenna generating a circularly polarized elliptical beam," *IEEE Trans. Antennas Propagat.*, vol. 22, pp. 746–751, November 1974.

[45] A. K. Bhattacharyya and G. Goyette, "A novel horn radiator with high aperture efficieny and low cross-polarization and applications in arrays and multibeam reflector antennas," *IEEE Trans. Antennas Propagat.*, vol. 52, pp. 2850– 2859, November 2004.

[46] P. Clarricoats and R. F. D. A. Olver, "High performance compact corrugated horn," *IEE Proc.-Microw. Antennas Propag.*, vol. 151, pp. 519–524, December 2004.

[47] A. D. Olver and J. Xiang, "Design of profiled corrugated horns," *IEEE Trans. Antennas Propagat.*, vol. 36, pp. 936–940, July 1988.

[48] A. S. Slobelev and P.-S. Kildal, "Analysis of a hard strip-loaded conical horn by the method of generalized scattering matrix," *IEEE Trans. Antennas Propagat.*, vol. 51, pp. 2918–2925, July 2003.